LUND INSTITUTE OF TECHNOLOGY
Division of Structural Mechanics
Report TVSM-1002
LUND SWEDEN 1986

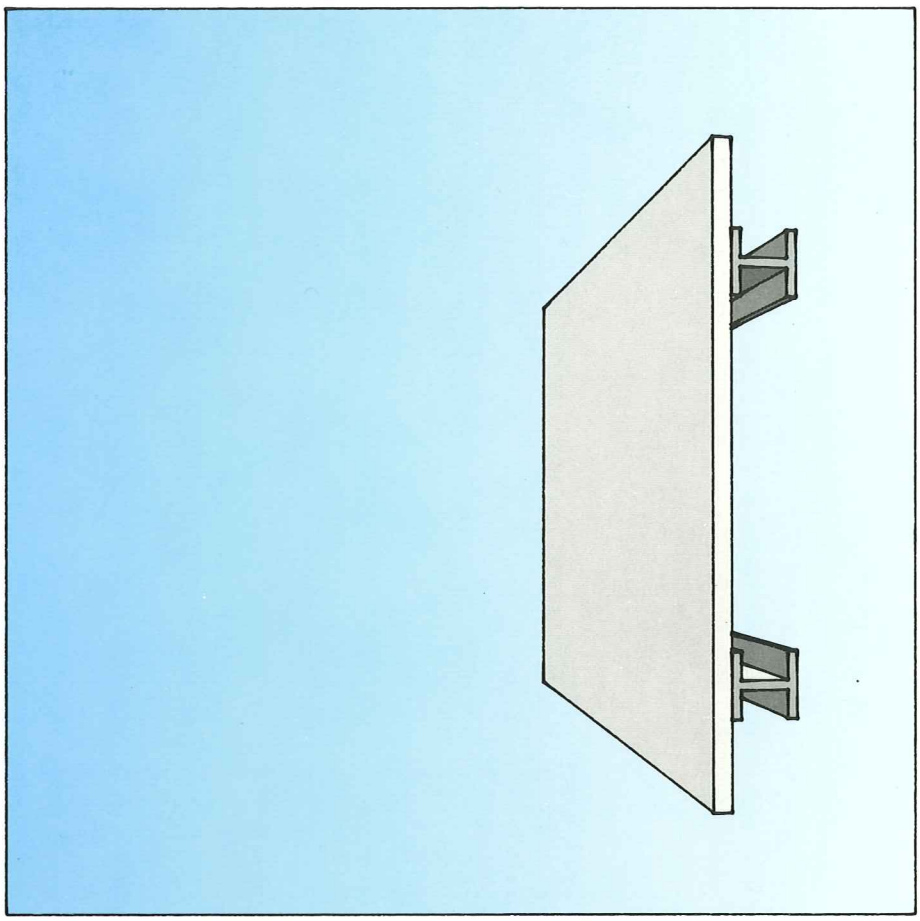

GÖRAN SANDBERG

FINITE ELEMENT MODELLING OF FLUID-STRUCTURE INTERACTION

LUND INSTITUTE OF TECHNOLOGY
Division of Structural Mechanics
Report TVSM-1002
CODEN: LUTVDG/(TVSM-1002)/1-148/(1986)

GÖRAN SANDBERG

FINITE ELEMENT MODELLING OF FLUID-STRUCTURE INTERACTION

To those who matter
Henrik and Håkan

Printed in Sweden
Jabe-Offset AB
Lund 1986

ACKNOWLEDGEMENTS

The research presented in this thesis has been carried out at the division of Structural Mechanics, Lund Institute of Technology, starting during the academic year 1983/84. Financial support has been given by the Swedish Council for Building Research.

I wish to express my gratitude to Professor Hans Petersson, the supervisor during this work, for his guidance. His enthusiasm, even during small talk, proved contagious and for that I am thankful. I also want to thank Docent Sven Thelandersson for suggesting improvements to the manuscript and Docent Niels Saabye Ottosen for many discussions.

Special thanks are also due to Tech.Dr. Anders Peterson and Tech.Lic. Ola Dahlblom for their never-ending patience in discussing computational anomalies, and to Tech.Lic. Pål Hansson for being available when computer graphics were going wrong. Their willingness is appreciated.

My thanks are also directed to Professor Sven Lindblad and Tech.Dr. Björn Petersson, both at the division of Engineering Acoustics, for valuable discussions.

I would also like to thank Mrs. Tarja Aunola-Möller for her skill in typing the manuscript and above all for her doing so with never-ending enthusiasm even when time was short. Many thanks to Mr. Bo Zadig for preparing the drawings and figures and also to L.J. Gruber and Dr. Charles Stuart for checking the English. My thanks are also directed to all other friends at the Division of Structural Mechanics for their support and interest.

To my children, Henrik and Håkan: My gratitude for your instinctive understanding and for your joy. With your wakening in the middle of the night and your 'shouldn't you go to bed Dad', this work has constantly projected against the real values. To my parents for their assistance: Thank you.

Lund, 'between bird-cherry and lilac', May 1986.

Göran Sandberg

ABSTRACT

The dynamic interaction between a non-viscid, compressible fluid and an elastic structure is studied. Finite element formulations, using the weighted residual method, are derived. Different primary variables in the fluid domain are used and different source functions are considered.

When a potential field is used, the dynamic interaction between fluid and structure yields nonsymmetric matrices. In addition to these, new symmetric formulations for transient analysis are presented.

Some nonlinear fluid behaviour is taken into consideration. Applications to a cavitating fluid due to elastic wave propagation are described.

Numerical experiments show good agreement with what could be expected from a physical point of view. The nonlinear formulation shows good agreement with analytical results.

Key words

Finite element method, coupled problem, fluid-structure interaction, transient, acoustics, cavitation, time stepping, symmetric, nonlinear acoustics, submerged structures.

Page

1. INTRODUCTION

1.1 Finite elements in fluid-structure analysis

During the last 25 years, the Finite Element Method as a tool for solving problems in structural mechanics and continuum mechanics has developed from an exclusive research area into an everyday reality for both researchers and practising engineers. The reason for this dynamic development of the Finite Element Method is of course its close relation to the everyday engineering need for analyzing complex structures, along with the development of powerful computers. During this process, mathematicians have given the finite element method a firm mathematical form, using standard mathematical tools such as calculus of variation, weak solution technique, Rayleigh-Ritz method and the whole apparatus in error analysis. It would seem that these two branches have developed quite independently (see Vichnevetsky [46]). As computer capacity expanded, there was an increasing wish to explore more sophisticated physical phenomena and to do so with increasing precision by the use of the Finite Element Method. In the early seventies, finite element research began in the field of fluid mechanics and in 1974 the first conference on that topic was held at Swansea, UK. In a paper at that conference O.C. Zienkiewicz answered the question 'Why Finite Elements?' from the 1974 horizon. (See Zienkiewicz [48]). Almost a decade later (1982) the same author was able to present a far more detailed answer to that question in a retrospective paper presented at the fifth International Symposium of Finite Elements for Flow Problems (see Zienkiewicz et al [49]). In that paper the use of the Finite Element Method is divided into subareas such as

* slow viscid flow
* laminar flow
* turbulent flow
* shallow water flow
* meteorology
* acoustic phenomena
* fluid-structure interaction

and arguments are made about research penetrations and the advantages and drawbacks of the Finite Element Method. I

shall not repeat these arguments here but refer instead to that paper for such a discussion. A series of proceedings (see [55]), of which the paper cited above is a representative, gives a good idea of the state of research in applied finite elements in fluid mechanics.

The present work is confined to the last two areas listed above. Subsection 1.2 gives examples of the objectives of this work and in the introduction to Chapter 2 a formal definition is given. Let us just note that in this work, the fluid is regarded as compressible and inviscid.

Among the first working in this field were Gladwell and Zimmermann who presented two papers in the middle of the 1960s (see Gladwell at al [19] and Gladwell [20]). In these papers, finite element formulations are derived for coupled fluid-structure vibrations, using both displacement and fluid pressure as fluid unknowns, although the former did not work satisfactorily. Some years later Cragg, in a series of papers dated 1970-1973, presented a variational formulation of the coupled problem in terms of fluid pressure (Cragg [8]-[10]).

Fluid-structure interaction touches upon other finite element disciplines and questions in discrete analysis. Eigenvalue analysis is discussed by Daniel [12], [13]. Basically fluid-structure formulations lead to nonsymmetric matrices. However, this can be avoided, for example by matrix manipulations as is done by Tong [43] and Felippa [18], although the latter is closely related to formulations that may be achieved directly via the differential equations. When passing from continuous formulations to discrete ones, infinite domains must be truncated. Different methods can be applied, such as boundary element methods used by Amin and Wilton [1] where arguments are made for high order polynomials compared to low order polynomials. In Szmidt [44], a transmitting boundary is constructed by using the fluid eigenmodes. Infinite elements are used by many authors such as Bettess [4], Bettess and Zienkiewicz [5], Sharan [39]. Time stepping routines for transient analysis are developed by, for example, Zienkiewicz and Taylor [47] for nonsymmetric, coupled problems such as fluid-structure interaction. A nonlinear problem arises because the fluid lacks the ability to withstand negative absolute pressure. Such problems are discussed, inter alia, by Newton [23]-[26].

An excellent review of the state of the art in fluid-structure analysis is presented by Zienkiewicz et al [50] and a good insight can be obtained in Hinton et al [27]. A discussion of the finite element method in practical acoustics is given in Stanko et al [37]. Finally, methods for dealing with non-linearized fluid flow without elastic boundaries are presented by Hughes et al [21] and Duncan et al [14].

1.2 The aim of the present analysis

The present work is confined to fluid-structure interaction and acoustic phenomena. The aim is to present, within the restrictions given in Chapter 2, general finite element descriptions using different primary variables and allowing different source terms in the fluid, some of which are illustrated and checked numerically.

In order to give a physical interpretation of the aim of this work some examples to which the theory is applicable are presented in the following.

A liquid container is exposed to external transient structural load. What are the stresses in the container due to this load? The liquid is part of the overall behaviour as it interacts with the structure.

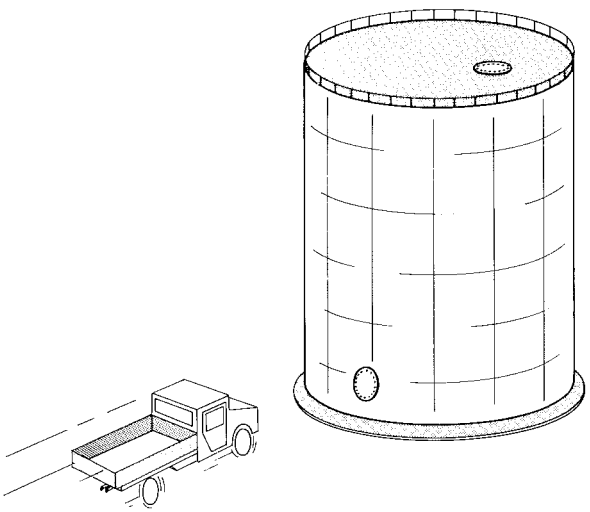

Figure 1.1. Filled or partially filled liquid container exposed to external transient load

In a chemical industry there is a safety valve. When the valve blows, the air pressure may reach very high levels. How high? Can it cause ear damage to people close to the valve?

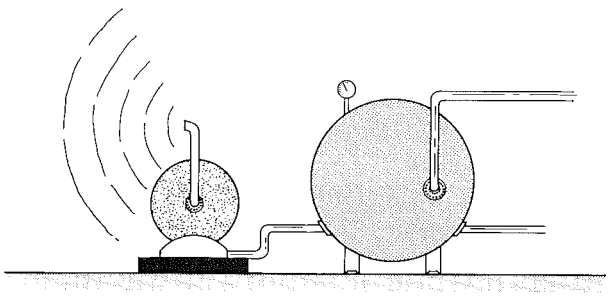

Figure 1.2. Sudden release of air under pressure

A vibrating equipment is placed in an enclosed space with elastic walls. As the equipment vibrates, the wall does likewise. What air pressure levels are we likely to get at a certain point outside the walls?

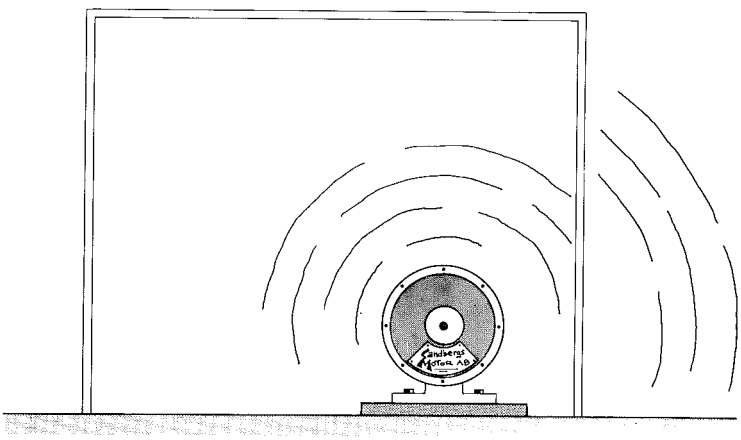

Figure 1.3. Vibrating equipment in an enclosed space with elastic walls

Finally, a submerged structure is exposed to underwater blast loading. The blast wave reaches the structure, which deforms, and the reflected wave causes the fluid to cavitate.

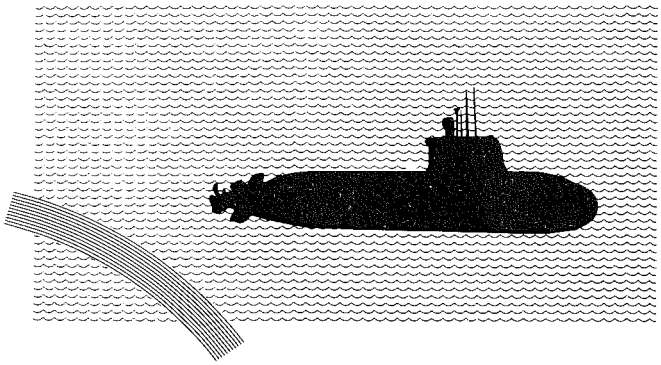

Figure 1.4. Submerged structure exposed to underwater explosions

1.3 Summary of contents

Chapter 2 starts with a formal definition of the goal of this work: what effects should the model consider? Little attention is given to the structure on its own The aim is to describe the fluid and the interaction between fluid and structure using different variables in the fluid description. Some nonlinear behaviour is also taken into consideration.

In Chapter 3, finite element models are derived. Different primary variables are used to describe the fluid. The scalar field descriptions are non-symmetric, but three symmetric formulations are also given. Finally, a model for nonlinear wave propagation is given, with special application to cavitation.

Chapter 4 deals with the computer programming needed during the course of the work.

Numerical examples verifying the models and illustrating the different possibilities within the models are presented in Chapter 5.

Finally, Chapter 6 contains some concluding remarks: general results achieved, original features and ideas for future research and development.

1.4 Notations

Appendix A contains a list of the notations used here. Some general remarks must be made however. In Chapter 2 $\partial/\partial t$ is used for time derivatives but in Chapter 3, in passing to finite element modelling, $\dot{}$ is used. As scalar product we use '$\cdot$' and as vectorial product '$\times$'. Vectors are written in boldface.

The finite element formulations using different primary variables or the symmetric formulations give different coupling matrices and load matrices. Nevertheless, the same notation is used in all formulations for a matrix connected with a specific phenomenon. For instance the coupling mass matrix is always called M_c even if its content or location in a global matrix changes when another formulation is used. It is my belief, however, that the confusion in doing so is less than the confusion that would arise if new notations were introduced in each new formulation.
There are notations not listed in Appendix A, but these are used only locally in specific subsections and are never referred to from any other subsection.

References are made by name and a number in square brackets which refers to the list in Appendix D.

2. MATHEMATICAL DESCRIPTION

In this chapter, a mathematical description and a mathematical derivation are given. The main interest is the study of the structural behaviour as it interacts with some fluid. Since the fluid is the reason for the structural behaviour, the main effort will be directed at deriving and describing the mathematics of the fluid and the fluid-structure interaction, and only little attention will be given to the structural parts on their own.

By way of introduction, in the previous chapter we listed some applications for the model presented here. These applications can be interpreted as a working definition of our model and they are easily restated into a verbal definition. A structure surrounds, or is surrounded by, a fluid. We allow the structure to have openings and the fluid to be infinite. The structure is subjected to forces or prescribed motions, the fluid to body forces or mass inflow. The fluid is thought of as an inviscid and compressible fluid, and its boundary consists of structural members or a free surface with a prescribed external pressure. On this free surface we allow gravitational (linearized) waves. The fluid is regarded as a continuum in areas not subjected to a mass inflow, that is, the fluid particles maintain the same topological relationship at all times in those areas. Along the structural members, the fluid recognizes the structural displacements and the structural members recognize the fluid pressure as a distributed load.

2.1 Structure

The structural components can be formulated as

$$L(\mathbf{u}_s) = \mathbf{F}_s(\mathbf{r},t), \tag{2.1}$$

where L is a partial differential operator with respect to time and space. $\mathbf{u}_s$ is the structural displacement vector, which is a function of location $\mathbf{r}$ and time t. Finally, $\mathbf{F}_s$ is an external time dependent load.

The fluid influence on the structure will manifest itself through the surface load vector (the subscript 's' denotes structure and 'f' fluid)

$$\mathbf{F}_f(\mathbf{r},t) = p(\mathbf{r},t)\mathbf{n}, \tag{2.2}$$

where p is the unsteady fluid pressure and $\mathbf{n}$ is the outward unit normal vector at the fluid-structure interface.

2.2 Fluid

The governing equations for the fluid can be obtained from most books on fluid dynamics (see Cole [7]), but it is useful to make a complete derivation of these equations so as to fully understand the simplifications that are made along the way.

Mass balance for an arbitrary material volume V(t) gives

$$\frac{d}{dt}\left(\int_{V(t)} \hat{\rho}\ dV\right) = \int_{V(t)} q\ dV, \tag{2.3}$$

where $\hat{\rho}$ is the density and q is the added fluid mass per unit volume and time. Reversal of the order between differentiation and integration (see Appendix B) yields

$$\int_{V(t)} \left(\frac{d\hat{\rho}}{dt} + \hat{\rho}\ \nabla\cdot\mathbf{v}\right)dV = \int_{V(t)} q\ dV,$$

where $\mathbf{v}$ is the fluid velocity field. Because the volume V(t) is arbitrary, we have

$$\frac{d\hat{\rho}}{dt} + \hat{\rho}\ \nabla\cdot\mathbf{v} = q. \tag{2.4}$$

We neglect viscosity, although later on when the system matrices are defined a Rayleigh-type damping can be taken into consideration. Internal forces acting upon a volume V(t) in the fluid act at the boundary S(t) of that volume. Furthermore, they are perpendicular to the boundary, which is a consequence of the fluid being inviscid. External forces are the body forces $\mathbf{b}$ (per mass unit). Conservation of linear momentum yields

$$\frac{d}{dt}\int_{V(t)} \hat{\rho}\mathbf{v}\ dV = -\int_{S(t)} \hat{p}\mathbf{n}\ dS + \int_{V(t)} \hat{\rho}\mathbf{b}\ dV + \int_{V(t)} q\mathbf{v}_q\ dV, \tag{2.5}$$

where $\mathbf{v}_q$ is the velocity of the added fluid mass.
Applying Appendix B to the left-hand side and Gauss theorem the first term on the right-hand side, we have

$$\int_{V(t)} \left[\frac{d}{dt}(\hat{\rho}\mathbf{v}) + \hat{\rho}\mathbf{v}(\nabla\cdot\mathbf{v})\right] dV = \int_{V(t)} (-\nabla\hat{p} + \hat{\rho}\mathbf{b} + q\mathbf{v}_q) dV.$$

As before, the volume is arbitrary so we have

$$\frac{d}{dt}(\hat{\rho}\mathbf{v}) + \hat{\rho}\mathbf{v}(\nabla\cdot\mathbf{v}) = -\nabla\hat{p} + \hat{\rho}\mathbf{b} + q\mathbf{v}_q. \tag{2.6}$$

Now, using Eq. (2.4),

$$\frac{d}{dt}(\hat{\rho}\mathbf{v}) = \frac{d\hat{\rho}}{dt}\mathbf{v} + \hat{\rho}\frac{d\mathbf{v}}{dt} = q\mathbf{v} - \hat{\rho}(\nabla\cdot\mathbf{v})\mathbf{v} + \hat{\rho}\frac{d\mathbf{v}}{dt}.$$

Combining this result with Eq. (2.6) we obtain

$$\hat{\rho}\frac{d\mathbf{v}}{dt} = -\nabla\hat{p} + \hat{\rho}\mathbf{b} - q(\mathbf{v} - \mathbf{v}_q). \tag{2.7}$$

Eqs. (2.4) and (2.7) are sufficient if we consider an incompressible fluid for which $\hat{\rho}$ is a known and time-invariant quantity. These equations can then be solved with respect to $\hat{p}$ and $\mathbf{v}$. If we consider a compressible fluid, we need one more relation containing $\hat{\rho}$ and $\hat{p}$. We assume the fluid motion to be independent of temperature and therefore the additional equation (equation of state) is

$$\hat{p} = \hat{p}(\hat{\rho}). \tag{2.8}$$

Summing up the results so far

$$\begin{cases} \dfrac{d\hat{\rho}}{dt} + \hat{\rho}\,\nabla\cdot\mathbf{v} = q, \\[2ex] \hat{\rho}\dfrac{d\mathbf{v}}{dt} + \nabla\hat{p} = \hat{\rho}\mathbf{b} - q(\mathbf{v} - \mathbf{v}_q), \\[2ex] \hat{p} = \hat{p}(\hat{\rho}). \end{cases} \tag{2.9}$$

2.2.1 Linear fluid

The physical model of the fluid, as expressed by Eq. (2.9), contains effects that can be neglected for our purpose. These deletions are discussed in this subsection.

The variation of the density is divided into two parts, one that contains a time-dependent part (ρ) and one that contains the static value (ρ_s). Thus

$$\hat{\rho} = \rho_s + \rho,$$

where $\nabla\rho_s = 0$. The first equation of (2.9) can be rewritten

$$\frac{d\rho}{dt} + \rho_s(1 + \frac{\rho}{\rho_s})\nabla\cdot\mathbf{v} = q.$$

If we assume the variation in time to be far less than the static value, that is

$$\frac{|\rho|}{\rho_s} << 1,$$

we have

$$\frac{d\rho}{dt} + \rho_s\nabla\cdot\mathbf{v} = q.$$

If we deal with the second equation of (2.9) in the same way, we end up with the system

$$\begin{cases} \dfrac{d\rho}{dt} + \rho_s\nabla\cdot\mathbf{v} = q, \\ \rho_s \dfrac{d\mathbf{v}}{dt} + \nabla\hat{p} = \rho_s\mathbf{b} - q(\mathbf{v} - \mathbf{v}_q), \\ \hat{p} = \hat{p}(\hat{\rho}). \end{cases} \tag{2.10}$$

The total time derivatives of ρ and $\mathbf{v}$ are

$$\frac{d\rho}{dt} = \frac{\partial\rho}{\partial t} + \mathbf{v}\cdot\nabla\rho,$$

$$\frac{d\mathbf{v}}{dt} = \frac{\partial\mathbf{v}}{\partial t} + (\mathbf{v}\cdot\nabla)\mathbf{v}.$$

The convective terms in these expressions and the influence of the added fluid mass q on the second equation in Eq. (2.10) are without significance under certain conditions, namely that the fluid velocity is considerably smaller than the speed of sound (these are discussed in detail in Appendix C). Under such conditions Eq. (2.10) yields

$$\frac{\partial\rho}{\partial t} + \rho_s\nabla\cdot\mathbf{v} = q, \tag{2.11}$$

$$\rho_s\frac{\partial\mathbf{v}}{\partial t} + \nabla\hat{p} = \rho_s\mathbf{b}. \tag{2.12}$$

These two equations together with the equation of state constitute a physical model for a linearized flow. They will be used further in the next subsection (2.2.2) as a basis for a cavitation model.

We can simplify the equations further. As was done in the case of density, we divide the pressure into two parts, p and p_s (same notation as for $\hat{\rho}$), and by linearizing the equation of state we write

$$\hat{p} = p_s + p \approx p_s + \rho\left(\frac{dp}{d\hat{\rho}}\right)_{\hat{\rho}=\rho_s},$$

where p_s is assumed constant. By introducing a new constant

$$c = \sqrt{\left(\frac{dp}{d\hat{\rho}}\right)_{\hat{\rho}=\rho_s}}$$

we have

$$p = c^2\rho. \tag{2.13}$$

Eq. (2.11) is then differentiated with respect to time

$$\frac{\partial^2 \rho}{\partial t^2} + \nabla\cdot(\rho_s \frac{\partial \mathbf{v}}{\partial t}) = \frac{\partial q}{\partial t}.$$

Eq. (2.12) is substituted into this expression, yielding

$$\frac{\partial^2 \rho}{\partial t^2} + \nabla\cdot(\rho_s \mathbf{b} - \nabla\hat{p}) = \frac{\partial q}{\partial t}.$$

In this relation, p is replaced by ρ using Eq. (2.13) and $\hat{p}$ is replaced by $p + p_s$, implying

$$\frac{\partial^2 \rho}{\partial t^2} = c^2\nabla^2\rho + \nabla^2 p_s - \rho_s\nabla\cdot\mathbf{b} + \frac{\partial q}{\partial t}.$$

From the definition of p_s above, the term $\nabla^2 p_s = 0$ so the final result reduces to a wave equation with source terms

$$\frac{\partial^2 \rho}{\partial t^2} = c^2\nabla^2\rho - \rho_s\nabla\cdot\mathbf{b} + \frac{\partial q}{\partial t}. \qquad (2.14)$$

By using Eq. (2.13) we may instead express the wave equation in terms of the pressure

$$\frac{\partial^2 p}{\partial t^2} = c^2\nabla^2 p - c^2\rho_s\nabla\cdot\mathbf{b} + c^2\frac{\partial q}{\partial t}. \qquad (2.15)$$

We now return to Eqs. (2.11-12). We apply the gradient to the first and the partial time derivative to the second of these equations, and solve with respect to $\mathbf{v}$ to get

$$\frac{\partial^2 \mathbf{v}}{\partial t^2} = c^2\nabla(\nabla\cdot\mathbf{v}) + \frac{\partial \mathbf{b}}{\partial t} - \frac{c^2}{\rho_s}\nabla q. \qquad (2.16)$$

It may be noted that

$$\nabla(\nabla\cdot\mathbf{v}) = \nabla^2\mathbf{v} + \nabla\times(\nabla\times\mathbf{v}).$$

For a perfect fluid, as long as the body forces are derivable from a potential function, the velocity field once irrotational remains that way. Thus

$$\nabla\times\mathbf{v} = 0.$$

This may also be regarded as a constraint - we are only interested in conservative solutions. If this constraint is imposed on Eq. (2.16) we once again obtain the wave equation, now in terms of the velocity field,

$$\frac{\partial^2\mathbf{v}}{\partial t^2} = c^2\nabla^2\mathbf{v} + \frac{\partial\mathbf{b}}{\partial t} - \frac{c^2}{\rho_s}\nabla q. \tag{2.17}$$

If the displacement field $\mathbf{u}_f$ of the fluid is introduced,

$$\mathbf{v} = \frac{\partial\mathbf{u}_f}{\partial t},$$

we can integrate Eq. (2.17) with respect to time, (disregarding the initial state for $\mathbf{u}_f$ and $\mathbf{b}$ and the convective term as before), obtaining

$$\frac{\partial^2\mathbf{u}_f}{\partial t^2} = c^2\nabla^2\mathbf{u}_f + \mathbf{b} - \frac{c^2}{\rho_s}\nabla Q, \tag{2.18}$$

where

$$Q = \int_0^t q\, d\tau.$$

Hence the displacement field also satisfies the wave equation.

The assumption that the velocity field is irrotational implies that the displacement field also has this property, i.e.

$$\mathbf{u}_f = \nabla\psi, \tag{2.19}$$

where ψ is a potential function to be introduced. Let us further introduce the potential associated with the body forces

$$\mathbf{b} = \nabla\phi. \tag{2.20}$$

Eq. (2.18) yields

$$\nabla\left[\frac{\partial^2\psi}{\partial t^2} - c^2\nabla^2\psi - \phi + \frac{c^2}{\rho_s} Q\right] = 0$$

and therefore the function inside the brackets is independent of position and depends on time only. Because we can add an extra function of time to ψ without changing the displacement field $\mathbf{u}_f$, we have with no loss of generality

$$\frac{\partial^2\psi}{\partial t^2} = c^2\nabla^2\psi + \phi - \frac{c^2}{\rho_s} Q. \tag{2.21}$$

Summing up the alternative formulations obtained in this subsection we have

$$\frac{\partial^2\rho}{\partial t^2} = c^2\nabla^2\rho - \rho_s\nabla\cdot\mathbf{b} + \frac{\partial q}{\partial t}, \tag{2.22a}$$

$$\frac{\partial^2 p}{\partial t^2} = c^2\nabla^2 p - c^2\rho_s\nabla\cdot\mathbf{b} + c^2\frac{\partial q}{\partial t}, \tag{2.22b}$$

$$\frac{\partial^2\mathbf{v}}{\partial t^2} = c^2\nabla^2\mathbf{v} + \frac{\partial\mathbf{b}}{\partial t} - \frac{c^2}{\rho_s}\nabla q, \tag{2.22c}$$

$$\frac{\partial^2\mathbf{u}_f}{\partial t^2} = c^2\nabla^2\mathbf{u}_f + \mathbf{b} - \frac{c^2}{\rho_s}\nabla Q, \tag{2.22d}$$

$$\frac{\partial^2 \psi}{\partial t^2} = c^2 \nabla^2 \psi + \phi - \frac{c^2}{\rho_s} Q. \qquad (2.22e)$$

In the derivation of these equations, we introduced **b** as the source of influence inside the fluid. Later, we assumed the existence of a potential ϕ to the body forces. The relation $b = \nabla\phi$ might be introduced into Eq. (2.22b), which would then change to

$$\frac{\partial^2 p}{\partial t^2} = c^2 \nabla^2 (p - \rho_s \phi) + c^2 \frac{\partial q}{\partial t}, \qquad (2.23)$$

where $\rho_s \phi$ can be interpreted as a prescribed pressure quantity applied inside the fluid domain.

2.2.2 Nonlinear fluid

Up to now we have regarded the fluid as a linear continuum. There has been a linear relationship between internal stresses and displacements or, by using the nomenclature of Subsection 2.2.1

$$p = c^2 \rho.$$

Under some circumstances, this linear relationship does not adequately describe what is actually happening in the fluid. When an elastic wave that propagates through a fluid reaches a structure boundary it will reflect. Depending on the density of the fluid, the mass and the stiffness of the structure boundary, the reflection factor may take any value between -1 and +1. If the fluid is comparatively incompressible (in some sense) and the structure is pliable, say a steel construction in water, the reflection factor is likely to be negative. The result is that the incident wave carrying a high positive pressure will give rise to a reflected wave with high negative pressure. As long as the magnitude of the negative pressure is well above the hydrostatic pressure, this is acceptable, but when the absolute pressure drops below zero this is not acceptable.

Observations indicate that when the absolute pressure drops below zero (possibly depending not only on the magnitude of the pressure but also on the rate of pressure drop) a field of micro-bubbles called cavities is formed (see Cole [7], and Plesset [35]). This formation of micro-bubbles is not discrete but allows a continuum treatment of the phenomenon. A zone containing cavities has only limited ability to withstand negative absolute pressure, but the exact physical behaviour of cavity formation is not yet fully understood.

In the following derivation of a cavitating fluid model, we proceed from Eqs. (2.11) and (2.12)

$$\frac{\partial \rho}{\partial t} + \rho_s \nabla \cdot \mathbf{v} = q, \tag{2.24}$$

$$\rho_s \frac{\partial \mathbf{v}}{\partial t} + \nabla \hat{p} = \rho_s \mathbf{b}. \tag{2.25}$$

By differentiating Eq. (2.24) with respect to time and eliminating the velocity field we have

$$\frac{\partial^2 \rho}{\partial t^2} - \nabla^2 \hat{p} = -\rho_s \nabla \cdot \mathbf{b} + \frac{\partial q}{\partial t}. \tag{2.26}$$

A constitutive equation linking density and pressure might be written as

$$\hat{p} = p_s + p = p_s + \sigma(\rho, \frac{\partial \rho}{\partial t}), \tag{2.27}$$

where p_s is the reference pressure, p the ambient value of the pressure and σ is a suitable, nonlinear function of ρ and $\partial\rho/\partial t$. Because we might assume that $\nabla^2 p_s = 0$, we have

$$\frac{\partial^2 \rho}{\partial t^2} - \nabla^2 p = -\rho_s \nabla \cdot \mathbf{b} + \frac{\partial q}{\partial t}. \tag{2.28}$$

Experiment show that a fluid has some slight ability to withstand tensile forces (See Cole [7]), but there is no

agreement on the magnitude of the parameters that might be involved in σ.

Still, quite an elaborate constitutive law would be

$$p = \sigma(\rho, \frac{\partial \rho}{\partial t}) = \alpha(\rho)\rho + \beta(\rho)\frac{\partial \rho}{\partial t} \qquad (2.29)$$

which, in the numerical experiments presented in Chapter 5, is simplified to

$$\beta(\rho) \equiv 0, \qquad (2.30)$$

$$\alpha(\rho) = c^2 \qquad \text{when } \rho \geq -p_s/c^2, \qquad (2.31a)$$

$$\alpha(\rho) = -p_s/\rho \qquad \text{when } \rho \leq -p_s/c^2, \qquad (2.31b)$$

although nothing in this formulation excludes more elaborate forms of constitutive equations. In fact, in the formulation we use σ without specifying its content. The consequence of Eqs.(2.30-31) is that, as long as the absolute pressure is above zero, there is a linear relation between the ambient value of density and pressure and that, when the ambient pressure drops to $-p_s$, this value is maintained during expansion.

Eq. (2.28) together with the constitutive law in Eq. (2.29) constitutes a nonlinear wave equation and is of course also valid for other problems with a nonlinear propagating velocity in addition to a cavitating fluid.

2.2.3 Boundary conditions

At the beginning of this chapter we listed some features our model should be able to take into consideration. These primarily concerned the fluid boundary. Later on in Section 2.2.1, more features were introduced in the fluid domain resulting in a simplified mathematical fluid model as compared to the basic equations stated in Eq. (2.9). In this subsection, the fluid boundary conditions listed in the introduction of this chapter are given a mathematical description. We divide the fluid boundary into four different parts according to their properties, namely

S_1 The wet surface, i.e., the fluid-structure interface.

S_2 A free surface with prescribed external pressure where we allow linearized waves (gravitational waves).

S_3 Fixed surface with prescribed external pressure.

S_4 An energy absorbing surface, i.e., a surface able to transmit the incident wave.

We assume that the fluid mass inflow $q \equiv 0$ in the neighbourhood of the boundary and we are thereby able to treat the fluid close to the boundary as a continuum. A consequence of the continuum hypothesis is that the displacement field at any time must be a continous mapping of the initial state. Boundary particles must therefore remain as boundary particles and interior particles remain as interior particles at all times.

For each part of the boundary we wish to express the boundary conditions in different primary variables according to the finite element formulation in mind. In Chapter 3, the pressure, the displacement and the displacement potential are used for finite element discretization.

We want to formulate boundary relations for the following quantities

$\frac{\partial \mathbf{v}}{\partial t} \cdot \mathbf{n}$ for the pressure and density formulation,

$(\nabla \cdot \mathbf{u}_f)$ for the displacement formulation,

$\nabla\psi \cdot \mathbf{n}$ for the displacement potential formulation,

where $\mathbf{n}$ is the outward normal to the fluid boundary.

S_1

S_1 is the most essential part of the fluid boundary in the sense of this work. The motion of the structure and the

normal component of the fluid motion coincide, that is

$$\mathbf{u}_f \cdot \mathbf{n} = u_{sf}. \tag{2.32}$$

Here, u_{sf} is the structural displacement component perpendicular to the fluid boundary. Changing to the displacement potential according to Eq. (2.19) we have

$$\nabla\psi \cdot \mathbf{n} = u_{sf}. \tag{2.33}$$

The second time derivative applied to Eq. (2.32) yields

$$\frac{\partial \mathbf{v}}{\partial t} \cdot \mathbf{n} = \frac{\partial^2 u_{sf}}{\partial t^2}. \tag{2.34}$$

By combining Eqs. (2.11) and (2.13), we have

$$\frac{\partial}{\partial t}\left(\frac{1}{c^2} p + \rho_s \nabla \cdot \mathbf{u}_f\right) = 0$$

if no fluid is added at the fluid-structure interface. Assuming the initial state to be at rest, we have

$$\rho_s c^2 \nabla \cdot \mathbf{u}_f = -p. \tag{2.35}$$

$\underline{S_2}$

The pressure at a point on the surface depends on the height of the wave created at the surface and on the external pressure p_e. We have

$$p = \rho_s g(\mathbf{u}_f \cdot \mathbf{n}) + p_e, \tag{2.36}$$

where $\mathbf{n}$ is a unit vector normal to the surface in the initial state, which is thus independent of time. $\rho_s g(\mathbf{u}_f \cdot \mathbf{n})$ is essentially the weight of the wave created at the surface and g is the acceleration due to gravity.

Differentiating twice with respect to time, we have

$$\rho_s\left(\frac{\partial \mathbf{v}}{\partial t}\cdot\mathbf{n}\right) = \frac{1}{g}\frac{\partial^2(p-p_e)}{\partial t^2}. \tag{2.37}$$

Eq. (2.12) states that

$$\rho_s \frac{\partial^2 \mathbf{u}_f}{\partial t^2} = -\nabla p,$$

if no body force is present. Therefore, by changing from displacement to displacement potential according to Eq. (2.19), we obtain

$$\nabla\left(\rho_s \frac{\partial^2 \psi}{\partial t^2} + p\right) = 0.$$

This relation is satisfied if

$$\rho_s \frac{\partial^2 \psi}{\partial t^2} + p = 0. \tag{2.38}$$

Substituting Eq. (2.36) into Eq. (2.38) yields

$$\rho_s \frac{\partial^2 \psi}{\partial t^2} + \rho_s g(\mathbf{u}_f\cdot\mathbf{n}) + p_e = 0$$

or

$$g\,\nabla\psi\cdot\mathbf{n} = -\frac{\partial^2 \psi}{\partial t^2} - \frac{p_e}{\rho_s}. \tag{2.39}$$

Finally combining Eqs. (2.36) and (2.35) we obtain

$$\rho_s c^2\,\nabla\cdot\mathbf{u}_f = -\rho_s g\,\mathbf{u}_f\cdot\mathbf{n} - p_e. \tag{2.40}$$

S_3

On the surface with no waves the displacement perpendicular to the surface is assumed to be zero, so

$$\mathbf{u}_f \cdot \mathbf{n} = 0 \tag{2.41}$$

or

$$\nabla\psi \cdot \mathbf{n} = 0. \tag{2.42}$$

The second time derivative of Eq. (2.41) yields

$$\frac{\partial \mathbf{v}}{\partial t} \cdot \mathbf{n} = 0. \tag{2.43}$$

Substituting the prescribed zero motion of Eq. (2.41) into Eq. (2.40) we have

$$\nabla \cdot \mathbf{u}_f = - \frac{p_e}{\rho_s c^2}. \tag{2.44}$$

Eqs. (2.42)-(2.44) give the desired expression to be used in the finite element formulation. At the S_2 boundary the external pressure p_e enters directly via the boundary condition, while in this case it does so only when the displacement is the primary variable. In the case of the pressure formulation the external pressure is taken into consideration as a prescribed value of the pressure along the S_3 boundary. Finally, in the case of the displacement potential formulation, Eq. (2.39) gives

$$\frac{\partial^2 \psi}{\partial t^2} = - \frac{p_e}{\rho_s} \tag{2.45}$$

because $\nabla\psi \cdot \mathbf{n} = 0$. That is, the external pressure enters the solution via a prescribed value of the acceleration of the displacement potential along the S_3 boundary.

S_4

In a discrete analysis, an infinite or semi-infinite domain must be truncated. This can be achieved in different ways, for instance by infinite element techniques or boundary integral methods. Infinite elements have been proposed by Bettess and Zienkiewicz [4], by Bettess [5] and also by Olson and Bathe [33]. The latter uses doubly asymptotic approximation (DAA), that is the infinite fluid is described as the sum of the plane wave approximation at high frequencies and the added mass approximation at low frequencies. The DAA method is also used in connection with bilinear fluid analysis by Felippa and DeRuntz [17] and by Wawa and DiMaggio [45] in connection with shock waves. DAA for fluid-structure interactions was originally developed by Geers [57]. One of the first to use boundary integral methods was Berkhoff [3]. Perhaps the most elegant way is that proposed by Smith [41]. If a wave reflects against a free boundary (i.e. of Neumann type), then the reflected wave will be of the opposite sign while if the boundary is fixed (i.e. of Dirichlet type) the reflected wave will have the same sign. For linearized problems Smith superposes these two cases and the reflected wave cancels out.

Another approach was proposed by Sommerfield [42]. This method is exact if the incident wave is perpendicular to the boundary. If the boundary is located at a large distance from structural members and from the sources of disturbances, it is quite accurate. The method is easily implemented. A derivation of the necessary expressions is given below.

Assume that the boundary consists of a series of dampers. The force developed in a damper is

$$C_d \frac{\partial \mathbf{u}_f}{\partial t} \cdot \mathbf{n},$$

where C_d is the unknown value of the damping constant and $(\partial \mathbf{u}_f/\partial t)\cdot\mathbf{n}$ is the velocity component perpendicular to the boundary. This term should equal the fluid pressure, thus

$$p + p_s = C_d \frac{\partial \mathbf{u}_f}{\partial t} \cdot \mathbf{n}. \tag{2.46}$$

Then

$$\frac{\partial p}{\partial t} = C_d \frac{\partial^2 \mathbf{u}_f}{\partial t^2} \cdot \mathbf{n} = C_d \, c^2 \nabla(\nabla \cdot \mathbf{u}_f) \cdot \mathbf{n}$$

where we have used the wave equation given by Eq. (2.22d) with $\mathbf{b} = 0$ and $\nabla Q = 0$. By the use of Eq. (2.35)

$$\frac{\partial p}{\partial t} = -C_d \frac{1}{\rho_s} \nabla p \cdot \mathbf{n}. \tag{2.47}$$

Far away from any disturbances, the wave propagates at the speed of sound c. Therefore

$$\frac{\partial p}{\partial t} = -c \nabla p \cdot \mathbf{n},$$

which is just the D'Alembert's solution to wave equation, so

$$C_d = \rho_s c, \tag{2.48}$$

which determines the value of the damping constant. Eq. (2.47) can thus be written

$$\nabla p \cdot \mathbf{n} = -\frac{1}{c} \frac{\partial p}{\partial t} \tag{2.49}$$

or according to Eq. (2.11)

$$\rho_s \frac{\partial \mathbf{v}}{\partial t} \cdot \mathbf{n} = \frac{1}{c} \frac{\partial p}{\partial t}. \tag{2.50}$$

The feature of the boundary condition as expressed in Eq. (2.49) is to transmit a right-angle incident wave. Because the unknown p is only a scalar quantity satisfying the wave equation in the interior of the domain, then, for any scalar quantity satisfying the wave equation, Eq. (2.49)

constitutes a transmitting boundary just by replacing the variable. The displacement potential should thus satisfy

$$\nabla\psi\cdot\mathbf{n} = -\frac{1}{c}\frac{\partial\psi}{\partial t}. \tag{2.51}$$

Finally, differentiating Eq. (2.51) with respect to time and applying Eq. (2.22e), we have

$$\frac{\partial}{\partial t}(\nabla\psi)\cdot\mathbf{n} = -\frac{1}{c}\frac{\partial^2\psi}{\partial t^2} = -\frac{1}{c}c^2\nabla^2\psi.$$

Replacing $\nabla\psi$ by u_f yields

$$\frac{\partial \mathbf{u}_f}{\partial t}\cdot\mathbf{n} = -c\ \nabla\cdot\mathbf{u}_f$$

or

$$\nabla\cdot\mathbf{u}_f = -\frac{1}{c}\frac{\partial \mathbf{u}_f}{\partial t}\cdot\mathbf{n}. \tag{2.52}$$

Boundary	Formulation		
	p	ψ	$\mathbf{u}_f$
S_1	$\frac{\partial \mathbf{v}}{\partial t} \cdot \mathbf{n} = \frac{\partial^2 u_{sf}}{\partial t^2}$	$\nabla\psi \cdot \mathbf{n} = u_{sf}$	$\rho_s c^2 \nabla \cdot \mathbf{u}_f = -p$
S_2	$g\rho_s \frac{\partial \mathbf{v}}{\partial t} \cdot \mathbf{n} = = \frac{\partial^2 (p - p_e)}{\partial t^2}$	$g\nabla\psi \cdot \mathbf{n} = = -\frac{\partial^2 \psi}{\partial t^2} - \frac{p_e}{\rho_s}$	$\rho_s c^2 \nabla \cdot \mathbf{u}_f = = -\rho_s g \mathbf{u}_f \cdot \mathbf{n} - p_e$
S_3	$\frac{\partial \mathbf{v}}{\partial t} \cdot \mathbf{n} = 0$ prescribed $p = p_e$	$\nabla\psi \cdot \mathbf{n} = 0$ prescribed $\frac{\partial^2 \psi}{\partial t^2} = -\frac{p_e}{\rho_s}$	$\rho_s c^2 \nabla \cdot \mathbf{u}_f = -p_e$
S_4	$\rho_s \frac{\partial \mathbf{v}}{\partial t} \cdot \mathbf{n} = = -\frac{1}{c}\frac{\partial p}{\partial t}$	$\nabla\psi \cdot \mathbf{n} = = -\frac{1}{c}\frac{\partial \psi}{\partial t}$	$\nabla \cdot \mathbf{u}_f = -\frac{1}{c}\frac{\partial \mathbf{u}_f}{\partial t} \cdot \mathbf{n}$

Table 2.1. Required boundary quantities using different fluid formulations

3. FINITE ELEMENT MODELLING

This chapter contains the discretization of the equations derived in the previous chapter using the finite element method. In the fluid domain, we derive finite element formulations using pressure, displacement potential and displacement as independent variables. Reformulation is carried out using the weak formulation and Galerkin's method of choosing the test functions, but first some notes concerning structural discretization.

3.1 Structure

As stated in Section 2.1, the structural behaviour is governed by

$$L(\mathbf{u}_s) = \mathbf{F}_s(\mathbf{r},t) \tag{3.1}$$

with the boundary condition

$$\mathbf{F}_f(\mathbf{r},t) = p(\mathbf{r},t)\cdot\mathbf{n}$$

due to the distributed pressure load along the fluid boundary.

A discretized formulation for the structure yields, in matrix notation

$$M_s\ddot{U}_s + C_s\dot{U}_s + K_sU_s = L_s^e + L_f, \tag{3.2}$$

where M_s, C_s and K_s are the structural mass matrix, damping matrix and stiffness matrix, respectively. L_s^e is the load vector due to the external structural loads and L_f is the load vector due to the coupling effects.

As mentioned above, the test functions and the trial functions are taken from the same set of functions. This set may differ from the one to be used in the fluid domain. The functions in the set to be used in the structural domain are designated by a subscript 's' i.e., $\mathbf{N}_s$ and the

function set by $\{\mathbf{N}_s\}$. The coupling vector, L_f, between the structural and fluid domains is thus

$$L_f = \int_{S_1} \mathbf{N}_s \cdot \mathbf{n}\, p\, dS. \tag{3.3}$$

Using previously derived relations between pressure and displacement, we have, according to Eq. (2.35)

$$L_f = -\int_{S_1} \mathbf{N}_s \cdot \mathbf{n}\, c^2 \rho_s (\nabla \cdot \mathbf{u}_f) dS, \tag{3.4}$$

when a displacement formulation is used for the fluid. Using Eqs. (2.35) and (2.22e) the relation between pressure and displacement potential implies

$$L_f = -\int_{S_1} \mathbf{N}_s \cdot \mathbf{n}\, \rho_s \frac{\partial^2 \psi}{\partial t^2}\, dS + \int_{S_1} \mathbf{N}_s \cdot \mathbf{n}\, \rho_s \phi\, dS \tag{3.5}$$

in case of a displacement potential formulation for the fluid. This concludes the finite element formulation of the structure.

3.2 Linear fluid

3.2.1 Pressure formulation

The wave equation using the pressure as independent variable, Eq. (2.22b), is

$$\frac{\partial^2 p}{\partial t^2} = c^2 \nabla^2 p + c^2 \frac{\partial q}{\partial t} - c^2 \rho_s \nabla \cdot \mathbf{b}. \tag{3.6}$$

Multiplication by a test function $w = w(x,y,z)$ yields

$$w \frac{\partial^2 p}{\partial t^2} - c^2 w \nabla^2 p = c^2 w \frac{\partial q}{\partial t} - c^2 \rho_s w \nabla \cdot \mathbf{b}$$

and integration over the total fluid domain V gives

$$\int_V w \frac{\partial^2 p}{\partial t^2}\, dV - c^2 \int_V w\nabla^2 p\, dV = c^2 \int_V w \frac{\partial q}{\partial t}\, dV - c^2 \rho_s \int_V w\nabla\cdot\mathbf{b}\, dV. \tag{3.7}$$

Using Green's first formula, the second integral becomes

$$\int_V w\nabla^2 p\, dV = \int_S w(\nabla p)\cdot\mathbf{n}\, dS - \int_V (\nabla w)\cdot(\nabla p) dV,$$

where S is the boundary of V and $\mathbf{n}$ is the outward normal of S. Hence

$$\int_V w \frac{\partial^2 p}{\partial t^2}\, dV + c^2 \int_V (\nabla w)\cdot(\nabla p) dV = c^2 \int_S w\nabla p\cdot\mathbf{n}\, dS +$$

$$+ c^2 \int_V w \frac{\partial q}{\partial t}\, dV - c^2 \rho_s \int_V w\nabla\cdot\mathbf{b}\, dV. \tag{3.8}$$

According to Eq. (2.12)

$$\nabla p = -\rho_s \frac{\partial \mathbf{v}}{\partial t} + \rho_s \mathbf{b}.$$

Note that $\nabla\hat{p} = \nabla p$. Now, study the following part of Eq. (3.8)

$$c^2 \int_S w\, \nabla p\cdot\mathbf{n}\, dS - c^2 \rho_s \int_V w\nabla\cdot\mathbf{b}\, dV =$$

$$= -c^2 \rho_s \int_S w \frac{\partial \mathbf{v}}{\partial t}\cdot\mathbf{n}\, dS + c^2 \rho_s \int_S w\mathbf{b}\cdot\mathbf{n}\, dS -$$

$$-c^2 \rho_s \int_V w\nabla\cdot\mathbf{b}\, dV =$$

$$= -c^2 \rho_s \int_S w \frac{\partial \mathbf{v}}{\partial t}\cdot\mathbf{n}\, dS + c^2 \rho_s \int_V \nabla w\cdot\mathbf{b}\, dV.$$

We split the surface integral in Eq. (3.8) into four parts according to the boundary in Table 2.1. Hence

$$c^2\rho_s \int_{S_1} w \frac{\partial \mathbf{v}}{\partial t} \cdot \mathbf{n}\, dS = c^2\rho_s \int_{S_1} w \frac{\partial^2 u_{sf}}{\partial t^2}\, dS, \tag{3.9a}$$

$$c^2\rho_s \int_{S_2} w \frac{\partial \mathbf{v}}{\partial t} \cdot \mathbf{n}\, dS = \frac{c^2}{g} \int_{S_2} w \frac{\partial^2 (p-p_e)}{\partial t^2}\, dS, \tag{3.9b}$$

$$c^2\rho_s \int_{S_3} w \frac{\partial \mathbf{v}}{\partial t} \cdot \mathbf{n}\, dS = 0, \tag{3.9c}$$

$$c^2\rho_s \int_{S_4} w \frac{\partial \mathbf{v}}{\partial t} \cdot \mathbf{n}\, dS = c \int_{S_4} \frac{\partial p}{\partial t}\, dS. \tag{3.9d}$$

Finally Eq. (3.8) becomes

$$\int_V w \frac{\partial^2 p}{\partial t^2}\, dV + c^2 \int_V (\nabla w)\cdot(\nabla p) dV = -c^2\rho_s \int_{S_1} w \frac{\partial^2 u_{sf}}{\partial t^2}\, dS +$$

$$+ \frac{c^2}{g} \int_{S_2} w \frac{\partial^2 (p-p_e)}{\partial t^2}\, dS - c \int_{S_4} w \frac{\partial p}{\partial t}\, dS + c^2 \int_V w \frac{\partial q}{\partial t}\, dV -$$

$$+ c^2\rho_s \int_V (\nabla w)\cdot\mathbf{b}. \tag{3.10}$$

In the absence of body force and external applied pressure (p_e) this reduces to

$$\int_V w \frac{\partial^2 p}{\partial t^2} dV + c^2 \int_V (\nabla w)\cdot(\nabla p) dV = -c^2 \rho_s \int_{S_1} w \frac{\partial^2 u_{sf}}{\partial t^2} dS -$$

$$- \frac{c^2}{g} \int_{S_2} w \frac{\partial^2 p}{\partial t^2} dS - c \int_{S_4} w \frac{\partial p}{\partial t} dS + c^2 \int_V w \frac{\partial q}{\partial t} dV. \quad (3.11)$$

Discretization of Eq. (3.11) is carried out by expanding the pressure p in terms of finite element basis functions or shape functions, each one associated with a unique nodal point. The shape functions in the fluid domain are designated by a subscript 'f', i.e. N_f, and the function set by $\{N_f\}$.

The expression for the pressure p then takes the form

$$p(\mathbf{r},t) = \sum_j N_f^j(\mathbf{r})\ P_j(t), \quad (3.12)$$

where summation is over the number of shape functions and $P_j(t)$ is the value of the pressure at the associated nodal point at time t. Clearly we have

$$\frac{\partial^2 p(\mathbf{r},t)}{\partial t^2} = \sum_j N_f^j(\mathbf{r}) \cdot \frac{d^2 P_j(t)}{dt^2} . \quad (3.13)$$

Using the standard Galerkin formulation with

$$w \in \{N_f\},$$

the discretized form of Eq. (3.10) is

$$M_f \ddot{P} + C_f \dot{P} + K_f P = -L_s + L_q + L_b + L_e, \quad (3.14)$$

where

P = column matrix for the unknown nodal values of the pressure,

$$(M_f)_{ij} = \int_V N_f^i \, N_f^j \, dV + \frac{c^2}{g} \int_{S_2} N_f^i \, N_f^j \, dS,$$

$$(C_f)_{ij} = c \int_{S_4} N_f^i \, N_f^j \, dS,$$

$$(K_f)_{ij} = c^2 \int_V (\nabla N_f^i) \cdot (\nabla N_f^j) dV,$$

$$(L_s)_i = c^2 \rho_s \int_{S_1} N_f^i \, \ddot{u}_{sf} \, dS,$$

$$(L_q)_i = c^2 \int_V N_f^i \, \frac{\partial q}{\partial t} \, dV,$$

$$(L_b)_i = c^2 \rho_s \int_V (\nabla N_f^i) \cdot \mathbf{b} \, dV,$$

$$(L_e)_i = \frac{c^2}{g} \int_{S_1} N_f^i \, \frac{\partial^2 p_e}{\partial t^2} \, dS$$

(i = row index, j = column index).

The matrix denoted L_s couples the fluid domain with the structural domain and is dealt with in Section 3.3. This concludes the finite element formulation using pressure as independent variable.

3.2.2 Displacement potential formulation

The procedure in this subsection is very much the same as that in the previous subsection. The wave equation using displacement potential as the primary variable reads

$$\frac{\partial^2\psi}{\partial t^2} = c^2\nabla^2\psi + \phi - \frac{c^2}{\rho_s} Q. \tag{3.15}$$

Multiplying by a test function $w = w(x,y,z)$ and integrating over the fluid domain,

$$\int_V w \frac{\partial^2\psi}{\partial t^2}\, dV = \int_V wc^2\nabla^2\psi\, dV + \int_V w\phi\, dV - \frac{c^2}{\rho_s}\int_V wQ\, dV. \tag{3.16}$$

Using Green's first formula on the right-hand side and rearranging terms,

$$\int_V w \frac{\partial^2\psi}{\partial t^2}\, dV + c^2 \int_V (\nabla w)\cdot(\nabla\psi) dV = c^2 \int_S w(\nabla\psi)\cdot\mathbf{n}\, dS +$$

$$+ \int_V w\phi\, dV - \frac{c^2}{\rho_s}\int_V wQ\, dV. \tag{3.17}$$

The first term on the right-hand side is rewritten using the boundary conditions in Table 2.1. Hence

$$\int_{S_1} w(\nabla\psi)\cdot\mathbf{n}\, dS = \int_{S_1} wu_{sf}\, dS,$$

$$\int_{S_2} w(\nabla\psi)\cdot\mathbf{n}\, dS = -\frac{1}{g}\int_{S_2} w\frac{\partial^2\psi}{\partial t^2} - \frac{1}{g\rho_s}\int_{S_2} wp_e\, dS,$$

$$\int_{S_3} w(\nabla\psi)\cdot\mathbf{n}\, dS = 0,$$

$$\int_{S_4} w(\nabla\psi)\cdot\mathbf{n}\, dS = -\frac{1}{c}\int_{S_4} w\frac{\partial\psi}{\partial t}.$$

Eq. (3.17) then reads

$$\int_V w \frac{\partial^2 \psi}{\partial t^2} dV + c^2 \int_V (\nabla w)\cdot(\nabla \psi) dV = c^2 \int_{S_1} w u_{sf} \, dS +$$

$$+ \int_V w(\phi - \frac{c^2}{\rho_s} Q) dV + \frac{c^2}{g} \int_{S_2} w(- \frac{\partial^2 \psi}{\partial t^2} - \frac{p_e}{\rho_s}) dS -$$

$$- c \int_{S_4} w \frac{\partial \psi}{\partial t} \, dS. \qquad (3.18)$$

In the abscence of body forces and external pressure we have

$$\int_V w \frac{\partial^2 \psi}{\partial t^2} dV + c^2 \int_V (\nabla w)\cdot(\nabla \psi) dV = c^2 \int_{S_1} w u_{sf} \, dS -$$

$$- \frac{c^2}{\rho_s} \int_V wQ \, dV - \frac{c^2}{g} \int_{S_2} w \frac{\partial^2 \psi}{\partial t^2} dS - c \int_{S_4} w \frac{\partial \psi}{\partial t}. \qquad (3.19)$$

Expanding ψ in terms of a set of shape functions N_f (we use the same notation for the shape functions as in the previous subsection) yields

$$\psi(\mathbf{r},t) = \sum_j N_f^j(\mathbf{r})\cdot\Psi_j(t),$$

where summation is over the number of shape functions and Ψ_j holds the value of ψ at the j:th node associated with N_f^j.

Choosing w according to the Galerkin method with

$$w \in \{N_f\},$$

the discretized form of Eq. (3.18) is

$$M_f\ddot{\Psi} + C_f\dot{\Psi} + K_f\Psi = L_s + L_b - L_q - L_e, \qquad (3.20)$$

where

Ψ = column matrix for the unknown nodal values of the displacement potential,

$$(M_f)_{ij} = \int_V N_f^i N_f^j \, dV + \frac{c^2}{g} \int_{S_2} N_f^i N_f^j \, dS,$$

$$(C_f)_{ij} = c \int_{S_4} N_f^i N_f^j \, dS,$$

$$(K_f)_{ij} = c^2 \int_V (\nabla N_f^i)\cdot(\nabla N_f^j) dV,$$

$$(L_s)_i = c^2 \int_{S_1} N_f^i \, u_{sf} \, dS,$$

$$(L_b)_i = \int_V N_f^i \, \phi \, dV,$$

$$(L_q)_i = \frac{c^2}{\rho_s} \int_V N_f^i \, Q \, dV,$$

$$(L_e)_i = \frac{c^2}{g\rho_s} \int_{S_2} N_f^i \, p_e \, dS$$

(i = row index, j = column index).

(The same notation is used as in the previous section, when the matrix represents the same mathematical phenomenon).

3.2.3 Displacement formulation

The major difference between this subsection and the two previous ones is that the independent variable is no longer a scalar quantity but a vector field.

Eq (2.22d) shows that each displacement component satisfies the wave equation

$$\frac{\partial^2 \mathbf{u}_f}{\partial t^2} = c^2 \nabla^2 \mathbf{u}_f + \mathbf{b} - \frac{c^2}{\rho_s} \nabla Q. \tag{3.21}$$

A straightforward Galerkin approach applied to each component yields for the x-component in a Euclidean space

$$\int_V w \frac{\partial^2 u_{xf}}{\partial t^2} \, dV = c^2 \int_V w \nabla^2 u_{xf} \, dV + \int_V w(b_x - \frac{c^2}{\rho_s} \frac{\partial Q}{\partial x}) dV. \tag{3.22}$$

Green's formula applied to the second term gives

$$\int_V w \nabla^2 u_{xf} dV = -\int_V (\nabla w) \cdot (\nabla u_{xf}) dV + \int_S w(\nabla u_{xf}) \cdot \mathbf{n} \, dS. \tag{3.23}$$

The drawback in this process is now evident. We are not able to make any statements about the surface integral in Eq. (3.23).

The derivation of Eq. (3.21) used the following formula

$$\nabla(\nabla \cdot \mathbf{u}_f) = \nabla^2 \mathbf{u}_f + \nabla \times (\nabla \times \mathbf{u}_f) \tag{3.24}$$

or rather its equivalence for the velocity field. Because the displacement field is irrotational the last term vanishes. Eq. (3.21) thus originates from

$$\frac{\partial^2 \mathbf{u}_f}{\partial t^2} = c^2 \nabla(\nabla \cdot \mathbf{u}_f) + \mathbf{b} - \frac{c^2}{\rho_s} \nabla Q. \tag{3.25}$$

The drawback now is that there is no guarantee of an irrotational displacement field because this condition is not imposed on Eq. (3.25). A weak form of Eq. (3.25) using Green's formula will by necessity couple the different components contrary to our wish. The remedy is to replace $\nabla^2 \mathbf{u}_f$ in Eq. (3.21) using the formula (3.24), thereby creating a rotational stiffness in order to prevent a rotational displacement field. Thus

$$\frac{\partial^2 \mathbf{u}_f}{\partial t^2} = c^2 \nabla(\nabla \cdot \mathbf{u}_f) - c^2 \kappa \, \nabla \times (\nabla \times \mathbf{u}_f) + \mathbf{b} - \frac{c^2}{\rho_s} \nabla Q, \qquad (3.26)$$

where κ allows control of the degree of rotational stiffness. The weak formulation yields

$$\int_V \mathbf{w} \cdot \frac{\partial^2 \mathbf{u}_f}{\partial t^2} \, dV = c^2 \int_V \mathbf{w} \cdot \nabla(\nabla \cdot \mathbf{u}_f) dV - \kappa c^2 \int_V \mathbf{w} \cdot \nabla \times (\nabla \times \mathbf{u}_f)) dV +$$

$$+ \int_V \mathbf{w} \cdot (\mathbf{b} - \frac{c^2}{\rho_s} \nabla Q), \qquad (3.27)$$

where

$$\mathbf{w} = (w_x, w_y, w_z).$$

Using the following derivative formulae

$$\nabla \cdot (\mathbf{w}(\nabla \cdot \mathbf{u}_f)) = (\nabla \cdot \mathbf{w})(\nabla \cdot \mathbf{u}_f) + \mathbf{w} \cdot (\nabla(\nabla \cdot \mathbf{u}_f)),$$

$$\nabla((\nabla \times \mathbf{u}_f) \times \mathbf{w}) = \mathbf{w} \cdot (\nabla \times (\nabla \times \mathbf{u}_f)) - (\nabla \times \mathbf{w}) \cdot (\nabla \times \mathbf{u}_f),$$

we obtain

$$\int_V \mathbf{w} \cdot (\nabla(\nabla \cdot \mathbf{u}_f)) dV = -\int_V (\nabla \cdot \mathbf{w})(\nabla \cdot \mathbf{u}_f) dV + \int_S \mathbf{w}(\nabla \cdot \mathbf{u}_f) \cdot \mathbf{n} \, dS \qquad (3.28)$$

and

$$\int_V \mathbf{w}\cdot(\nabla\times(\nabla\times\mathbf{u}_f))dV = \int_V (\nabla\times\mathbf{w})\cdot(\nabla\times\mathbf{u}_f)dV + \int_S ((\nabla\times\mathbf{u}_f)\times\mathbf{w})\cdot\mathbf{n}\ dS. \tag{3.29}$$

The surface integral in Eq. (3.28) can be reformulated using the boundary conditions in Table 2.1. We have

$$c^2 \int_{S_1} \mathbf{w}(\nabla\cdot\mathbf{u}_f)\cdot\mathbf{n}\ dS = -\frac{1}{\rho_s}\int_{S_1} \mathbf{w}p\cdot\mathbf{n}\ dS,$$

$$c^2 \int_{S_2} \mathbf{w}(\nabla\cdot\mathbf{u}_f)\cdot\mathbf{n}\ dS = -g\int_{S_2} \mathbf{w}(\mathbf{u}_f\cdot\mathbf{n})\cdot\mathbf{n}\ dS -$$

$$-\frac{1}{\rho_s}\int_{S_2} \mathbf{w}p_e\cdot\mathbf{n}\ dS,$$

$$c^2 \int_{S_3} \mathbf{w}(\nabla\cdot\mathbf{u}_f)\cdot\mathbf{n}\ dS = -\frac{1}{\rho_s}\int_{S_3} \mathbf{w}p_e\cdot\mathbf{n}\ dS,$$

$$c^2 \int_{S_4} \mathbf{w}(\nabla\cdot\mathbf{u}_f)\cdot\mathbf{n}\ dS = -c\int_{S_4} \mathbf{w}\left[\frac{\partial\mathbf{u}_f}{\partial t}\cdot\mathbf{n}\right]\cdot\mathbf{n}\ dS.$$

The surface integral in formula (3.29) vanishes naturally at the boundary. This is based on the fact that fluid particles at the boundary remains there at all times. See further the discussion at the beginning of Subsection 2.2.3. Therefore, $\nabla\times\mathbf{u}_f$ must be parallel to $\mathbf{n}$ and $(\nabla\times\mathbf{u}_f)\times\mathbf{w}$ is perpendicular to $\mathbf{n}$ for any $\mathbf{w}$. The discretization of Eq. (3.27) is carried out by expanding $\mathbf{u}_f(\mathbf{r},t)$ in terms of shape functions, the same for all components

$$\mathbf{u}_f = \sum_j N_f^j(\mathbf{r})\mathbf{u}_f^j(t), \tag{3.30}$$

where

$$\mathbf{u}_f^j(t) = (u_{xf},\ u_{yf},\ u_{zf})_j$$

is the value of $\mathbf{u}_f$ at the j:th nodal point which is associated with the shape function N_f^j.

Eq. (3.30) is equivalent to

$$\mathbf{u}_f = \begin{bmatrix} N_f^1 & 0 & 0 & N_f^2 & 0 & \dots \\ 0 & N_f^1 & 0 & 0 & N_f^2 & \dots \\ 0 & 0 & N_f^1 & 0 & 0 & \dots \end{bmatrix} U_f = \begin{bmatrix} N_f \end{bmatrix} U_f,$$

where U_f is a column matrix for the unknown nodal values of $\mathbf{u}_f$. (Dimension (U_f) = 3 times the number of nodal points).

Using the same test functions as shape functions, a typical set of three test functions is

$$\begin{bmatrix} N_f^i & 0 & 0 \\ 0 & N_f^i & 0 \\ 0 & 0 & N_f^i \end{bmatrix}.$$

In Eq.(3.24) we used $\nabla\times\mathbf{u}_f$ for the curl of $\mathbf{u}_f$. At this stage it is better to use the matrix formulation of the curl

$$\nabla\times\mathbf{u}_f = \tilde{\nabla}\mathbf{u}_f,$$

where

$$\tilde{\nabla} = \begin{bmatrix} 0 & -\frac{\partial}{\partial z} & \frac{\partial}{\partial y} \\ \frac{\partial}{\partial z} & 0 & -\frac{\partial}{\partial x} \\ -\frac{\partial}{\partial y} & \frac{\partial}{\partial x} & 0 \end{bmatrix}$$

and where $\mathbf{u}_f$ on the right-hand side is a column vector. Finally, introducing the notation $[\tilde{N}_f]$ for the matrix multiplication $[n_x\ n_y\ n_z][N_f]$, the discretized form of Eq. (3.27), using Eqs. (3.28) and (3.29), is

$$M_f\ddot{U}_f + C_f\dot{U}_f + K_fU_f = L_b - L_q - L_s + L_e, \tag{3.31}$$

where

$$M_f = \rho_s \int_V [N_f]^T [N_f] dV,$$

$$C_f = c\rho_s \int_{S_4} [\tilde{N}_f]^T [\tilde{N}_f] dS,$$

$$K_f = c^2\rho_s \int_V (\nabla[N_f])^T (\nabla[N_f]) dV +$$

$$+ \kappa c^2 \rho_s \int_V (\tilde{\nabla}[N_f])^T (\tilde{\nabla}[N_f])\ dV - g\rho_s \int_{S_2} [\tilde{N}_f]^T [\tilde{N}_f] dS,$$

$$L_b = \rho_s \int_V [N_f]^T \mathbf{b}\ dV,$$

$$L_q = c^2 \int_V [N_f]^T \nabla Q\ dV,$$

$$L_s = \int_{S_1} [\tilde{N}_f]^T\ p\ dS,$$

$$L_e = \int_{S_2+S_3} [\tilde{N}_f]^T p_e.$$

3.3 Fluid-structure interaction

In Sections 3.1 and 3.2 the finite element discretizations lead to a system of matrices for each domain and the link between these domains appears as the coupling terms L_f and L_s on the right-hand side. When using a time-stepping algorithm for transient analysis of the coupled system or solving for harmonic excitation, it may be possible to iterate between the systems (apart from the iteration needed within each system in transient analysis) until the residual coupling vectors are sufficiently small. In this section, however, the aim is to assemble the systems, so there is no need for separate coupling iterations between the systems.

For the sake of brevity, we use the same matrix notation for the same mathematical phenomena, although the content depends on the independent variable.

3.3.1 Pressure formulation

The two sets of equations given in Eqs. (3.2) and (3.14) are

$$M_s \ddot{U}_s + C_s \dot{U}_s + K_s U_s = L_s^e + L_f \tag{3.32}$$

for the solid region and

$$M_f \ddot{P} + C_f \dot{P} + K_f P = -L_s + L_q + L_b + L_e \tag{3.33}$$

for the fluid region. Here, L_f is a function of fluid pressure and L_s is a function of structural displacement and thus carry the interaction features of the model. All other vectors on the right-hand side are true load vectors.

The definitions of L_s and L_f read

$$(L_s)_i = c^2 \rho_s \int_{S_1} N_f^i \, \ddot{u}_{sf} \, dS$$

and

$$(L_f)_i = \int_{S_1} \mathbf{N}_s^i \cdot \mathbf{n}\ p\ dS$$

Because

$$u_{sf} = \mathbf{u}_s \cdot \mathbf{n} = \sum_j \mathbf{N}_s^j \cdot \mathbf{n}\ U_s^j,$$

where the nodal index j runs through the set of structural trial functions, we have

$$L_s = M_c\ \ddot{U}_s, \tag{3.34}$$

where

$$(M_c)_{ij} = c^2\ \rho_s \int_{S_2} N_f^i\ \mathbf{N}_s^j \cdot \mathbf{n}\ dS.$$

In the same way we have

$$p = \sum_j N_f^j\ P_j$$

and thus

$$L_f = K_c\ P, \tag{3.35}$$

where

$$(K_c)_{ij} = \int_{S_1} \mathbf{N}_s^i \cdot \mathbf{n}\ N_f^j\ dS.$$

As pointed out above, we need only consider those structural degrees of freedom that are involved in displacements perpendicular to the fluid boundary. The same is true for the fluid degrees of freedom, i.e., we need only consider pressure nodes along structural members that are linked to the structure.

The assembled system of equations is

$$\begin{bmatrix} M_s & 0 \\ M_c & M_f \end{bmatrix} \ddot{X} + \begin{bmatrix} C_s & 0 \\ 0 & C_f \end{bmatrix} \dot{X} + \begin{bmatrix} K_s & -K_c \\ 0 & K_f \end{bmatrix} X = \begin{bmatrix} L_s^e \\ L_q + L_b + L_e \end{bmatrix} \quad (3.36)$$

where

$$X = \begin{bmatrix} U_s \\ P \end{bmatrix}$$

It is obvious that $M_c = c^2 \rho_s K_c^T$ and that most elements in these matrices are zero.

3.3.2 Displacement potential formulation

Eq. (3.2) describing the structural behaviour still holds,

$$M_s \ddot{U}_s + C_s \dot{U}_s + K_s U_s = L_s^e + L_f,$$

although we have another definition of the coupling vector

$$(L_f)_i = -\int_{S_1} \mathbf{N}_s^i \cdot \mathbf{n}\, \ddot{\psi}\, dS + \int_{S_1} \mathbf{N}_s^i \cdot \mathbf{n}\, \rho_s \ddot{\phi}\, dS.$$

In the fluid domain we have

$$M_f \ddot{\Psi} + C_f \dot{\Psi} + K_f \Psi = L_s + L_b - L_q - L_e, \quad (3.37)$$

where

$$(L_s)_i = c^2 \int_{S_1} N_f^i u_{sf}\, dS.$$

Because

$$u_{sf} = \mathbf{u}_s \cdot \mathbf{n} = \sum_j \mathbf{N}_s^j \cdot \mathbf{n}\, U_s^j$$

and

$$\psi = \sum_j N_f^j \Psi_j$$

we have

$$L_s = K_c U_s, \tag{3.38}$$

where

$$(K_c)_{ij} = c^2 \int_{S_1} N_f^i \, \mathbf{N}_s^j \cdot \mathbf{n} \, dS.$$

Further, for the solid equations

$$L_f = -M_c \ddot{\psi} + L_{bs}, \tag{3.39}$$

where

$$(M_c)_{ij} = \rho_s \int_{S_1} \mathbf{N}_s^i \cdot \mathbf{n} \, N_f^j \, dS$$

and

$$(L_{bs})_i = \int_{S_1} \mathbf{N}_s^i \cdot \mathbf{n} \, \rho_s \phi \, dS.$$

The total system using displacement potential formulation reads

$$\begin{bmatrix} M_s & M_c \\ 0 & M_f \end{bmatrix} \ddot{X} + \begin{bmatrix} C_s & 0 \\ 0 & C_f \end{bmatrix} \dot{X} + \begin{bmatrix} K_s & 0 \\ -K_c & K_f \end{bmatrix} X = \begin{bmatrix} L_s^e + L_{bs} \\ L_b - L_q \; -L_e \end{bmatrix}, \tag{3.40}$$

where

$$X = \begin{bmatrix} U_s \\ \Psi \end{bmatrix}$$

and we have

$$c^2 M_c = \rho_s K_c^T.$$

3.3.3 Displacement formulation

The two systems to be assembled are

$$M_s \ddot{U} + C_s \dot{U}_s + K_s U_s = L_s^e + L_f$$

and

$$M_f \ddot{U}_f + C_f \dot{U}_f + K_f U_f = -L_s + L_b - L_q - L_e, \qquad (3.41)$$

where

$$(L_f)_i = \int_{S_1} \mathbf{N}_s^i \cdot \mathbf{n}\, p\, dS$$

and

$$(L_s)_i = \int_{S_1} \tilde{N}_f^i\, p\, dS.$$

Here, $\tilde{N}_f^i$ is an entry in the matrix $[\tilde{N}_f]$ defined in connection with Eq. (3.31).
The degrees of freedom are divided into three groups where only U_{sf} participates in the interaction between fluid and structure.

Then the assembled system is

$$\begin{bmatrix} M_s & & \\ & & \\ & & M_f \end{bmatrix} \ddot{U} + \begin{bmatrix} C_s & & \\ & & \\ & & C_f \end{bmatrix} \dot{U} + \begin{bmatrix} K_s & & \\ & & \\ & & K_f \end{bmatrix} U =$$

$$= \begin{bmatrix} L_s^e & & \overline{L_f - L_s} \\ & & \\ \overline{L_b - L_q - L_e} & & \end{bmatrix}, \qquad (3.42)$$

where

$$U = \begin{bmatrix} U_{ss} \\ U_{sf} \\ U_{ff} \end{bmatrix}.$$

The elements at the intersection between M_s and M_f and between K_s and K_f are the added quantities of corresponding elements.

The load matrix

$$(L_f - L_s)_i = \int_{S_1} (\tilde{N}_f^i - \mathbf{N}_s^i \cdot \mathbf{n}) p \, dS$$

vanishes if the same interpolants are used along the interface. Otherwise it produces fictitious loads.

3.4 Symmetric formulation of fluid-structure interaction

In Section 3.3, the formulations using a fluid potential lead to nonsymmetric matrices. For several reasons, it is desirable that the discrete system is symmetric. Many common computer codes depend on this and time stepping algorithms for symmetric problems are far better understood. The displacement formulation has this property but has the drawback of an increase in the number of unknowns, especially in three dimensional applications.

In the literature, symmetrization is sometimes achieved by means of matrix manipulations (see Tong [43]) or modal techniques (see. Daniel [12]-[13]). In Everstine [15] the velocity potential is added to the unsymmetric pressure formulation, leading to a fictitious damped symmetric system. True symmetric formulations have been introduced using variational principles for harmonic problems (see Ohayon [28]-[31]). Recently, a symmetric formulation using pressure and velocity potential as fluid unknowns was proposed (see Olson et al [32]). The drawback in this formulation is still the introduction of a damping matrix, although the system is conservative.

The object of this section is to introduce a symmetric formulation for transient analysis using the same method as in Subsection 3.2.1-2. A striking result in those subsections is the way the unsymmetric coupling matrices enter the system. They change in a symmetric manner in passing from the pressure formulation to the displacement potential formulation (see Eq. (3.36) and (3.40)). The idea is to combine the formulations and in that way obtain a symmetric formulation.

The structural part of the system presented in Subsections 3.3.1 and 3.3.2 reads

$$M_s \ddot{U}_s + K_s U_s - M_c P = L_s^e \tag{3.43}$$

and

$$M_s \ddot{U}_s + K_s U_s + \rho_s M_c \ddot{\psi} = L_s^e, \tag{3.44}$$

where

$$M_c = \int_{S_1} \mathbf{N}_s^i \cdot \mathbf{n}\, N_f^j \, dS$$

if we neglect structural damping. Furthermore, there are two relations between pressure and displacement potential given in subsection 2.2.1 (Eqs. (2.11), (2.12), (2.13) and (2.19))

$$\frac{1}{c^2}\dot{p} + \rho_s \nabla^2\dot{\psi} = q, \tag{3.45}$$

$$\frac{1}{\rho_s}\nabla p + \nabla\ddot{\psi} = \mathbf{b}. \tag{3.46}$$

Symmetrization can now be achieved in two ways by combining one of the structural equations and the relations between pressure and displacement potential. Differentation of Eq. (3.45) with respect to time yields

$$\frac{1}{c^2}\ddot{p} + \rho_s \nabla^2\ddot{\psi} = \dot{q}. \tag{3.47}$$

The weak form using Green's second formula is

$$\frac{1}{c^2}\int_V w\ddot{p}\, dV - \rho_s \int_V \nabla w \cdot \nabla\ddot{\psi}\, dV + \rho_s \int_S w\nabla\ddot{\psi}\cdot\mathbf{n}\, dS =$$

$$= \int_V w\dot{q}\, dV. \tag{3.48}$$

The surface integral is reformulated using the boundary condition at the fluid-structure interface

$$\int_{S_1} w\nabla\ddot{\psi}\cdot\mathbf{n}\, dS = \int_{S_1} w\ddot{u}_{sf}\, dS.$$

The formulation does not allow a fluid boundary of type S_2. Other boundary conditions enters according to Table 2.1. Spatial integration of Eq. (3.46) yields

$$\frac{1}{\rho_s}p + \ddot{\psi} = \phi \tag{3.49}$$

because an arbitrary function of time could be added to ψ and the weak form of Eq. (3.49) is

$$\frac{1}{\rho_s}\int_V wp\ dV + \int_V w\ddot{\psi}\ dV = \int_V w\phi\ dV. \tag{3.50}$$

Expanding p, ψ and u_{sf} in a set of shape functions

$$p = \sum_j N_p^j\ P_j,$$

$$\psi = \sum_j N_\psi^j\ \Psi_j,$$

$$u_{sf} = \mathbf{u}_s\cdot\mathbf{n} = \sum_j \mathbf{N}_s^j\cdot\mathbf{n}\ U_s^j.$$

(Note that shape functions in the p-field need not be the same as in the ψ-field.) Using N_ψ^i as test functions in Eq. (3.48) and N_p^i as test function in Eq. (3.50) yields

$$\frac{1}{c^2}A\ddot{P} - \rho_s K_f\ddot{\Psi} + \rho_s M_c^T\ddot{U}_s = L_q \tag{3.51}$$

and

$$\frac{1}{\rho_s c^2}M_f P + \frac{1}{c^2}A^T\ddot{\Psi} = L_b, \tag{3.52}$$

where

$$(A)_{ij} = \int_V N_\psi^i\ N_p^j\ dV,$$

$$(K_f)_{ij} = \int_V \nabla N_\psi^i\cdot\nabla N_\psi^j\ dV,$$

$$(M_f)_{ij} = \int_V N_p^i\ N_p^j\ dV,$$

$$(L_q)_i = \int_V N_\psi^i\ \dot{q}\ dV,$$

$$(L_b)_i = \frac{1}{c^2} \int_V N_p^i \, \phi \, dV.$$

M_c is defined in connection with Eqs. (3.43) and (3.44). Note that by that definition $N_f = N_\psi$. If the same shape function set is used in both the p-field and the ψ-field then A is symmetric and

$$A = M_f.$$

Assembling Eqs. (3.44), (3.51) and (3.52)

$$\begin{bmatrix} M_s & \rho_s M_c & 0 \\ \rho_s M_c^T & -\rho_s K_f & \frac{1}{c^2} A \\ 0 & \frac{1}{c^2} A^T & 0 \end{bmatrix} \ddot{X} + \begin{bmatrix} K_s & 0 & 0 \\ 0 & 0 & 0 \\ 0 & 0 & \frac{1}{\rho_s c^2} M_f \end{bmatrix} X =$$

$$= \begin{bmatrix} L_s^e \\ L_q \\ L_b \end{bmatrix}, \qquad (3.53)$$

where

$$X = \begin{bmatrix} U_s \\ \Psi \\ P \end{bmatrix}.$$

Note that the source vectors L_b and L_q influence the p-field and the ψ-field, respectively. Besides the fact that it is possible to use different interpolants in the two fields it is also possible to use different numbers of interpolants. This is basically the same formulation as was derived by Ohayon [28] for free vibrations.

The other symmetric formulation is achieved in a similar manner. Integration of Eq. (3.45) results in

$$\frac{1}{\rho_s c^2} p + \nabla^2\psi = \frac{1}{\rho_s} Q. \tag{3.54}$$

The weak form is

$$\frac{1}{\rho_s c^2} \int_V wp \, dV - \int_V \nabla w \cdot \nabla\psi \, dV + \int_S w u_{sf} \, dS =$$

$$= \frac{1}{\rho_s} \int_V wQ \, dV \tag{3.55}$$

using the boundary condition at the fluid-structure interface. The weak form of (3.46) is found by using ∇w as test function

$$\int_V \nabla w \cdot \nabla p \, dV + \rho_s \int_V \nabla w \cdot \nabla\ddot{\psi} \, dV = \rho_s \int_V \nabla w \cdot \mathbf{b} \, dV. \tag{3.56}$$

Expanding p and ψ in different sets of shape functions, $\{N_p\}$ and $\{N_\psi\}$, using $\{N_p\}$ as test function set in Eq. (3.55) and using $\{N_\psi\}$ in Eq. (3.56) results in

$$\frac{1}{\rho_s c^2} M_f P - B^T \Psi + M_c^T U_s = L_q, \tag{3.57}$$

$$BP + \rho_s K_f \ddot{\Psi} = L_b, \tag{3.58}$$

where M_f and K_f are as above (Eq. 3.52). In M_c we set $N_f = N_p$ and so

$$B = \int_V \nabla N_\psi \cdot \nabla N_p \, dV,$$

$$L_q = \frac{1}{\rho_s} \int_V N_p Q \, dV,$$

$$L_b = \rho_s \int_V \nabla N_\psi \cdot \mathbf{b} \, dV.$$

The assembled system, using Eq. (3.43), is

$$\begin{bmatrix} M_s & 0 & 0 \\ 0 & \rho_s K_f & 0 \\ 0 & 0 & 0 \end{bmatrix} \ddot{X} + \begin{bmatrix} K_s & 0 & -M_c \\ 0 & 0 & B \\ -M_c^T & B^T & -\frac{1}{\rho_s c^2} M_f \end{bmatrix} X =$$

$$= \begin{bmatrix} L_s^e \\ L_b \\ -L_q \end{bmatrix}, \qquad (3.59)$$

where

$$X = \begin{bmatrix} U_s \\ \psi \\ P \end{bmatrix}.$$

This latter symmetric formulation is quite attractive in connection with static condensation. Regarding U_s and ψ as master variables and P as slave variables, no equivalent masses are attached to the slave variables. The slave variables are assumed to be unloaded, i.e., $L_q \equiv 0$. If

$$T = \rho_s c^2 M_f^{-1} \begin{bmatrix} -M_c^T & B \end{bmatrix}$$

and

$$T^* = \begin{bmatrix} I \\ T \end{bmatrix},$$

where I is the identity matrix, we get the condensed form

$$M^{*}\ddot{X} + K^{*}X = (T^{*})^{T}\begin{bmatrix} L_s^e \\ L_b \\ 0 \end{bmatrix}, \tag{3.60}$$

where

$$X = \begin{bmatrix} U_s \\ \Psi \end{bmatrix},$$

$$K^{*} = (T^{*})^{T}KT^{*} = \begin{bmatrix} K_s+\rho_s M_c M_f^{-1} M_c^{T} & -\rho_s c^2 M_c M_f^{-1} B^{T} \\ -\rho_s c^2 B M_f^{-1} M_c^{T} & \rho_s c^2 B^{T} M_f^{-1} B^{T} \end{bmatrix},$$

$$M^{*} = (T^{*})^{T}MT^{*} = \begin{bmatrix} M_s & 0 \\ 0 & \rho_s K_f \end{bmatrix}.$$

M and K are the original mass matrix and stiffness matrix.

3.5 Non-linear fluid

The aim in this and the next section is to give a fairly general formulation of a nonlinear wave propagation problem although the application in mind is the cavitating fluid. Cavitating fluids due to underwater shocks were first given a finite element formulation by Newton [23]-[26] using the displacement potential in the fluid. Later, Zienkiewicz et al [51] studied the effect on dams in connection with earthquakes. Recently Felippa et al [17] reported studies on hull cavitations using staggered time-integration routines and special boundary techniques. Using the displacement potential is advantageous in some sense. Being a primitive variable it is likely to be robust in numerical discretization.

Studies by Newton [23]-[25] indicated that the cavitating fluid might cause spurious pressure oscillations that generate pressurized zones within the cavitated region and vice versa. This phenomenon has been named frothing. The remedy is to introduce numerical damping (see Felippa et al

[17]). (This is discussed further in section 4.3). The introduction of numerical damping calls for the calculation of, basically, $\partial^3\psi/\partial t^3$, which is not naturally present in the time stepping routine when using ψ as a primary variable. On the other hand, when ρ is used as primary variable, numerical damping is generated via $\partial\rho/\partial t$, which is very much present. Above all, ρ is a physical variable allowing more general constitutive laws, and boundary conditions that naturally occur, such as pressurized boundaries, need no special treatment.

Recall the equations given in Subsection 2.2.2

$$\ddot{\rho} - \nabla^2 p = -\rho_s \nabla\cdot\mathbf{b} + \dot{q}, \tag{2.28}$$

$$p = \sigma(\rho, \dot{\rho}). \tag{2.27}$$

In conformity with the procedure in section 3.2 we have

$$\int_V w\ddot{\rho}\, dV + \int_V (\nabla w)\cdot(\nabla p) dV = \int_S w(\nabla p)\cdot\mathbf{n}\, dS -$$

$$- \rho_s \int_V w\nabla\cdot\mathbf{b}\, dV + \int_V w\dot{q}\, dV. \tag{3.61}$$

The discussion concerning the surface integral in Eq. (3.8) also applies to Eq. (3.61), and therefore Eqs. (3.9a-c) can still be used to reformulate the surface integral. At the transmitting boundary (S_4), the fluid is not cavitating because this part of the boundary should be located far away from any irregularity. Hence

$$p = c^2\rho$$

and from Eq. (2.49) we have

$$\int_{S_4} w(\nabla p)\cdot\mathbf{n}\, dS = -c \int_{S_4} w\dot{\rho}\, dS.$$

The outcome of the S_4-boundary is a damping matrix as in

Subsection 3.2.1. This matrix and the result of the S_2 and S_3 boundaries will be neglected in this section.

The conventional finite element scheme is derived as follows. Substituting the constitutive law given in Eq. (2.27) above into Eq. (3.61) yields

$$\int_V w\ddot{\rho}\, dV + \int_V \nabla w \nabla\sigma\, dV = -\rho_s \int_{S_1} w\ddot{u}_{sf}\, dS +$$

$$+ \rho_s \int_V \nabla w \cdot \mathbf{b}\, dV + \int_V w\dot{q}\, dV. \tag{3.62}$$

Because

$$\nabla\sigma = \frac{\partial\sigma}{\partial\dot{\rho}} \nabla\dot{\rho} + \frac{\partial\sigma}{\partial\rho} \nabla\rho \tag{3.63}$$

we get

$$\int_V w\ddot{\rho}\, dV + \int_V \nabla w \frac{\partial\sigma}{\partial\dot{\rho}} \nabla\dot{\rho}\, dV + \int_V \nabla w \frac{\partial\sigma}{\partial\rho} \nabla\rho\, dV =$$

$$= -\rho_s \int_{S_1} w\ddot{u}_{sf}\, dS + \rho_s \int_V \nabla w \cdot \mathbf{b}\, dV + \int_V w\dot{q}\, dV. \tag{3.64}$$

Expanding ρ in terms of a set of shape functions, $\{N_f\}$,

$$\rho(\mathbf{r},t) = \sum_j N_f^j(\mathbf{r}) \cdot \Pi_j(t), \tag{3.65}$$

where Π_j is the unknown value of ρ at node j and similarly for p. Further, if

$$w \in \{N_f\},$$

we get the discretized form of Eq. (3.61)

$$M_f \ddot{\Pi} + C_f \dot{\Pi} + K_f \Pi = -L_s + L_b + L_q, \tag{3.66}$$

where

$$(M_f)_{ij} = \int_V N_f^i \, N_f^j \, dV,$$

$$(C_f)_{ij} = \int_V (\nabla N_f^i) \cdot (\nabla N_f^j) \, \frac{\partial \sigma}{\partial \dot{\rho}} \, dV,$$

$$(K_f)_{ij} = \int_V (\nabla N_f^i) \cdot (\nabla N_f^j) \, \frac{\partial \sigma}{\partial \rho} \, dV,$$

$$(L_s)_i = \rho_s \int_{S_1} N_f^i \, \ddot{u}_{sf} \, dS,$$

$$(L_b)_i = \rho_s \int_V \nabla N_f^i \cdot \mathbf{b} \, dV,$$

$$(L_q)_i = \int_V N_f^i \, \dot{q} \, dV,$$

(i = row index, j = column index) and Π is a column matrix for unknown nodal values of ρ.

Writing σ as in Eq. (2.27)

$$\sigma(\rho, \dot{\rho}) = \alpha(\rho)\rho + \beta(\rho)\dot{\rho}$$

we get

$$\frac{\partial \sigma}{\partial \dot{\rho}} = \beta,$$

$$\frac{\partial \sigma}{\partial \rho} = \rho \, \frac{d\alpha}{d\rho} + \alpha + \dot{\rho} \, \frac{d\beta}{d\rho}, \tag{3.67}$$

and thus in Eq. (3.66) we have

$$(C_f)_{ij} = \int_V (\nabla N_f^i)\cdot(\nabla N_f^j)\beta \, dV,$$

$$(K_f)_{ij} = \int_V (\nabla N_f^i)\cdot(\nabla N_f^j)(\rho \frac{d\alpha}{d\rho} + \alpha + \dot{\rho} \frac{d\beta}{d\rho})dV. \qquad (3.68)$$

As a practical approach, we might choose α and β as piecewise constant functions. To each subdomain (i.e., to each element), we assign constant values α_e and β_e to α and β, respectively. The element contributions to the matrices in Eq. (3.68) are

$$(C_f)^e_{ij} = \beta_e \int_e (\nabla N_f^i)(\nabla N_f^j)dV,$$

$$(K_f)^e_{ij} = \alpha_e \int_e (\nabla N_f^i)(\nabla N_f^j)dV. \qquad (3.69)$$

The constant values α_e and β_e should then be choosen on the basis of the nodal values of ρ at nodal points belonging to that subdomain.

An attractive approach as compared to the conventional finite element procedure is mentioned by Hughes et al [21] and references are made there to several authors working along this line. Christie et al [58] have termed it 'product approximation', Spradley et al [59] called it the 'general interpolants method'. Fletcher [60] and Fletcher et al [61] have introduced the 'group finite element formulation'. Their investigation clearly indicates a considerable gain in

* computer economy,

* accuracy, in particular for high order elements,

when treating a nonlinear problem. Their conclusions apply particularly with regard to compressible fluid flow. The explanation is that the scheme does not connect the nonlinear contributions between nodes to the same degree as

the conventional procedure. This quality is central when computing a non-smooth solution, as is the case when the fluid is cavitating.

Both ρ and p are expanded in terms of the same set of trial functions

$$\rho(\mathbf{r},t) = \sum_j N_f^j(\mathbf{r}) \cdot \Pi_j(t), \tag{3.70}$$

$$p(\mathbf{r},t) = \sum_j N_f^j(\mathbf{r}) \cdot P_j(t), \tag{3.71}$$

where Π_j and P_j are the nodal values of ρ and p. Because

$$P_j(t) = \sigma(\Pi_j(t), \dot{\Pi}_j(t)) \tag{3.72}$$

we have

$$\nabla p(\mathbf{r},t) = \sum_j \nabla N_f^j \cdot \sigma(\Pi_j, \dot{\Pi}_j). \tag{3.73}$$

If

$$w \in \left[N_f\right]$$

we get the discretized form of Eq. (3.62)

$$M_f \ddot{\Pi} + K_f \sigma(\Pi, \dot{\Pi}) = -L_s + L_b + L_q, \tag{3.74}$$

where

$$(K_f)_{ij} = \int_V (\nabla N_f^i) \cdot (\nabla N_f^j) dV.$$

$\sigma(\Pi, \dot{\Pi})$ is a column matrix and at the i:th row we have

$$(\sigma(\Pi, \dot{\Pi}))_i = \sigma(\Pi_i, \dot{\Pi}_i).$$

The other matrices in Eq. (3.74) are defined in Eq. (3.66). Writing σ as in Eq. (2.27)

$$\sigma(\Pi_i, \dot{\Pi}_i) = \alpha(\Pi_i)\Pi_i + \beta(\Pi_i)\dot{\Pi}_i \tag{3.75}$$

and the second term in Eq. (3.65) becomes

$$K_f\sigma(\Pi,\Pi) = K_f A\ \Pi + K_f\ B\ \dot{\Pi}, \tag{3.76}$$

where A and B are diagonal matrices

$$A = \text{Diag}\ (\alpha(\Pi_i)),$$
$$B = \text{Diag}\ (\beta(\Pi_i)).$$

3.6 Nonlinear fluid-structure interaction

In Eq. (3.2) the fluid domain was coupled to the structural domain by the vector L_f where

$$(L_f)_i = \int_{S_1} \mathbf{N}_s^i \cdot \mathbf{n} p(\mathbf{r}, t) dS.$$

A quasi-linearized form of Eq. (3.77) is

$$(L_f)_i = \int_{S_1} \mathbf{N}_s^i \cdot \mathbf{n} \left(\frac{\partial \sigma}{\partial \rho}\ \rho + \frac{\partial \sigma}{\partial \dot{\rho}}\ \dot{\rho}\right) dS. \tag{3.78}$$

Expanding ρ in terms of the shape functions yields

$$L_f = C_c \dot{\Pi} + K_c \Pi, \tag{3.79}$$

where

$$(C_c)_{ij} = \int_{S_1} \mathbf{N}_s^i \cdot \mathbf{n} \, \frac{\partial \sigma}{\partial \dot{\rho}} \, N_f^j \, dS,$$

$$(K_c)_{ij} = \int_{S_1} \mathbf{N}_s^i \cdot \mathbf{n} \, \frac{\partial \sigma}{\partial \rho} \, N_f^j \, dS. \tag{3.80}$$

If the special form for σ in Eq. (2.27) is used we get

$$(C_c)_{ij} = \int_{S_1} \mathbf{N}_s^i \cdot \mathbf{n} \, \beta \, N_f^j \, dS,$$

$$(K_c)_{ij} = \int_{S_1} \mathbf{N}_s^i \cdot \mathbf{n} \, \alpha \, N_f^j \, dS. \tag{3.81}$$

Likewise, the coupling vector in Eq. (3.66) is rewritten using structural discretization

$$L_s = M_c \, \ddot{U}_s, \tag{3.82}$$

where

$$(M_c)_{ij} = \rho_s \int_{S_1} N_f^i \, \mathbf{N}_s^j \cdot \mathbf{n} \, dS.$$

Assembling Eqs. (3.2) and (3.66) yields

$$\begin{bmatrix} M_s & 0 \\ M_c & M_f \end{bmatrix} \begin{bmatrix} \ddot{U}_s \\ \ddot{\Pi} \end{bmatrix} + \begin{bmatrix} C_s & -C_c \\ 0 & C_f \end{bmatrix} \begin{bmatrix} \dot{U}_s \\ \dot{\Pi} \end{bmatrix} + \begin{bmatrix} K_s & -K_c \\ 0 & K_f \end{bmatrix} \begin{bmatrix} U_s \\ \Pi \end{bmatrix} =$$

$$= \begin{bmatrix} L_s^e \\ L_b + L_q \end{bmatrix}. \tag{3.83}$$

Finally, if instead the 'product approximation' scheme is applied to Eq. (3.77), we get

$$L_f = K_c \sigma(\Pi, \dot{\Pi}), \tag{3.84}$$

where

$$(K_c)_{ij} = \int_{S_1} \mathbf{N}_s^i \cdot \mathbf{n}\, N_f^j \, dS.$$

By using the constitutive law as expressed in Eq. (2.27) we obtain

$$L_f = K_c A\, \Pi + K_c\, B\, \dot{\Pi}. \tag{3.85}$$

Assembling the Eqs. (3.2) and (3.74) yields

$$\begin{bmatrix} M_s & 0 \\ M_c & M_f \end{bmatrix} \begin{bmatrix} \ddot{U}_s \\ \ddot{\Pi} \end{bmatrix} + \begin{bmatrix} C_s & 0 \\ 0 & 0 \end{bmatrix} \begin{bmatrix} \dot{U}_s \\ \dot{\Pi} \end{bmatrix} + \begin{bmatrix} K_s & -K_c \\ 0 & K_f \end{bmatrix} \begin{bmatrix} U_s \\ \sigma(\Pi, \dot{\Pi}) \end{bmatrix} =$$

$$= \begin{bmatrix} L_s^e \\ L_b + L_q \end{bmatrix} \tag{3.86}$$

or by using Eqs. (3.76) and (3.85)

$$\begin{bmatrix} M_s & 0 \\ M_c & M_f \end{bmatrix} \ddot{X} + \begin{bmatrix} C_s & -K_c B \\ 0 & K_f B \end{bmatrix} \dot{X} + \begin{bmatrix} K_s & -K_c A \\ 0 & K_f A \end{bmatrix} X =$$

$$= \begin{bmatrix} L_s^e \\ L_b + L_q \end{bmatrix}, \tag{3.87}$$

where $X = \begin{bmatrix} U_s & \Pi \end{bmatrix}^T$. The nonlinear part of the damping and stiffness matrices can be separated

$$\begin{bmatrix} C_s & -K_c B \\ 0 & K_f B \end{bmatrix} = \begin{bmatrix} C_s & -K_c \\ 0 & K_f \end{bmatrix} \begin{bmatrix} I & 0 \\ 0 & B \end{bmatrix},$$

$$\begin{bmatrix} K_s & -K_c A \\ 0 & K_f A \end{bmatrix} = \begin{bmatrix} K_s & -K_c \\ 0 & K_f \end{bmatrix} \begin{bmatrix} I & 0 \\ 0 & A \end{bmatrix},$$

where I is the identity matrix.

The gain in computer economy is obvious when one compares Eq. (3.87) to Eq. (3.83). In Eq. (3.87), the nonlinear contribution is separated in diagonal matrices. This is particularly beneficial when an explicit time stepping algorithm is employed.

4. PROGRAMMING

4.1 CAMFEM

In modern technology, the researcher often reaches the point where ideas must be transformed into computer code. The work involved in this, starting from an empty screen, should never be underestimated. In many cases, however, the researcher does so without being able to consider previous experience and to use existing computer codes, because they are developed for other applications or new routines are not easily added to the existing code. Much work is thus spent on routines for common data and matrix handling.

During the course of this study, those aspects of programming have been minimized by using a computer program, CAMFEM, designed for research purposes. CAMFEM is based on a command language in which a command in general consists of a logical name for a certain operation followed by arguments. The basic structure of the program is shown in Fig. 4.1 below.

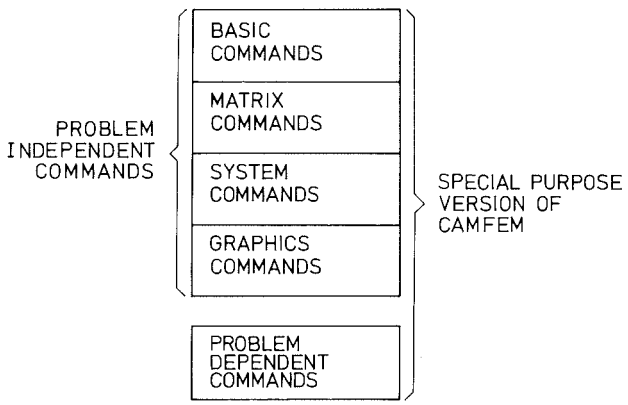

Figure 4.1. Structure of the program CAMFEM

The first four sets, called problem independent commands, are within the original frame of CAMFEM. The researcher adds to this his own problem dependent commands and obtains his own version of CAMFEM. For a more detailed description of the facilities of the CAMFEM concept, see Dahlblom and Peterson [11] and Peterson [34]. The problem dependent commands are of two types

* element routines,
* time stepping routines,

which are discussed in detail in the following sections.

4.2 Space discretization

The types of finite elements used for space discretization are of three kinds

* structural elements,
* fluid elements,
* coupling routines,

and are dealt with in the following subsections. The routines are constructed for two dimensional applications, but the intrinsic logic in the coupling routines has of course no two-dimensional limitation.

4.2.1 Structural elements

A simple two-dimensional beam element with 6 degrees of freedom is chosen as structural element. Finite element formulations for beams are standard procedure but because the beam is of interest in connection with the coupling routine, we will give a full description of the element chosen.

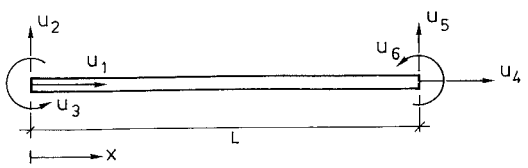

Figure 4.2. Structural element used in the numerical examples

The element has three degrees of freedom in each node, two displacements and one rotation. For a single beam, the restrictions of the trial functions for the left-hand node are

$$N_s^1 = 1 - \frac{x}{L},$$

$$N_s^2 = 1 - 3(\frac{x}{L})^2 + 2(\frac{x}{L})^3, \qquad (4.1)$$

$$N_s^3 = x - 2\frac{x^2}{L} + \frac{x^3}{L^2},$$

where L is the beam length. The right-hand node has similar trial functions.

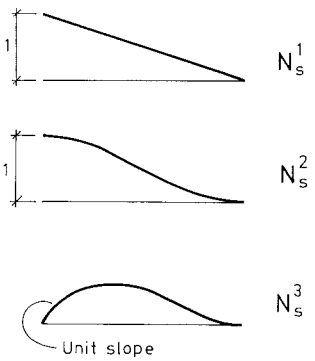

Figure 4.3. Trial functions for the left beam node

According to Euler-Bernoulli beam theory, the differential operator in Eq. (2.1) for axial displacement is

$$L_1 = \frac{\partial}{\partial x} EA \frac{\partial}{\partial x} - m \frac{\partial^2}{\partial t^2} \qquad (4.2)$$

and for transverse displacement

$$L_2 = \frac{\partial^2}{\partial x^2} EI \frac{\partial}{\partial x^2} + m \frac{\partial^2}{\partial t^2}, \qquad (4.3)$$

where E is Young's modulus, I the moment of inertia, A the cross sectional area, and m the beam mass per unit length.

Using standard Galerkin methods the differential operators together with the trial functions give the following element matrices (see for example Segerlind [38])

$$M_s^e = \frac{mL}{420}\begin{bmatrix} 140 & 0 & 0 & 70 & 0 & 0 \\ 0 & 156 & 22L & 0 & 54 & -13L \\ 0 & 22L & 4L^2 & 0 & 13L & -3L^2 \\ 70 & 0 & 0 & 140 & 0 & 0 \\ 0 & 54 & 13L & 0 & 156 & -22L \\ 0 & -13L & -3L^2 & 0 & -22L & 4L^2 \end{bmatrix} \tag{4.4}$$

$$K_s^e = \begin{bmatrix} \frac{EA}{L} & 0 & 0 & -\frac{EA}{L} & 0 & 0 \\ 0 & \frac{12EI}{L^3} & \frac{6EI}{L^2} & 0 & -\frac{12EI}{L^3} & \frac{6EI}{L^2} \\ 0 & \frac{6EI}{L^2} & \frac{4EI}{L} & 0 & -\frac{6EI}{L^2} & \frac{2EI}{L} \\ -\frac{EA}{L} & 0 & 0 & \frac{EA}{L} & 0 & 0 \\ 0 & -\frac{12EI}{L^3} & -\frac{6EI}{L^2} & 0 & \frac{12EI}{L^3} & -\frac{6EI}{L^2} \\ 0 & \frac{6EI}{L^2} & \frac{2EI}{L} & 0 & -\frac{6EI}{L^2} & \frac{4EI}{L} \end{bmatrix} \tag{4.5}$$

4.2.2 Fluid elements

In Chapter 3, the finite element derivation using a scalar field as a primary fluid unknown yields similar matrices. The primary difference between the pressure formulation and displacement potential formulation, apart from their different physical interpretations, lies not in their content but in the location of the coupling matrices. In the formulation for a nonlinear fluid in Section 3.6, the difference, besides the nonlinearity, is a multiplying constant. For this reason we need only develop one fluid

element and yet cover all fluid scalar field formulations presented in this work. The choice of fluid element has fallen upon a four node quadrilateral element (Fig. 4.4) made up of three triangular elements where the midnode (node number 5) is regarded as a slave node.

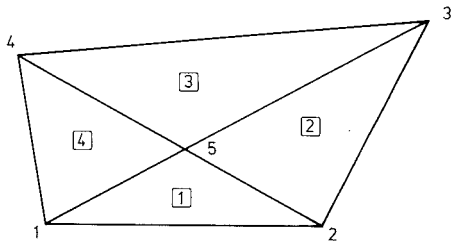

Figure 4.4. Four triangular elements constitute a quadrangle

In each triangle we have three nodes and thus the trial functions are first-order polynomials.

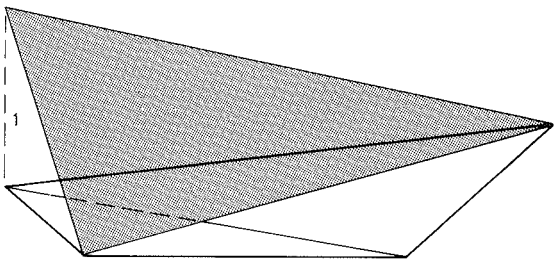

Figure 4.5. The restriction of the trial function at node 4 to the quadrangle

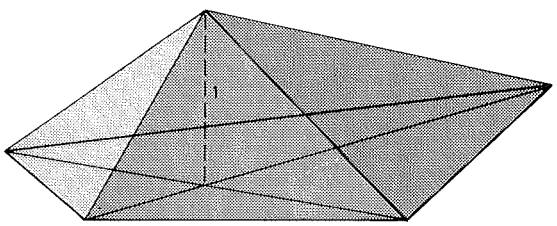

Figure 4.6. Trial function at node 5

From the triangle with nodes 1, 2 and 5 we have the following contribution. The trial functions are

$$\left[N_f^1 \quad N_f^2 \quad N_f^5\right] = \left[1 \; x \; y\right] \cdot C^{-1}, \tag{4.6}$$

where

$$C = \begin{bmatrix} 1 & x_1 & y_1 \\ 1 & x_2 & y_2 \\ 1 & x_5 & y_5 \end{bmatrix}$$

and (x_i, y_i) are the coordinates at node number i. The corresponding mass matrix (see Eqs. (3.14), (3.20), (3.66) and (3.74) give us

$$\left[\int_e N_f^i \, N_f^j \, dA\right] = C^{-T} \int_e \begin{bmatrix} 1 \\ x \\ y \end{bmatrix} \left[1 \; x \; y\right] dA \; C^{-1} =$$

$$= C^{-T} \int_e \begin{bmatrix} 1 & x & y \\ x & x^2 & xy \\ y & yx & y^2 \end{bmatrix} dA \; C^{-1}, \tag{4.7}$$

where the integration runs over the element e. The corresponding stiffness matrix is

$$\left[\int_e \nabla N_f^i \cdot \nabla N_f^j \, dA\right] = C^{-T} \int_e \left[\begin{bmatrix} \frac{\partial}{\partial x} \\ \frac{\partial}{\partial y} \end{bmatrix} \left[1 \; x \; y\right]\right]^T \begin{bmatrix} \frac{\partial}{\partial x} \\ \frac{\partial}{\partial y} \end{bmatrix} \left[1 \; x \; y\right] dA \; C^{-1} =$$

$$= C^{-1} \int_e \begin{bmatrix} 0 & 0 & 0 \\ 0 & 1 & 0 \\ 0 & 0 & 1 \end{bmatrix} dA \; C^{-1}. \tag{4.8}$$

The contributions from each one of the four triangles are assembled into matrices for the five node elements in Fig. 4.4. Static condensation is then performed on node number 5. If the quadrangle in Fig. 4.4 is a rectangle, these steps are easily performed using the side lengths as parameters.

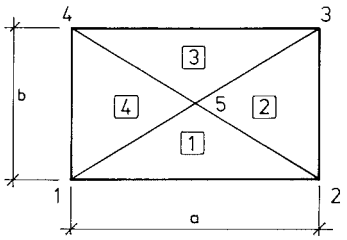

Figure 4.7. Rectangular element

The mass and stiffness contributions from element number 1 are

$$M_1 = \frac{ab}{48}\begin{bmatrix} 2 & 1 & 1 \\ 1 & 2 & 1 \\ 1 & 1 & 2 \end{bmatrix}, \tag{4.9}$$

$$K_1 = \frac{1}{4ab}\begin{bmatrix} a^2+b^2 & a^2-b^2 & -2a^2 \\ a^2-b^2 & a^2+b^2 & -2a^2 \\ -2a^2 & -2a^2 & 4a^2 \end{bmatrix}. \tag{4.10}$$

These contributions yield the following 5×5 matrices

$$M' = \frac{ab}{48}\begin{bmatrix} 4 & 1 & 0 & 1 & 2 \\ 1 & 4 & 1 & 0 & 2 \\ 0 & 1 & 4 & 1 & 2 \\ 1 & 0 & 1 & 4 & 2 \\ 2 & 2 & 2 & 2 & 8 \end{bmatrix}, \tag{4.11a}$$

$$K' = \frac{1}{4ab}\begin{bmatrix} 2A & B & 0 & -B & -2A \\ B & 2A & -B & 0 & -2A \\ 0 & -B & 2A & B & -2A \\ -B & 0 & B & 2A & -2A \\ -2A & -2A & -2A & -2A & 8A \end{bmatrix}, \tag{4.11b}$$

where $A = a^2+b^2$ and $B = a^2-b^2$.

Finally static condensation (see Zienkiewicz [52] pages 548-549) on an element level yields

$$M = \frac{ab}{96}\begin{bmatrix} 11 & 5 & 3 & 5 \\ 5 & 11 & 5 & 3 \\ 3 & 5 & 11 & 5 \\ 5 & 3 & 5 & 11 \end{bmatrix}, \qquad (4.12a)$$

$$K = \frac{1}{8ab}\begin{bmatrix} 3A & C & -A & D \\ C & 3A & D & -A \\ -A & D & 3A & C \\ D & -A & C & 3A \end{bmatrix}, \qquad (4.12b)$$

where A is as above and $C = a^2-3b^2$ and $D = -3a^2+b^2$.

4.2.3 Coupling routines between fluid and structure

The element size in the fluid domain and in the structural domain puts a limit to the possibility of detecting the high frequency content in a transient response. Required element sizes are easily computed as a function of the wavelength. For the structure elements, having a third degree polynomial approximation, the numerical solution is likely to imitate the physical behaviour as long as the element length is shorter than, say, half the wavelength. In the fluid, one might expect reasonable agreement if the element length is less than one fifth of the actual wavelength, because we have linear approximation within each element. These size estimations are of course rough upper bound estimates. Numerical resolution is thus linked to the wavelength. Furthermore, the wavelength is linked to the frequency (f) as f^{-1} in the fluid domain and as $f^{-1/2}$ in the structural domain. Because the coupling routines lock a certain number of structural elements to a certain number of fluid elements, it is only at a fixed frequency that the coupling routines produce numerical resolution of the same quality in both the structural and fluid domains. Away from the fixed frequency, either the fluid or the structure defines an upper bound for the size of the coupling element. Because the decrease of wavelength in the fluid as the frequency increases is faster than in the structure, the fluid element size will define the upper bound for an acceptable numerical resolution at higher frequencies.

The two-node beam in Fig. 4.8 has four degrees of freedom that affect the displacements perpendicular to the fluid boundary.

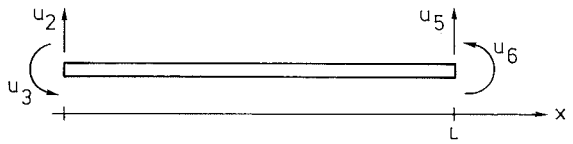

Figure 4.8. Structural degrees of freedom interacting with the fluid

The corresponding trial functions are

$$N_s^2 = 1-3\left[\frac{x}{L}\right]^2 + 2\left[\frac{x}{L}\right]^3, \qquad (4.13)$$

$$N_s^3 = x-2\frac{x^2}{L} + \frac{x^3}{L^2},$$

$$N_s^5 = 3\left[\frac{x}{L}\right]^2 - 2\left[\frac{x}{L}\right]^3,$$

$$N_s^6 = -\frac{x^2}{L} + \frac{x^3}{L^2}.$$

A case in which a beam interacts with three fluid elementis shown in Fig. 4.9. The trial functions for these elements are discussed below.

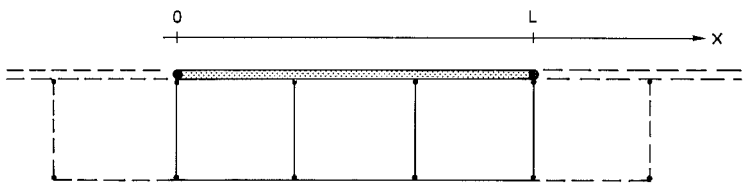

Figure 4.9. Fluid-structure element coupling

At the fluid-structure interface, the fluid trial functions at two fluid nodes are shown in Fig. 4.10.

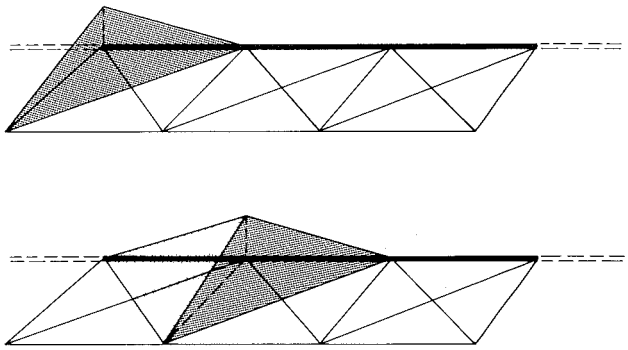

Figure 4.10. Fluid trial functions along the structural boundary

In Sections 3.3 and 3.6, we gave the expressions for the coupling matrices. The basic structure of these is

$$\int_{S_1} \mathbf{N}_s^i \cdot \mathbf{n}\, N_f^j \, dS \tag{4.14}$$

or its transpose, possibly multiplied by some constant. The expressions in Eq. (4.13) define the non-zero $\mathbf{N}_s^i \cdot \mathbf{n}$ for $\mathbf{n}$ parallel to the y-axis in a Cartesian coordinate system. It is obvious from Fig. 4.10 that the restrictions of N_f^j to the boundary are as follows

$$N_f^1(x) = \begin{cases} 1 - 3\,\dfrac{x}{L} & 0 \le x \le \dfrac{L}{3}, \\ 0 & \dfrac{L}{3} < x \le L \end{cases} \tag{4.15a}$$

$$N_f^2(x) = \begin{cases} 3\,\dfrac{x}{L} & 0 \le x \le \dfrac{L}{3} \\ 2\text{-}3\,\dfrac{x}{L} & \dfrac{L}{3} < x \le \dfrac{2L}{3}, \\ 0 & \dfrac{2L}{3} < x \le L \end{cases} \tag{4.15b}$$

$$N_f^3(x) = N_f^2(L-x), \tag{4.15c}$$

$$N_f^4(x) = N_f^1(L-x). \tag{4.15d}$$

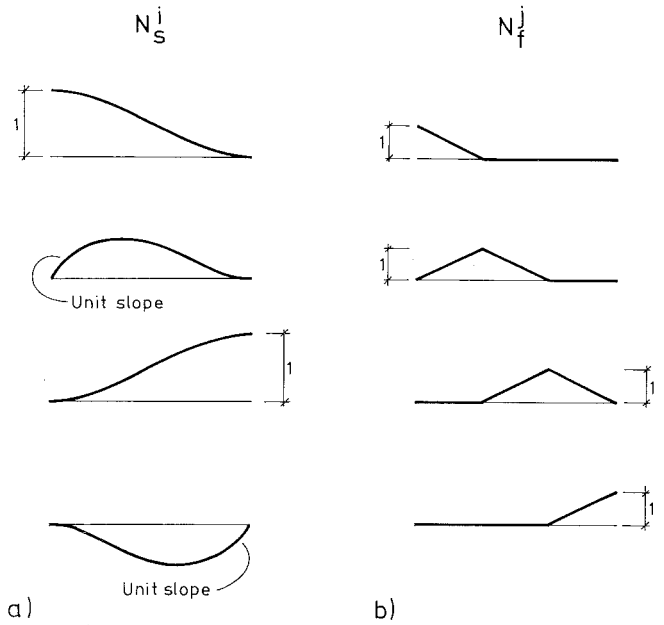

Figure 4.11. Trial functions at the fluid-structure interface for a) structure b) fluid. The figure shows the trial functions restricted to one structural element

The cross integrations between the two sets of trial functions are

$$\left[\int_0^L N_s^i \, N_f^j \, dx\right] = \frac{L}{1620}\begin{bmatrix} 257 & 390 & 150 & 13 \\ 21L & 70L & 40L & 4L \\ 13 & 150 & 390 & 257 \\ -4L & -40L & -70L & -21L \end{bmatrix}. \tag{4.16}$$

(Originally, N_s^i in Eq. (4.14) belongs to the set of test functions in the structural domain but, following the Galerkin method, they coincide).

If the structural element at the fluid boundary has a non-zero slope, the four fluid degrees of freedom interact with the six structural degrees of freedom, i.e., $\mathbf{N}_s^i \cdot \mathbf{n} \neq 0$ for $i = 1,\ldots,6$. The coupling matrix is therefore derived by making a rotation of the structural degrees of freedom as presented in Eq. (4.13).

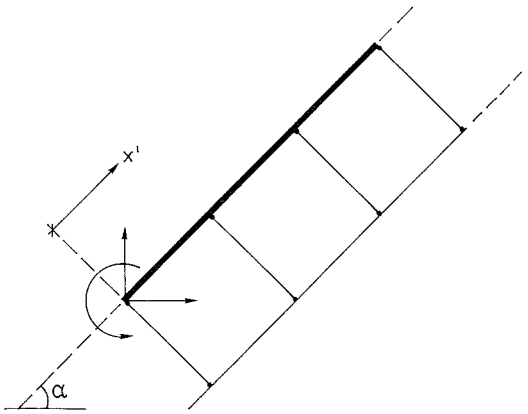

Figure 4.12. Non-horizontal fluid-structure interface

Let T be

$$T = \begin{bmatrix} -\sin\alpha & \cos\alpha & 0 & 0 & 0 & 0 \\ 0 & 0 & 1 & 0 & 0 & 0 \\ 0 & 0 & 0 & -\sin\alpha & \cos\alpha & 0 \\ 0 & 0 & 0 & 0 & 0 & 1 \end{bmatrix}. \tag{4.17}$$

The rotated coupling matrix is then

$$C = T^T \cdot \left[\int_0^L N_s^i \, N_f^j \, dx' \right]. \tag{4.18}$$

We once again stress the fact that, regardless of whether we use pressure formulation, displacement potential formulation or if we are dealing with a cavitating fluid, the coupling matrices have essentially the same structure. (See further Eqs. (3.34), (3.35), (3.38), (3.39), (3.82) and (3.84)). Some of the coupling matrices use the transpose of Eq. (4.18), i.e.,

$$\left[\int_0^L N_f^j \, N_s^i \, dx'\right] \cdot T. \tag{4.19}$$

This completes the derivation of the element routines.

4.3 Time discretization

In a transient analysis, the behaviour and the efficiency of the solution dependent on the time-stepping strategy. Such discussion is held in Belytschko et al [53]. Routines are also developed, especially for fluid-structure interaction, in Neishlos et al [22], Zienkiewicz and Taylor [47] and in Sharan and Gladwell [40]. The routines used in the present analysis are based on implicit schemes of Newmark-type closely related to those described in [56].

4.3.1 Linear fluid

The system to be solved by the time stepping algorithm is

$$M\ddot{X} + C\dot{X} + KX = L, \tag{4.20}$$

where X might be any of $\left[U_s \quad P\right]^T$, $\left[U_s \quad \Pi\right]^T$, $\left[U_s \quad \Psi\right]^T$ or $\left[U_s \quad \Psi \quad P\right]^T$ and the system matrices change according to the scalar field formulation used in the fluid domain. (See Eqs. (3.36), (3.40), (3.53) and (3.59)). The time interval of interest is divided into a set of time stations t_o, t_1, ... , t_n, t_{n+1}, ... , t_N.

During each time station, the equilibrium equation (4.20) takes the form

$$M\ddot{X}_{n+1} + C\dot{X}_{n+1} + KX_{n+1} = L_{n+1}, \tag{4.21}$$

where X_{n+1}, $\dot{X}_{n+1}$ and $\ddot{X}_{n+1}$ are the calculated approximations to $X(t_{n+1})$, $\dot{X}(t_{n+1})$ and $\ddot{X}(t_{n+1})$ and $L_{n+1} = L(t_{n+1})$. These approximations also satisfy the following equations

$$X_{n+1} = X^p_{n+1} + \Delta t_n^2 \beta \, \ddot{X}_{n+1}, \tag{4.22}$$

$$\dot{X}_{n+1} = \dot{X}^p_{n+1} + \Delta t_n \gamma \, \ddot{X}_{n+1}, \tag{4.23}$$

where

$$X^p_{n+1} = X_n + \Delta t_n \dot{X}_n + \Delta t_n^2 \left(\frac{1}{2} - \beta\right) \ddot{X}_n \tag{4.24}$$

is a predictor value to $X(t_{n+1})$ and

$$\dot{X}^p_{n+1} = \dot{X}_n + \Delta t_n (1-\gamma) \ddot{X}_n \tag{4.25}$$

is a predictor value to $\dot{X}(t_{n+1})$. β and γ are the Newmark parameters that control the accuracy and stability of the method and $\Delta t_n = t_{n+1} - t_n$.

Eliminating $\ddot{X}_{n+1}$ and $\dot{X}_n$ from Eq. (4.21) by the use of Eqs. (4.22)-(4.23) gives the following scheme:

1. Initialize X_o, $\dot{X}_o$ and $\ddot{X}_o$.

2. Form the effective stiffness matrix

$$K_{eff} = K + \frac{1}{\Delta t_n^2 \beta} M + \frac{\gamma}{\Delta t_n \beta} C.$$

3. Calculate the predictor values X^p_{n+1} and $\dot{X}^p_{n+1}$ according to (4.24) and (4.25).

4. Calculate the effective forces at time station t_{n+1}

$$F_{eff} = L_{n+1} + \frac{1}{\Delta t_n^2 \beta} M \, X^p_{n+1} + C\left[\frac{\gamma}{\beta \Delta t_n} X^p_{n+1} - \dot{X}^p_{n+1}\right].$$

5. Solve

$$K_{eff}\ X_{n+1} = F_{eff}.$$

6. Calculate acceleration and velocities at time station t_{n+1}

$$\ddot{X}_{n+1} = \frac{1}{\Delta t_n^2 \beta}(X_{n+1} - X^p_{n+1}),$$

$$\dot{X}_{n+1} = \dot{X}^p_{n+1} + \Delta t_n \gamma\ \ddot{X}_{n+1}.$$

Set n = n+1 and go to step 3 to continue the calculation at the next time station.

4.3.2 Nonlinear fluid

In this Subsection only the 'group finite element formulation' is continued.

If the fluid is allowed to cavitate, the governing equation is as was derived in section 3.6

$$\begin{bmatrix} M_s & 0 \\ M_c & M_f \end{bmatrix} \begin{bmatrix} \ddot{U}_s \\ \ddot{\Pi} \end{bmatrix} + \begin{bmatrix} C_s & 0 \\ 0 & 0 \end{bmatrix} \begin{bmatrix} \dot{U}_s \\ \dot{\Pi} \end{bmatrix} + \begin{bmatrix} K_s & -K_c \\ 0 & K_f \end{bmatrix} \begin{bmatrix} U_s \\ \sigma(\Pi, \dot{\Pi}) \end{bmatrix} =$$

$$= \begin{bmatrix} L^e_s \\ L_b + L_q \end{bmatrix}. \qquad (3.86)$$

As long as the fluid does not cavitate, Eq. (3.86) is equivalent to Eq. (4.20) and therefore a transient analysis of Eq. (3.86) starts with step 1-6 of the preceding subsection though in step 6, before going to the next time station, a check is made whether or not cavitation does occur. If so, the time stepping scheme is altered. This altered scheme needs the calculation of the tangential damping matrix (C_T) and the tangential stiffness matrix (K_T).

If by $F_I = F_I(U_s, \dot{U}_s, \Pi, \dot{\Pi})$ we mean the internal forces

$$F_I = \begin{bmatrix} C_s & 0 \\ 0 & 0 \end{bmatrix} \begin{bmatrix} \dot{U}_s \\ \dot{\Pi} \end{bmatrix} + \begin{bmatrix} K_s & -K_c \\ 0 & K_f \end{bmatrix} \begin{bmatrix} U_s \\ \sigma(\Pi, \dot{\Pi}) \end{bmatrix}, \tag{4.26}$$

we have

$$C_T = \frac{\partial F_I}{\partial(\dot{U}_s, \dot{\Pi})} = \begin{bmatrix} C_s & 0 \\ 0 & 0 \end{bmatrix} + \begin{bmatrix} K_s & -K_c \\ 0 & K_f \end{bmatrix} \begin{bmatrix} I & 0 \\ 0 & \dot{\Sigma} \end{bmatrix}, \tag{4.27}$$

where $\dot{\Sigma} = \text{Diag}\left[\frac{\partial\sigma(\Pi_j, \dot{\Pi}_j)}{\partial\dot{\Pi}_j}\right]$ and

$$K_T = \frac{\partial F_I}{\partial(U_s, \Pi)} = \begin{bmatrix} K_s & -K_c \\ 0 & K_f \end{bmatrix} \begin{bmatrix} I & 0 \\ 0 & \Sigma \end{bmatrix}, \tag{4.28}$$

where $\Sigma = \text{Diag}\left[\frac{\partial\sigma(\Pi_j, \dot{\Pi}_j)}{\partial\Pi_j}\right]$.

If we instead use Eq. (3.72), i.e.,

$$F_I = \begin{bmatrix} C_s & -K_c \\ 0 & K_f \end{bmatrix} \begin{bmatrix} I & 0 \\ 0 & B \end{bmatrix} \dot{X} + \begin{bmatrix} K_s & -K_c \\ 0 & K_f \end{bmatrix} \begin{bmatrix} I & 0 \\ 0 & A \end{bmatrix} X, \tag{4.29}$$

where $X = \begin{bmatrix} U_s & \Pi \end{bmatrix}^T$, we get

$$C_T = \frac{\partial F_I}{\partial \dot{X}} = \begin{bmatrix} C_s & -K_c \\ 0 & K_f \end{bmatrix} \begin{bmatrix} I & 0 \\ 0 & B \end{bmatrix} \tag{4.30}$$

and

$$K_T = \frac{\partial F_I}{\partial X} = \begin{bmatrix} C_s & -K_c \\ 0 & K_f \end{bmatrix} \begin{bmatrix} 0 & 0 \\ 0 & B' \end{bmatrix} + \begin{bmatrix} K_s & -K_c \\ 0 & K_f \end{bmatrix} \begin{bmatrix} I & 0 \\ 0 & A'+A \end{bmatrix}, \tag{4.31}$$

where

$$A' = \text{Diag} \left[\frac{\partial \alpha(\Pi_j)}{\partial \Pi_j} \cdot \Pi_j \right],$$

$$B' = \text{Diag} \left[\frac{\partial \beta(\Pi_j)}{\partial \Pi_j} \cdot \dot{\Pi}_j \right].$$

Finally, the constitutive law to be used in the numerical experiments described in (2.28)-(2.29) yields

$$C_T = \begin{bmatrix} C_s & 0 \\ 0 & 0 \end{bmatrix}, \tag{4.32}$$

$$K_T = \begin{bmatrix} K_s & -K_c \\ 0 & K_f \end{bmatrix} \begin{bmatrix} I & 0 \\ 0 & A'+A \end{bmatrix}, \tag{4.33}$$

and

$$A'+A = \text{Diag} \left[\frac{\partial \alpha(\Pi_j)}{\partial \Pi_j} \Pi_j + \alpha(\Pi_j) \right]$$

will have a zero diagonal element whenever the corresponding nodal point is cavitating i.e., when $\Pi_j \leq -p_0/c^2$, while those corresponding to a non-cavitating nodal point will take a constant value, c^2.

In order to prevent frothing (see Section 3.5), artifical damping is introduced in the following manner. Let

$$\sigma(\Pi_j, \dot{\Pi}_j) = D \, \Delta t \, c^2 \, \dot{\Pi}_j + \alpha(\Pi_j) \cdot \Pi_j,$$

where Δt is the time step used and D is a dimensionless damping coefficient. The matrix B in Eq. (4.29) becomes

$$B = D \cdot \Delta t \, c^2 \, I.$$

This does not affect K_T because B' = 0 but C_T is changed according to Eq. (4.30).

At any time station we wish to satisfy the following equation

$$M\ddot{X}_{n+1} + F_{I,n+1} = L_{n+1},$$

where M is defined in Eq. (3.71). $F_{I,n+1} = F_I(X_{n+1}, \dot{X}_{n+1})$ is the approximation to the internal forces at time station t_{n+1}, X_{n+1} is the calculated approximation to $X(t_{n+1})$ and similarly for $\dot{X}_{n+1}$ and $\ddot{X}_{n+1}$. Furthermore, the calculated approximations should satisfy Eqs. (4.22)-(4.23).

As mentioned at the beginning of this subsection, the nonlinear calculation starts with a linear one as described in subsection 4.3.2. When the check in step 6 of that scheme indicates a cavitating nodal point, we alter the scheme as follows:

1. Use the last non-cavitated values of X, $\dot{X}$ and $\ddot{X}$ as initial values.

2. Set the iteration counter i = 0.

3. Calculate the predictor values (see Eqs. (4.24)-(4.25))

$$X^i_{n+1} = X^p_{n+1},$$

$$\dot{X}^i_{n+1} = \dot{X}^p_{n+1},$$

$$\ddot{X}^i_{n+1} = 0.$$

4. Calculate the residual forces

$$F^{i}_{res} = L_{n+1} - M\ddot{X}^{i}_{n+1} - F_{I,n+1}.$$

5. Form, if necessary, the effective stiffness matrix

$$K_{eff} = \frac{1}{\Delta t_n^2 \beta} M + \frac{\gamma}{\Delta t_n \beta} C_T + K_T.$$

6. Solve

$$K_{eff} \cdot \Delta X^{i} = F^{i}_{res}.$$

7. Calculate the corrector values

$$X^{i+1}_{n+1} = X^{i}_{n+1} + \Delta X^{i},$$

$$\ddot{X}^{i+1}_{n+1} = (X^{i+1}_{n+1} - X^{p}_{n+1})/\Delta t_n^2 \beta,$$

$$\dot{X}^{i+1}_{n+1} = \dot{X}^{p}_{n+1} + \Delta t \gamma \ddot{X}^{i+1}_{n+1}.$$

8. Check the convergence condition

$$|\Delta X^{i}| < \text{error}.$$

If this is not satisfied set i = i+1 and go to step 4, otherwise continue.

9. Use the corrector values as calculated values at time station t_{n+1}

$$X_{n+1} = X^{i+1}_{n+1},$$

$$\dot{X}_{n+1} = \dot{X}^{i+1}_{n+1},$$

$$\ddot{X}_{n+1} = \ddot{X}^{i+1}_{n+1}.$$

Set n = n+1 and check whether the values indicate a cavitating nodal point. If so, continue the calculation at the next time station according to step 1-9 in this subsection, otherwise continue according to step 1-6 in the preceding subsection.

5. NUMERICAL EXAMPLES

The numerical examples presented in this chapter represent some of the different types of problems that this work is able to deal with. The geometry of the examples is deliberately kept simple, because only in a simple geometry can the reader's intuition guide his expectation of what happens in a specific problem. Also, if something unexpected happens, in a simple problem it is possible to trace this odd behaviour back as an outcome of the coupling between the two domains, and thereby to appreciate how well the models described in this work represent real conditions.

The examples are organized in three sections

excitation in the fluid,
excitation on the structure,
transient excitation with a cavitating fluid.

The first two sections are divided into two subsections, for harmonic excitation and transient excitation. In the linear cases we use pressure formulation in the fluid because pressure is an easily visualized field.

5.1 Excitation on the structure

The example chosen for illustrating excitation on the structure is a rectangular fluid domain with stiff boundaries and in the middle, dividing the fluid into two parts, a thin structure. The three dimensional counterpart is shown in Fig. 5.1: a metal sheet is mounted inside a closed room with rigid walls.

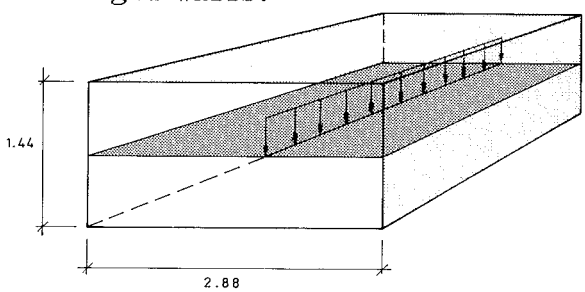

Figure 5.1. The three dimensional example for structural excitation

The air on one side of the steel sheet is not allowed to pass to the other side.

Both in the harmonic case and the transient case, the load is applied along the centre line of the metal sheet. The metal sheet is simply supported along the edges parallell to the load and is free to move along the other edges. The Poisson's ratio is set to zero. The membrane action is neglected.

The two dimensional counterpart, i.e. the cross-section of the room in Fig. 5.1, is divided into 648 fluid elements and 12 beam elements corresponding to 740 fluid degrees of freedom and 36 structural degrees of freedom. Each fluid element is square with a side length of 8 cm.

The beam elements are given data corresponding to a 2 mm steel sheet.

length = 24 cm,
E = $0.2 \cdot 10^{12}$ Pa,
A = $0.2 \cdot 10^{-2}$ m^2,
I = $0.67 \cdot 10^{-9}$ m^4,
Mass = 15.66 kg/m.

The fluid mesh is shown in Fig. 5.2. The problem has two symmetry axes that are taken into consideration in the calculation, and only one-quarter of the mesh is therefore used.

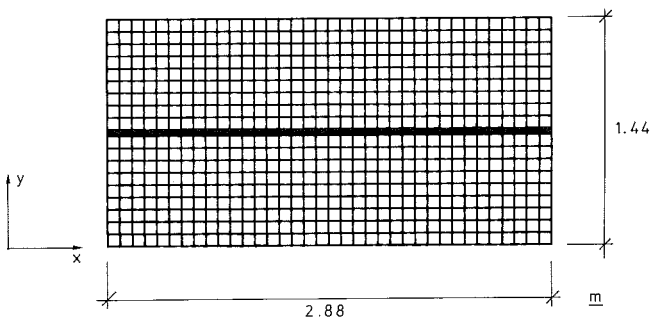

Figure 5.2. The fluid mesh and the intersecting beam

5.1.1 Harmonic excitation

The force applied to the structure is a vertical harmonic point load at the centre of the structure.

The discretized load vector is

$$L_s^e = [0...-1...0]^T e^{i\omega t} f(\omega) \qquad (5.1)$$

where the only non-zero element is the y-direction at the centre of the beam. If we neglect the initial state we get

$$(K - \omega^2 M)X = L_s^e \qquad (5.2)$$

This system is solved for $\omega/2\pi$ between 100 Hz and 400 Hz in steps of 2 Hz with $f(\omega) = 4.0$ and for three cases

A. A simple structure with no interaction,
B. The box filled with air,
C. The box filled with water.

'Filled with air' means that ρ = 1.29 kg/m^3 and c = 340 m/s while 'filled with water' means that ρ = 1000 kg/m^3 and c = 1500 m/s.

An eigenvalue calculation for the beam on its own gives the following six resonance frequencies in the interval between 100 Hz and 400 Hz:

101.4 Hz,
140.7 Hz,
191.8 Hz,
257.0 Hz,
333.4 Hz,
395.6 Hz.

Note that the last frequency corresponds to the highest bending mode that the structural discretization is able to deal with.

Below, in Figs. 5.3-5.5, the vertical displacement of the structure at three nodes is shown.

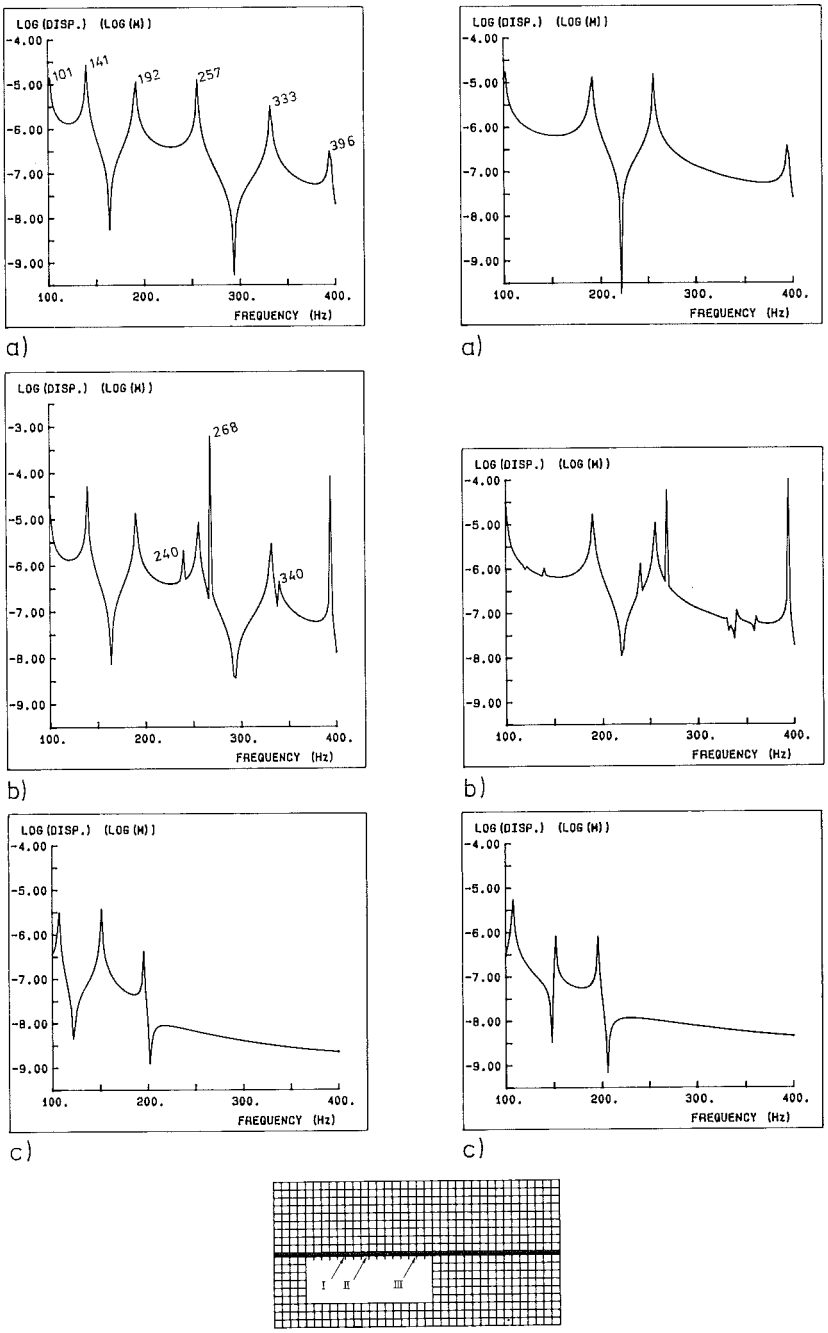

Figure 5.3-4. Logarithmic displacement in metres at node I (5.3) and node II (5.4) versus frequency
a) non-interacting beam, b) filled with air
c) filled with water

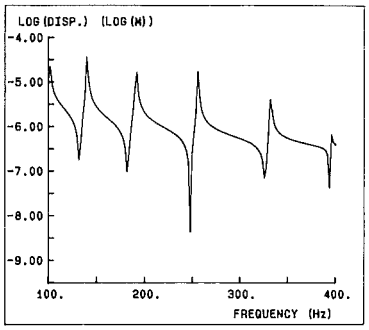

a)

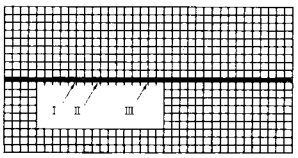

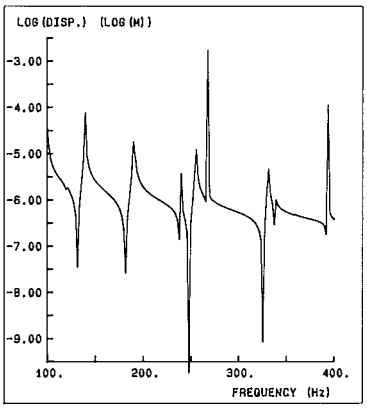

b)

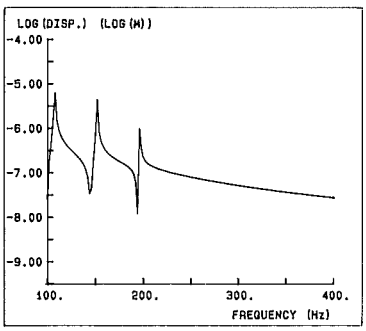

c)

Figure 5.5. Logarithmic displacement in metres at node III versus frequency
a) non-interacting beam, b) filled with air,
c) filled with water

When the beam interacts with air the displacement-frequency diagram shows that, apart from different amplitudes, new peaks have developed at 240 Hz, 268 Hz and 340 Hz. The first is close to a crucial wavelength for the fluid domain, namely 1.44 m, but 268 Hz is harder to identify. In Fig. 5.4, more fluid tracks can be traced; 118 Hz and 354 Hz correspond to the wave lengths 2.88 m and 0.96 m, respectively. The latter is one-third of the transverse dimension. When the structure interacts with water, it is clear that the resonance frequencies are considerably displaced towards lower values. The former highest structural resonance at 394 Hz is now located at 196 Hz.

Finally, the contour levels for air pressure measured in decibels for certain frequencies are shown. Note that the first frequency corresponds to a wave length equal to the horizontal transverse dimension, while the second frequency is in harmony with the height of the fluid domain. 340 Hz is just above a structural resonance which the pattern indicates, while at 360 Hz the fluid resonance is preferred; the horizontal transverse dimension is three times the wave length.

120 Hz

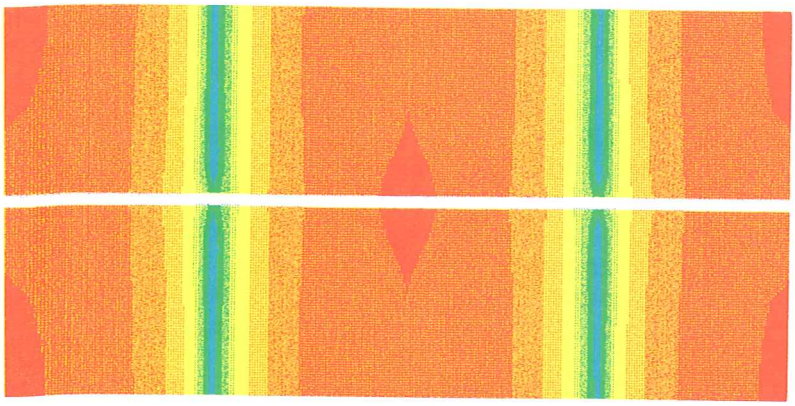

230 Hz

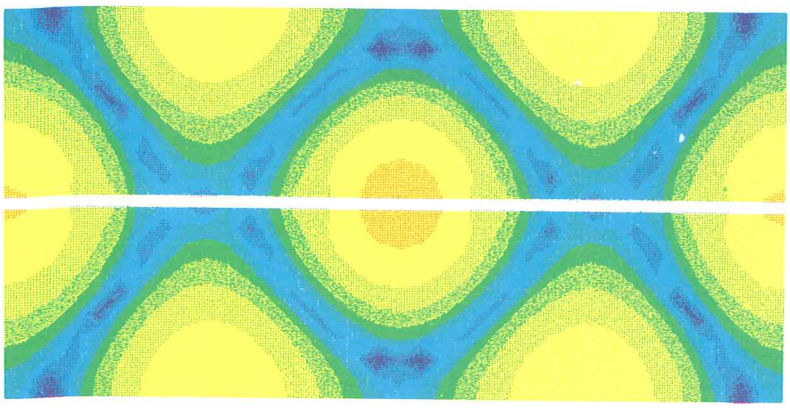

280 Hz

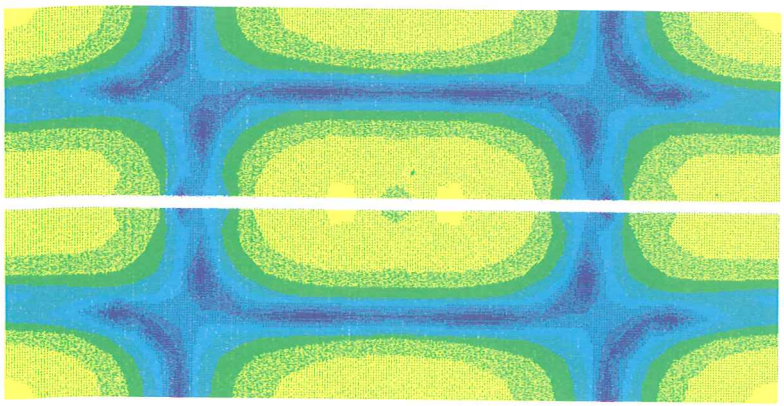

340 Hz

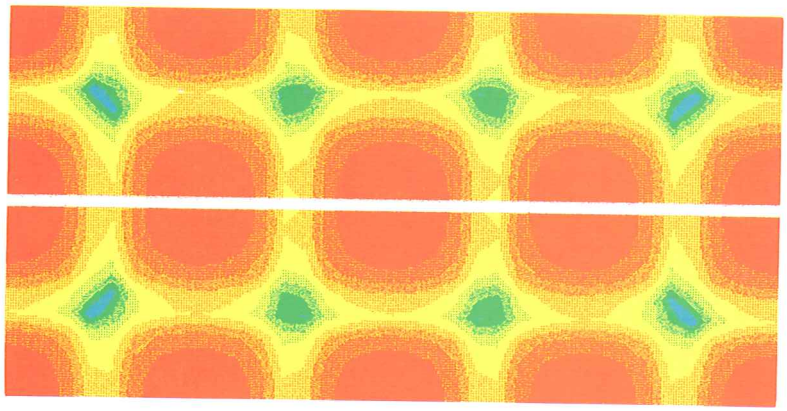

360 Hz

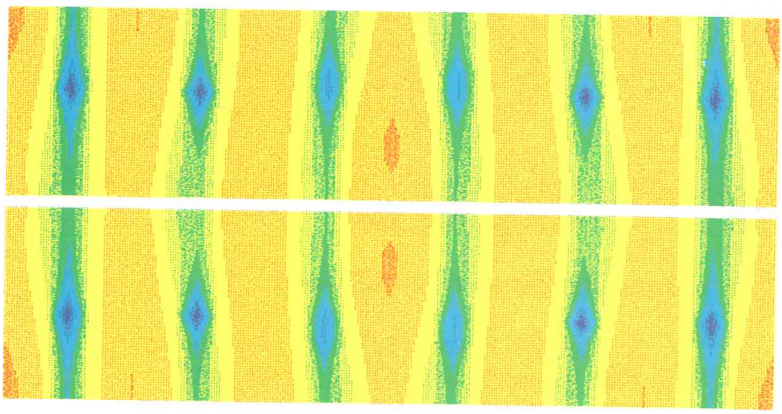

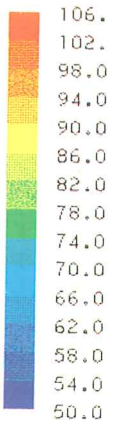

5.1.2 Transient excitation

The force applied to the structure is a vertical point load at the centre of the structure and the corresponding discretized load vector is

$$L_s^e = [0...-1...0]^T f(t) \qquad (5.3)$$

In the calculation, f(t) is given the following time history

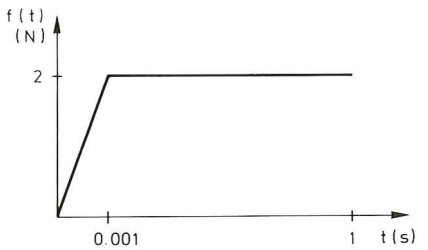

Figure 5.6. Time history for the applied transient structural load

Two calculations were performed,

A. A simple beam with no interaction,
B. The beam interacting with air.

The calculations were performed over 1 second using the implicit algorithm described in Section 4.3 using 4 time stations between 0 and 0.002 s and beyond that 499 time stations. During the first interval, all four result vectors were saved for plotting and every fourth vector was saved thereafter.

The structural displacement at the locations I, II and III (see Fig. 5.7) is shown below. At the centre where the load is applied, the non-interacting beam has a peak value of 14 mm while in the interacting case, the peak value is approximately 0.2 mm. This is natural because even small displacements of the structure create high fluid pressures in the closed box. What is somewhat more surprising is the way the high-frequency content is amplified for the interacting beam. Note also that, for the interacting beam, while the centre node (I) vibrates below its unloaded

position, node III vibrates above that position, quite contrary to the behaviour of the non-interacting beam.

Finally, the lower part of 'snapshots' of the air pressure levels at six time stations are shown.

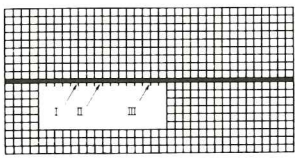

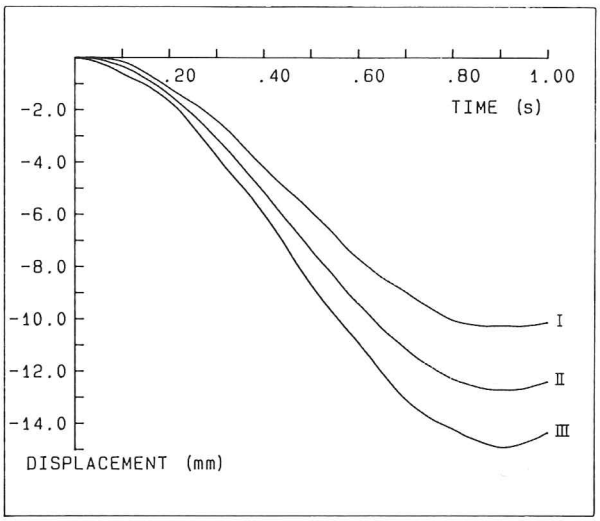

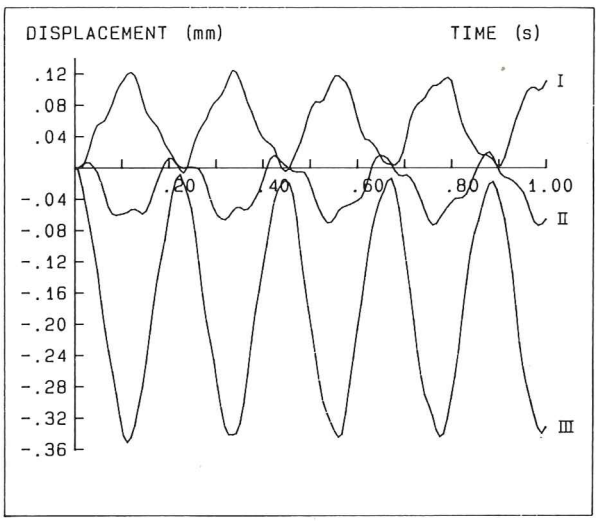

Figure 5.7. The displacement time history for a non-interacting beam (top) and an interacting beam (bottom).

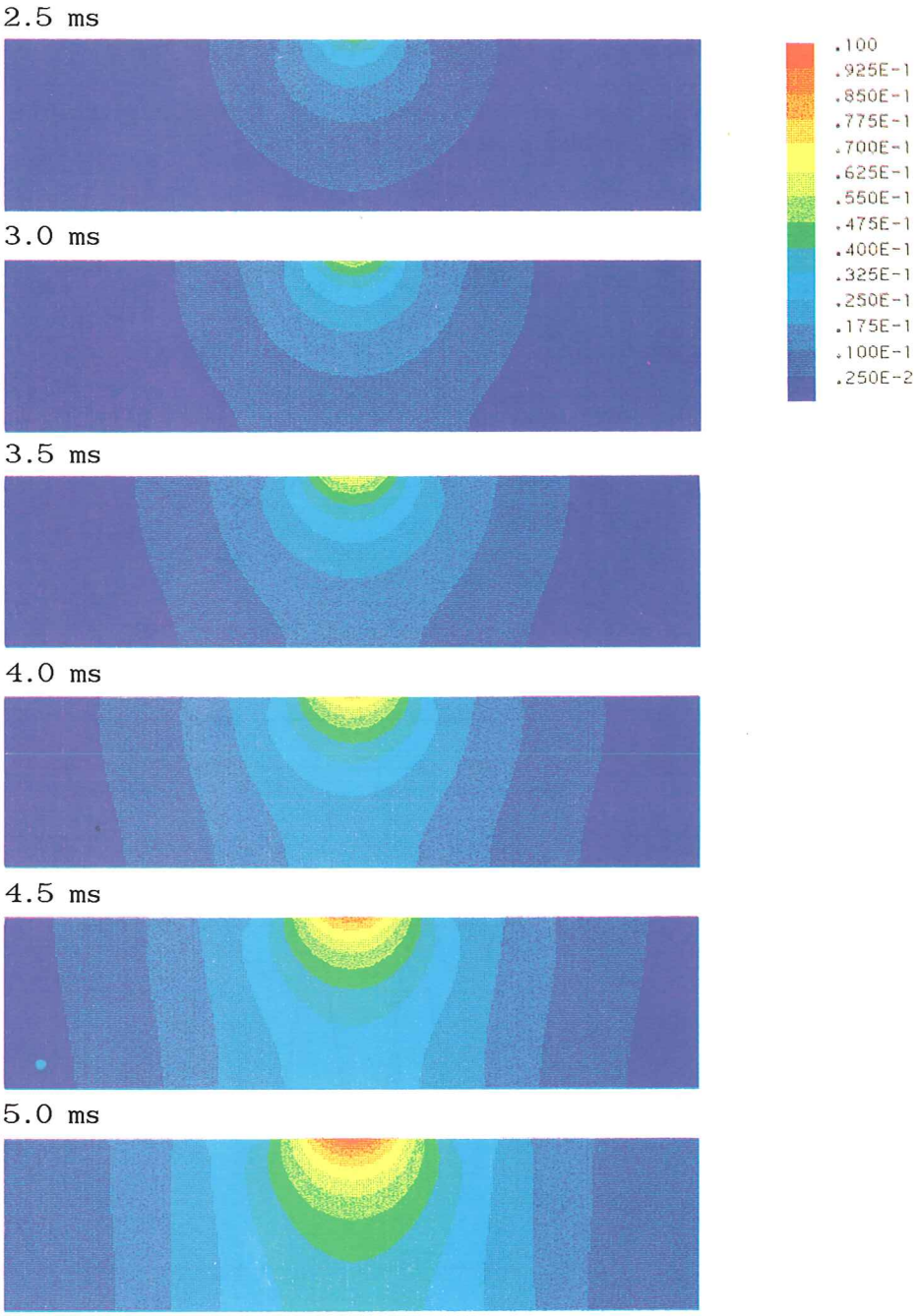
2.5 ms
3.0 ms
3.5 ms
4.0 ms
4.5 ms
5.0 ms
.100
.925E-1
.850E-1
.775E-1
.700E-1
.625E-1
.550E-1
.475E-1
.400E-1
.325E-1
.250E-1
.175E-1
.100E-1
.250E-2

5.2 Excitation in the fluid

The example chosen is a rectangle of dimensions indicated in Fig. 5.8.

The interior of the rectangle is divided into 648 fluid elements, corresponding to 703 fluid degrees of freedom. Each fluid element is square with a side length of 10 cm and has physical parameters corresponding to air, that is

$$\rho = 1.29 \text{ kg/m}^3,$$
$$c = 340 \text{ m/s}.$$

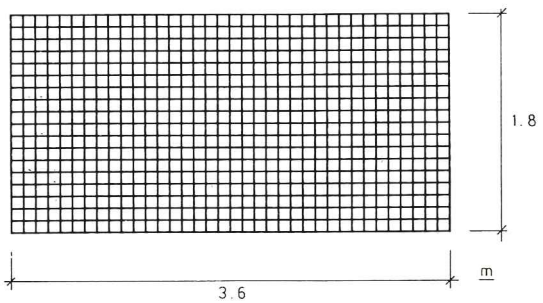

Figure 5.8. The dimensions and the mesh for the example

The boundary of the rectangle is divided into 36 beam elements corresponding to 108 degrees of freedom, where each beam element covers 3 fluid elements at the interface. The beam elements are given the following physical values

	Harmonic calculations		Transient calculations
Length (m)	0.3	0.3	0.3
E (Pa)	$0.2 \cdot 10^{12}$	$0.2 \cdot 10^{12}$	$0.2 \cdot 10^{12}$
A (m^2)	$0.1 \cdot 10^{-2}$	$0.2 \cdot 10^{-2}$	$0.4 \cdot 10^{-2}$
I (m^4)	$0.83 \cdot 10^{-11}$	$0.67 \cdot 10^{-9}$	$0.53 \cdot 10^{-8}$
mass (kg/m)	7.83	15.66	31.32

In both cases, the source of influence is placed in the centre of the rectangle as a point source. The displacements of the structure in the four corners are locked and the symmetric nature of the problem is exploited.

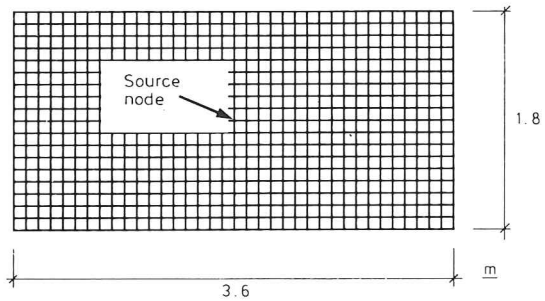

Figure 5.9. Location of the source node

This two-dimensional problem has a three-dimensional counterpart, a parallelepiped box whose two opposite sides are rigid. The other four sides are elastic and the source is a line source between the two rigid sides. (See Fig. 5.10). The data given to the structure correspond to a 1 mm and 2 mm steel sheet in the harmonic case and a 4 mm steel sheet in the transient case.

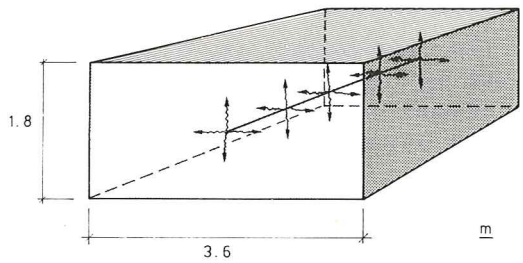

Figure 5.10. The three dimensional counterpart to the problem in this section

5.2.1 Harmonic excitation

The system is driven by the added fluid mass per unit area and time (volume velocity), denoted q in subsection 2.2. We assume

$$q(x,y,t) = A(\omega)\cdot\delta_c(x,y)\cdot e^{i\omega t}, \qquad (5.4)$$

i.e., that q has a harmonic variation in time (ω = angular frequency). δ_c is the Dirac function at the centre of the rectangle. $A(\omega)$ is a scalar function allowing an amplitude variation by frequency. Then

$$\frac{\partial q}{\partial t} = A(\omega)\ \delta_c(x,y) i\omega\ e^{i\omega t} \qquad (5.5)$$

and

$$(L_q)_r = \begin{cases} A(\omega)\cdot i\cdot\omega\ e^{i\omega t} & r = \text{centre node} \\ 0 & r \neq \text{centre node} \end{cases}$$

is the right-hand side as defined in Eq. (3.36), (see also Eq. (3.14)).

If we neglect the initial state

$$(K + \omega^2 M)X = A(\omega)\cdot i\cdot\omega\ \boldsymbol{\delta}, \qquad (5.6)$$

where $\boldsymbol{\delta}$ is a column matrix and

$$(\boldsymbol{\delta})_r = \begin{cases} 1 & r = \text{centre node} \\ 0 & r \neq \text{centre node} \end{cases}$$

and X contains the complex amplitude of the structural vibration and of the fluid pressure. The phase angle is obviously $\pm 90^o$ in every degree of freedom.

The system is solved for $\omega/2\pi$ between 50 Hz and 300 Hz in steps of 5 Hz and for three cases:

A. Stiff boundary,
B. Elastic boundary (2 mm steel sheet),
C. Elastic boundary (1 mm steel sheet).

The fluid pressure is measured in decibels. The displacement amplitude is also represented on a logarithmic scale, $\log|U_s|$, in the diagrams below. In Fig. 5.11 and

5.13 $A(\omega) \equiv 1$, i.e., the source has a constant amplitude variation. Fig. 5.11 a) and b) show the response in the centre node where q is applied.

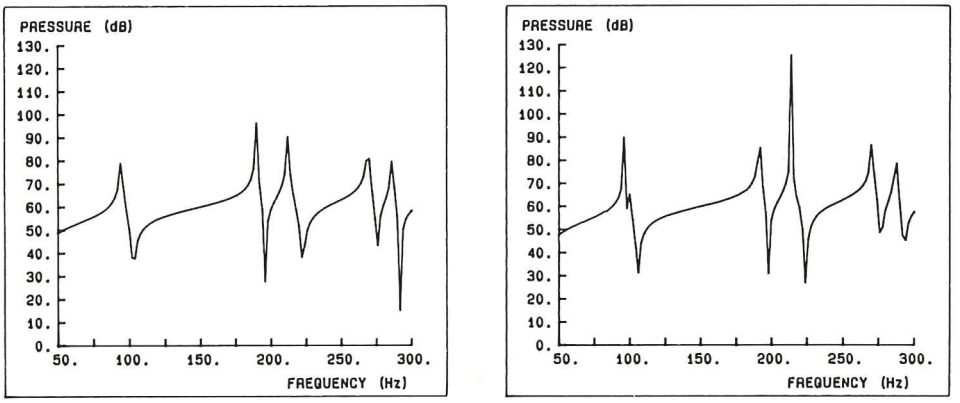

a) b)

Figure 5.11. The decibel (frequency) history at the centre node with a) stiff boundary b) elastic boundary (2 mm steel sheet)

The responses at three other fluid nodes and one structural node, located as indicated in Fig. 5.12 are presented below. In Fig. 5.13, the left column represents the case with a stiff boundary and the right column the case with a 2 mm steel sheet boundary.

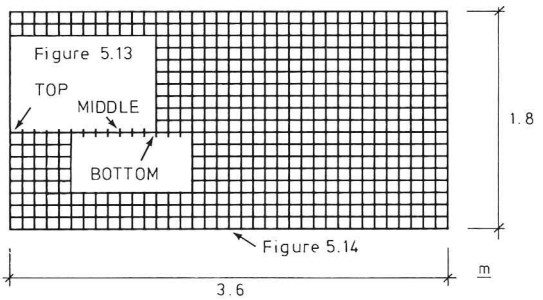

Figure 5.12. Location of nodes for frequency response presentation in Fig. 5.13-5.14

An eigenvalue analysis of the structure on its own gives the following eigenvalues in the range 50 Hz to 300 Hz: 98, 127, 154, 182, 220 and 247 Hz. In Fig. 5.14, these are marked '*'.

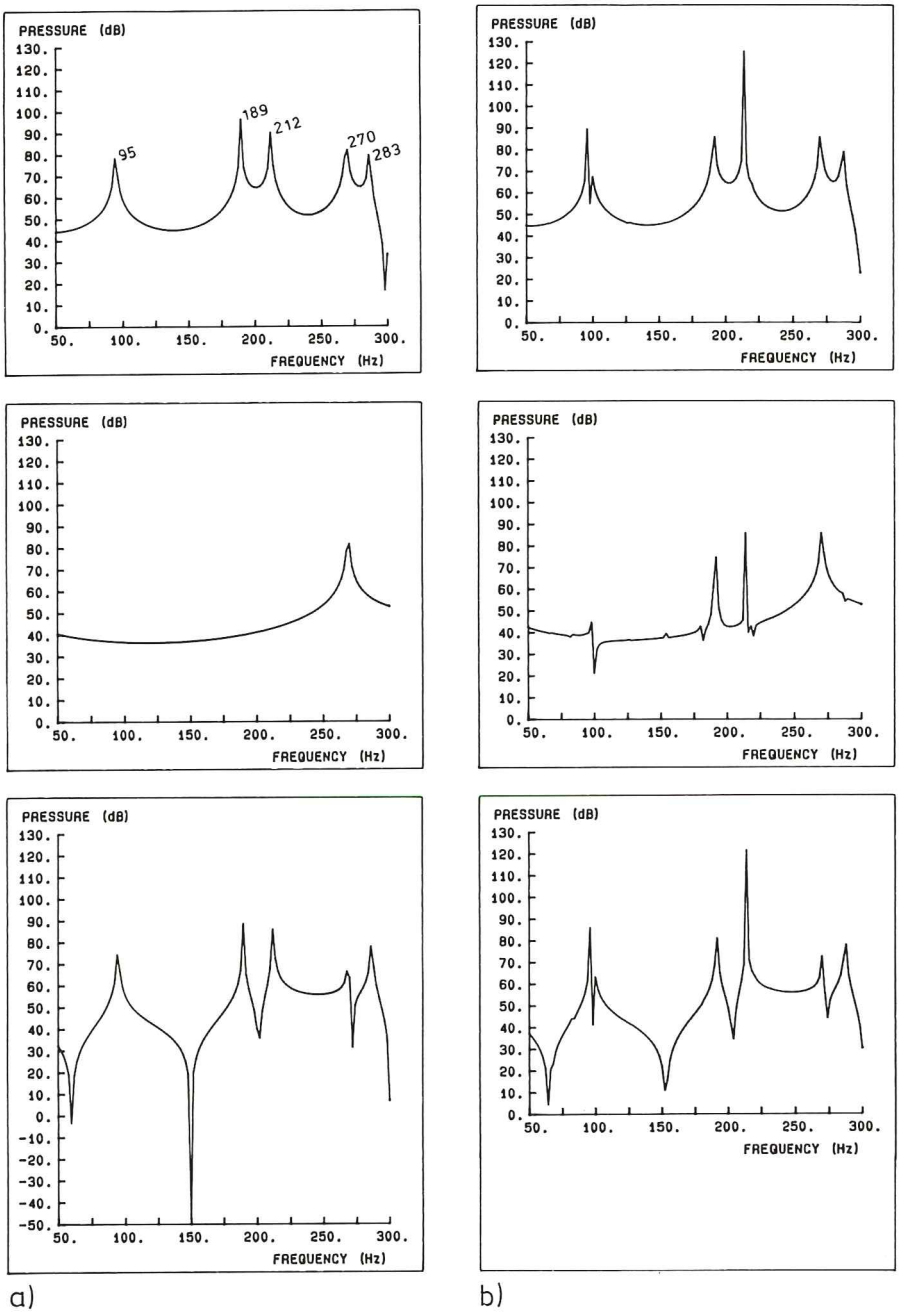

Figure 5.13 a) and b). Fluid pressure amplitude measured in decibels as a function of frequency at three different nodes, for a a) stiff and b) elastic boundary, respectively

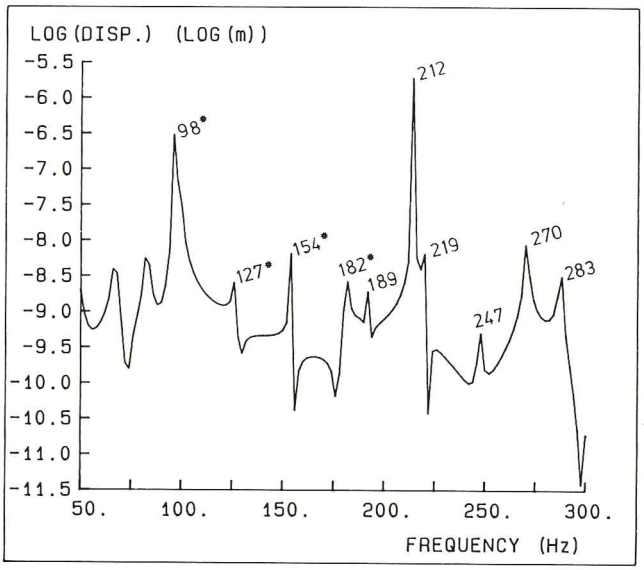

Figure 5.14. Structural displacement in the middle of the horizontal boundary (2 mm steel sheet) as a function of frequency

It is reasonable to expect resonance at frequencies for which the corresponding wavelengths are in harmony with the dimensions of the fluid domain (3.60 m × 1.80 m). Such frequencies are easily computed: 95, 189 and 283 Hz. In Fig. 5.13 (top left), these frequencies are indicated. Two other peaks are present at 212 Hz and 270 Hz. The latter corresponds to a wavelength in harmony with another characteristic distance in the fluid domain; $1.80/\sqrt{2}$. Those frequencies are also indicated in Fig. 5.14. Comparing the left column in Fig. 5.13 with the right column, representing the elastic boundary case, a new peak has entered representing the structural resonance at 98 Hz. Apart from this, the peaks differ in height and, above all, a careful measurement of their location shows that the peaks have shifted towards higher frequencies.

Some frequencies have been picked for colour plotting. The pictures show the air pressure level curves when the source node is normalized to 100 dB at all frequencies. In the elastic boundary case, the 1 mm steel sheet is chosen. At 100 Hz the wavelength almost coincides with the width of the fluid domain, which the colour plot clearly shows, while the frequency 190 Hz corresponds to a wavelength in harmony with both the height and the width of the fluid domain.

In Table 5.1, the original values at the centre are given. The difference between 100 dB and those values should be subtracted from the colour plots in order to achieve $A(\omega) \equiv 1$, as was used in the frequency response figures above.

Frequency (Hz)	a) Stiff boundary (dB)	b) Elastic boundary (dB)
100	51	82
145	59	59
190	96	73

Table 5.1. The original values at the centre node for certain frequencies.

Stiff boundary
100 Hz

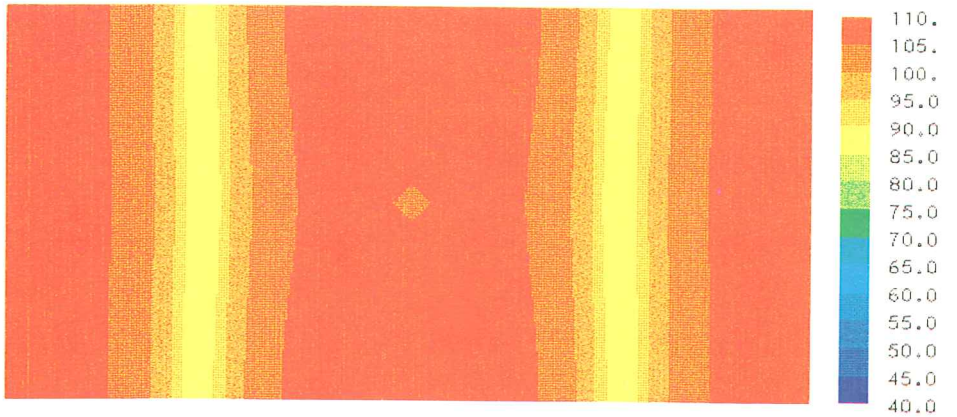

145 Hz

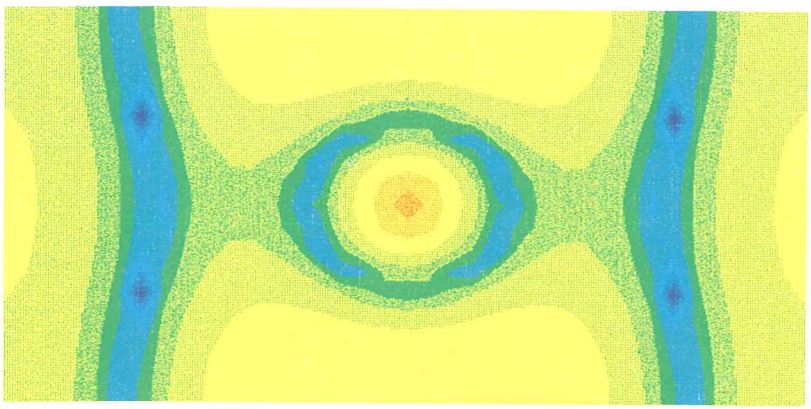

190 Hz

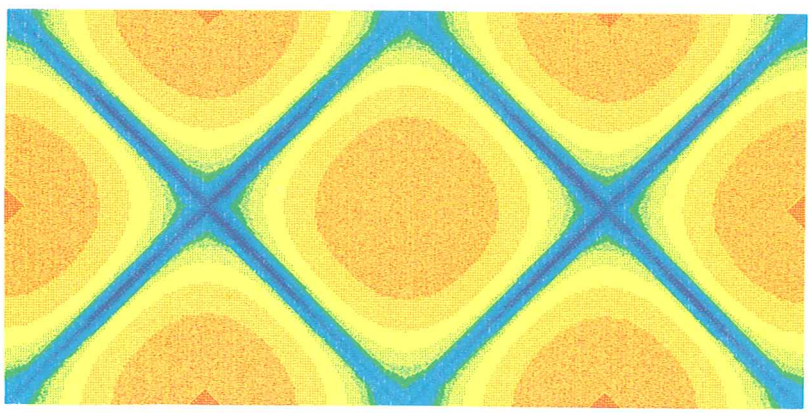

Elastic boundary (1 mm steel sheet)
100 Hz

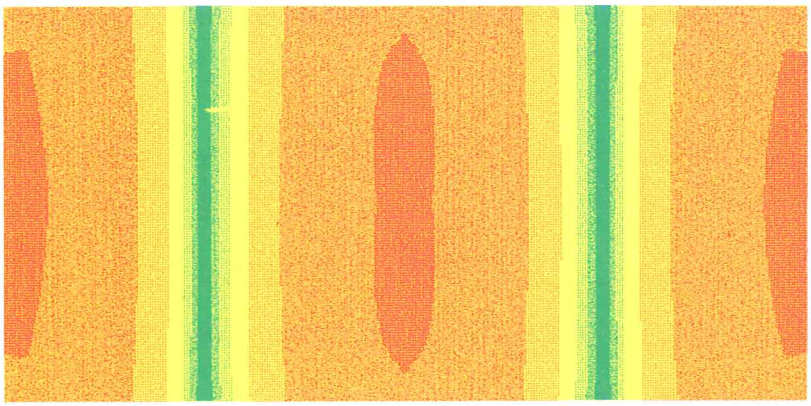

145 Hz

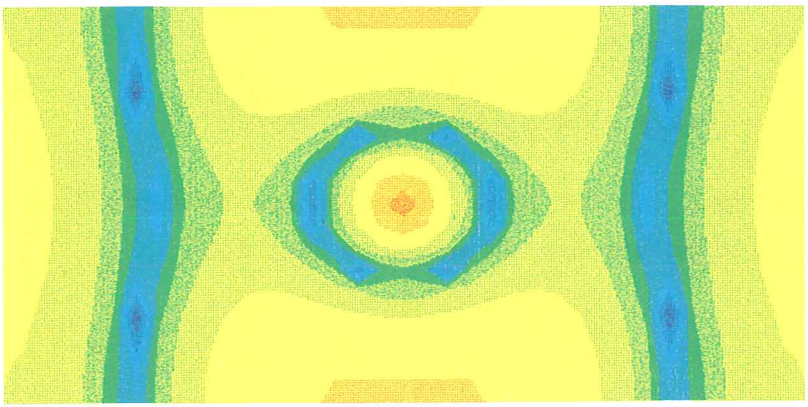

190 Hz

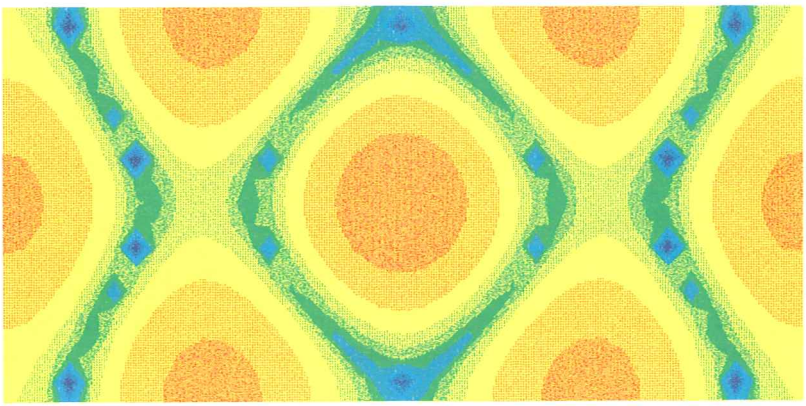

Fig. 5.15 shows the vibration shapes of the elastic boundary. The shapes are greatly exaggerated and only the displacement resultant is taken into consideration (no nodal rotation).

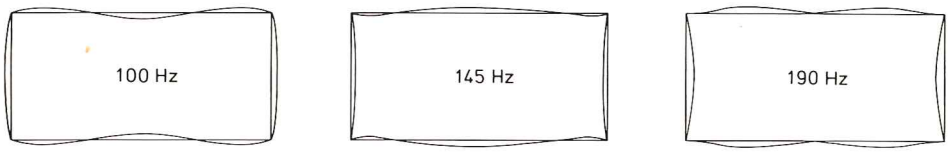

Figure 5.15. Vibration shapes for 1 mm steel sheet

5.2.2 Transient excitation

The fluid domain is exposed to a mass inflow represented by its second time derivative, $\dot{q}$

$$\dot{q}(x,y,t) = \delta_c(x,y) \cdot f(t), \tag{5.7}$$

where δ_c is the Dirac function and c stands for the centre. Its time history is shown in Fig. 5.16.

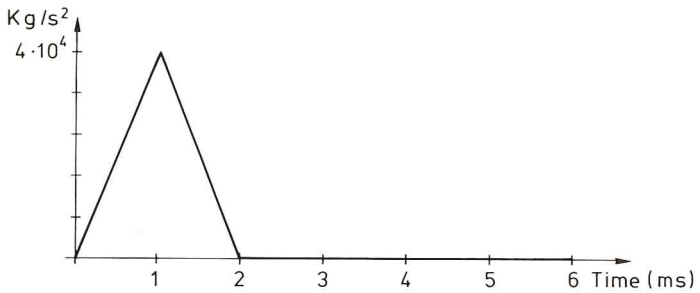

Figure 5.16. The source function applied at the centre

The corresponding mass velocity q is obtained by integration (see Fig. 5.17). A physical interpretation of q, as given in Fig. 5.17, would be a sudden discharge of fluid along the centre line in Fig. 5.10. The mass velocity rises during 2 ms to the sustained velocity.

The discrete system

$$M\ddot{X} + KX = L_q \tag{3.36}$$

is now solved, using the implicit algorithm described in Subsection 4.3.1. 300 time stations were used, equally distributed over the time interval 0 ms to 6 ms, i.e., the time steps used were $\Delta t = 2 \cdot 10^{-5}$ sec. In the interval from 0 ms to 2 ms, the results were saved for plotting every $4 \cdot 10^{-5}$ sec and, beyond that, every $16 \cdot 10^{-5}$ sec. In order to capture the high frequency content of the source function and to obtain a quantitatively reliable result in the neighbourhood of the source, a finer mesh is needed.

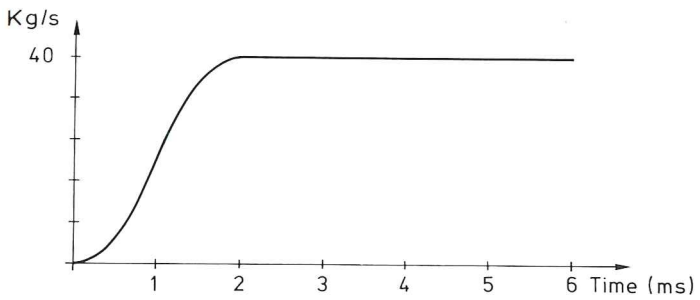

Figure 5.17. The volume velocity history to which the centre node is exposed

The colour plots show the pressure wave emerging from the centre. After 3 ms, the pressure wave reaches the closest structural part and starts to reflect against the wall. The incident wave and the reflected wave overlap at the boundary, which is well established after 4 ms. Finally, after 6 ms the wave reaches the most distant boundary and the reflected waves from the top and bottom overlap at the centre. Note that the colour scaling in the last 5 plots coincides.

1 ms

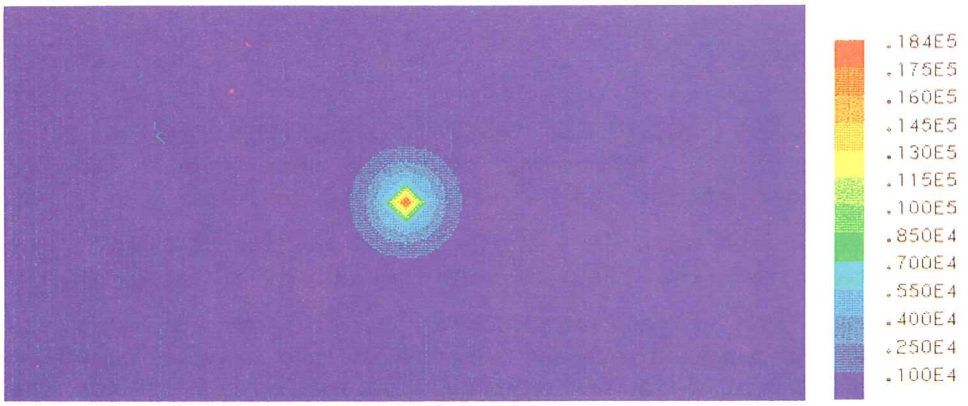
.184E5
.175E5
.160E5
.145E5
.130E5
.115E5
.100E5
.850E4
.700E4
.550E4
.400E4
.250E4
.100E4

2 ms

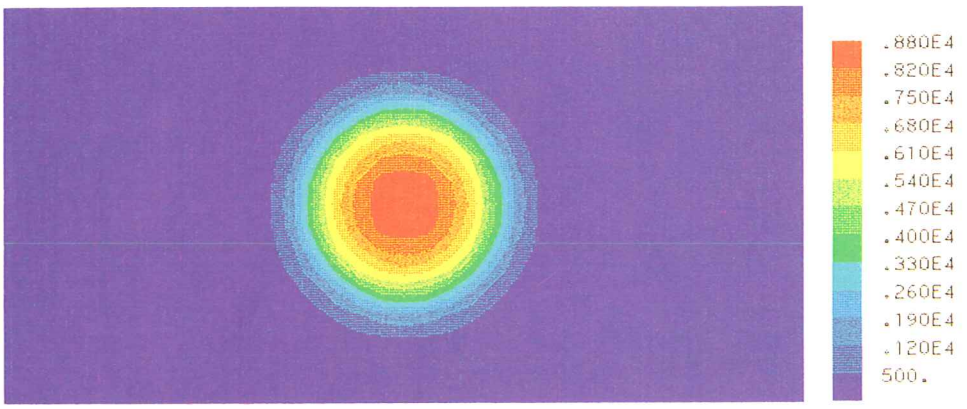
.880E4
.820E4
.750E4
.680E4
.610E4
.540E4
.470E4
.400E4
.330E4
.260E4
.190E4
.120E4
500.

3 ms

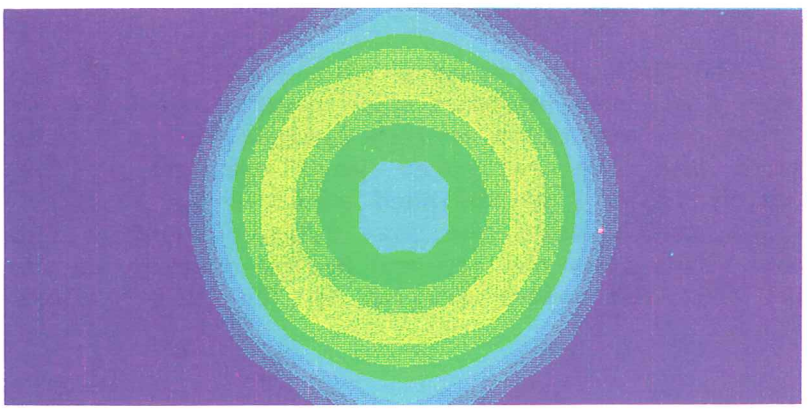

4 ms

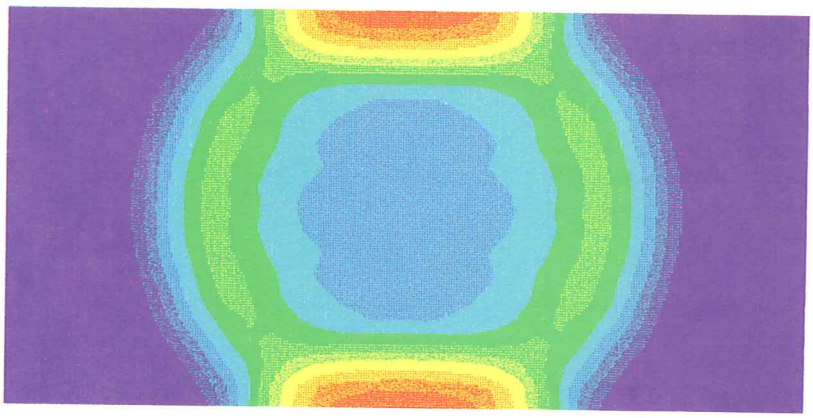

5 ms

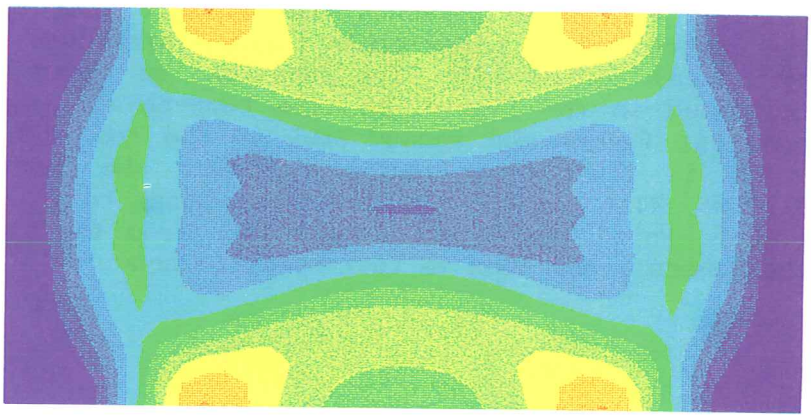

6 ms

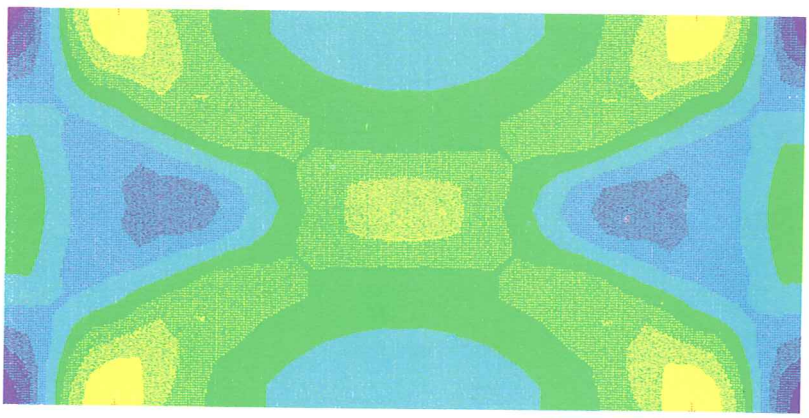

Fig. 5.18 shows the structural displacement during the last three milliseconds. The displacement is greatly exaggerated. In the left-hand picture, the maximum displacement is 0.9 mm.

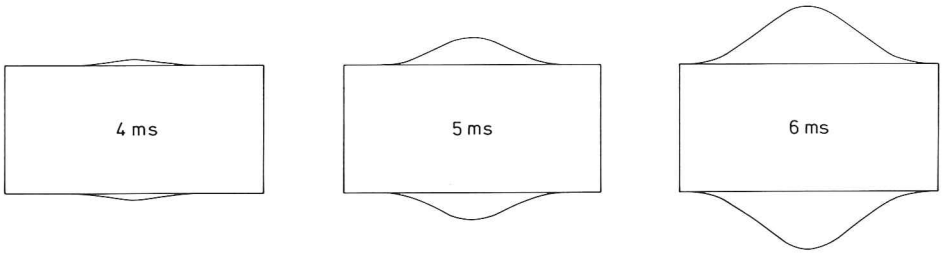

Figure 5.18. Deformed structural shape after 4 ms, 5 ms and 6 ms

Finally, Fig. 5.19 presents the pressure time history at the centre and at three other nodes distributed along the horizontal centre line. The locations of these nodes are indicated in the figure.The time between the peak in the top left figure and second peak in the top right figure, which is due to reflection against the boundary, is 4.12 ms. With c = 340 m/s this corresponds to approximately 1.40 m, which is the actual distance from the midpoint to the boundary and back to that specific node.

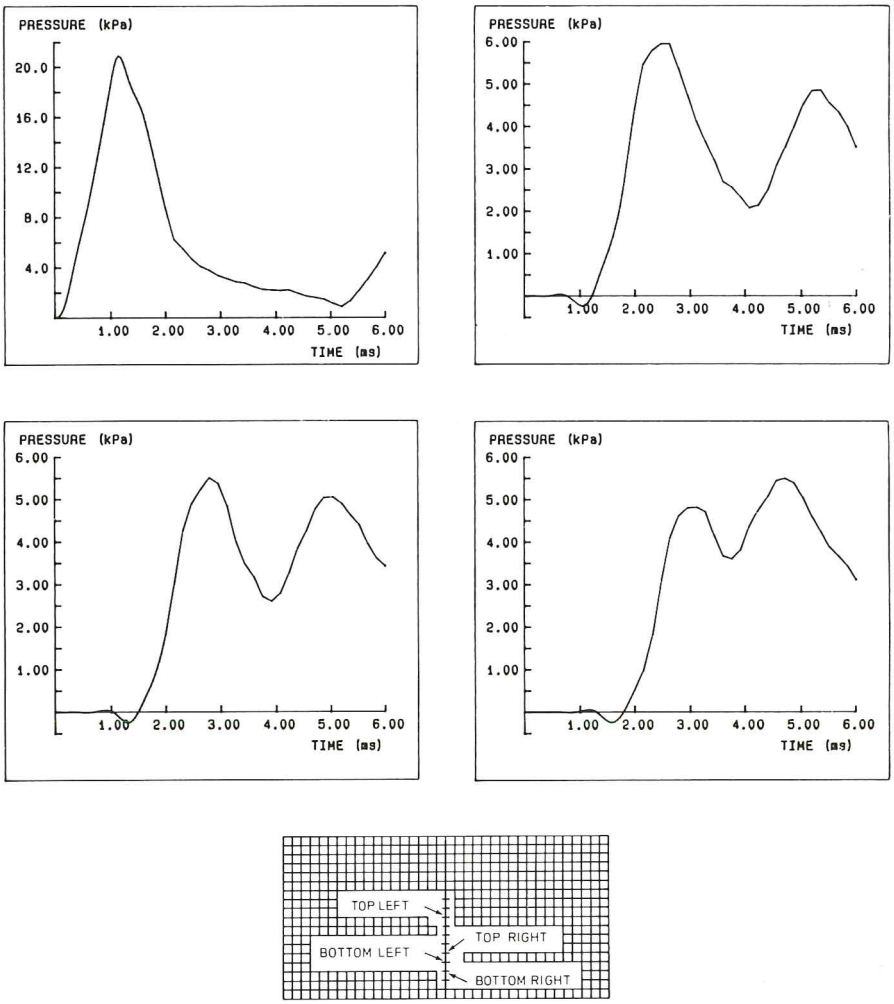

Figure 5.19. Pressure as a function of time

5.3 Transient excitation with regard to cavitation

The nonlinear fluid model presented in Sections 3.5-3.6 has been tested in one example. This example by Bleich-Sandler [6] is the only one in which an exact solution has been obtained. Originally, this is a one-dimensional problem, although the data for the numerical test correspond to the two-dimensional counterpart. The problem consists of a plate, initially at rest, on the surface of a semi-infinite space of fluid (Fig. 5.20). The surface mass is exposed to a plane pressure wave with a sudden rise and an exponential decay.

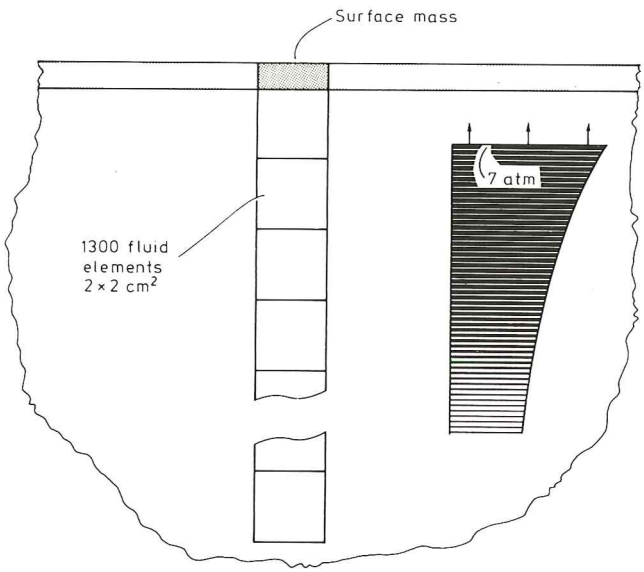

Figure 5.20. The Bleich-Sandler cavitating fluid example

The calculations were performed using 1300 fluid elements of 2 cm side length. This was enough to ensure that the boundary conditions at 'infinity' did not interfere with the interesting part of the solution. Physical data correspond to those used in Bleich-Sandler [6], although these are transformed into SI-units.

Speed of sound in the fluid $c = 1423.4$ m/s,
Speed of sound in the cavitated region $c_1 = 0$ m/s,

Density of the fluid $\rho_s = 999.83$ kg/m^3,

Surface mass density	$m_s = 144.68$ kg/m^2,
Atmospheric pressure	$P_A = 1.0133 \cdot 10^5$ Pa,
Peak value of the incident wave	$P_p = 7.1016 \cdot 10^5$ Pa,
Decay length of the incident wave	$L = 1.445$ m,
Acceleration due to gravity	$g = 9.8146$ m/s^2.

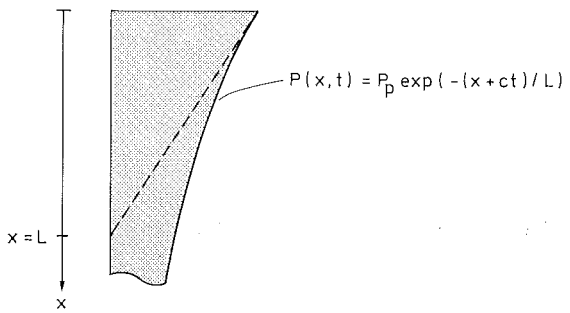

Figure 5.21. Incident plane pressure wave

The time integration procedure is described in Subsection 4.3.2. The check for convergence was made using the maximum norm, i.e.

$$\max_i \left| x_i \right| < \text{error}$$

and the error was set to 10^{-3}. Normally it took two iterations per time station to satisfy this condition, and never more than three iterations.

At the surface of the fluid, the hydrostatic pressure P_H was equal to the atmospheric pressure and increased linearly into the fluid half space consistent with the acceleration due to gravity and the fluid density. The calculations were performed over 13 milliseconds using 1950 time stations, i.e., the length of the time step was $6.667 \cdot 10^{-6}$ second. At time zero the pressure wave was initialized as though it was starting at infinity, i.e.,

$$\rho(x,0) = \frac{P_p \exp(-x/L)}{c^2},$$

$$\dot{\rho}(x,0) = -\frac{c}{L}\rho(x,0),$$

$$\ddot{\rho}(x,0) = \left(\frac{c}{L}\right)^2 \rho(x,0).$$

At each time station, a check was made for cavitating nodes, that is, whether

$$\rho(x,t) < P_H/c^2$$

In order to avoid numerical destruction of the wavefront it was 'ramped' over 5 elements and the time was measured from the arrival of half the 'ramped' front at the surface mass. This had no impact on the timing of the velocity peak but made the pressure wave act as intended behind the front. A check was also made to ensure that the pressure wave kept its profile. This check was located in time and space so as not to disturb the reflected wave or the cavitating zone. Four sets of runs were performed with different artificial damping coefficients D = 0.5, 0.25, 0.1 and 0. In Figs. 5.22, 5.23 and 5.25, the upward velocity of the surface mass for these cases is shown. The solid lines refer to the present analysis while the discrete symbols are taken from Bleich-Sandler [6]. (Note that the values in that paper are given in a non-dimensional form). The figures also show the upward velocity when no check for cavitation is made. As can be seen, the numerical results in the first cases are in excellent agreement with the analytical results and the smoothing effect of the artificial damping has only slight impact on the timing of the solution. The cavitating zone opens after 0.36 ms, i.e., after the peak velocity has occurred. After 6 ms the non-cavitating solution has a zero upward surface mass velocity while the cavitating fluid makes the surface mass velocity continue below zero. After 10.6 ms the cavitated zone closes and a secondary pressure wave reaches the surface mass after approximately 12 ms, which is clearly visible in Figures 5.22 and 5.23. Furthermore, there is a considerable difference in the peak displacement when the fluid is allowed to cavitate.

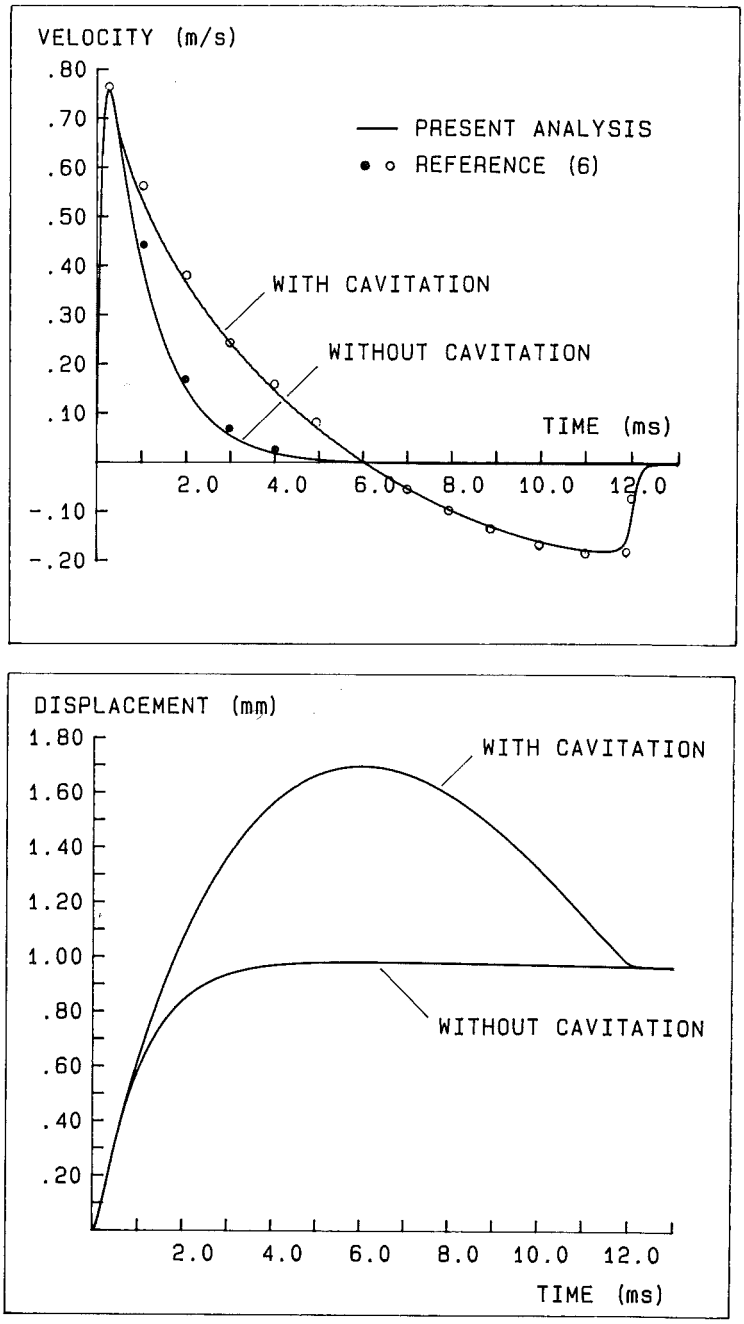

Figure. 5.22. Upward velocity and upward displacement of the surface mass, D = 0.5

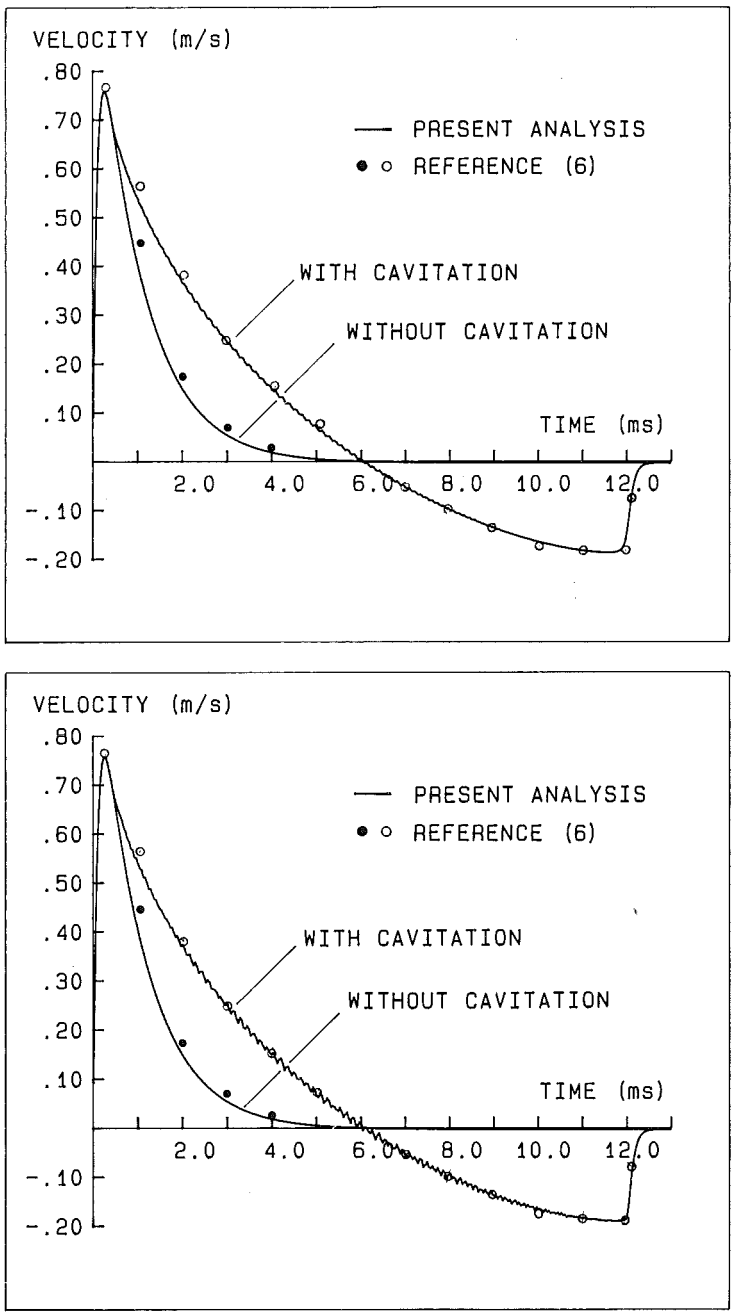

Figure 5.23. Upward velocity of the surface mass, D = 0.25 (top) and D = 0.1 (below)

In Fig. 5.24 the cavitating zone is shown for D = 0.5 and D = 0.1. The interfaces between cavitated and non-cavitated regions are made up of horizontal lines because only cavitated nodes are displayed. The result agree closely with those of Bleich-Sandler [6]. The cavitated region never reaches the surface and closes after 10.6 ms. For D = 0.1 the upper interface is 'fragmentized' due to the spurious pressure oscillations. These oscillations have a devastating effect on the solution when D = 0. Fig. 5.25 shows the upward velocity of the surface plate for this case.

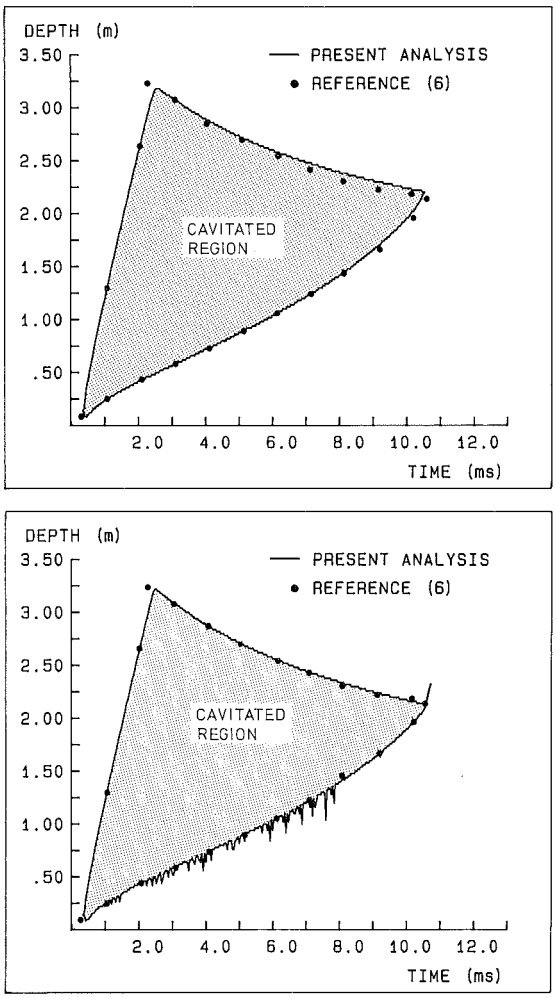

Figure 5.24. Time history of the cavitated region, D = 0.5 (top) and D = 0.1 (below)

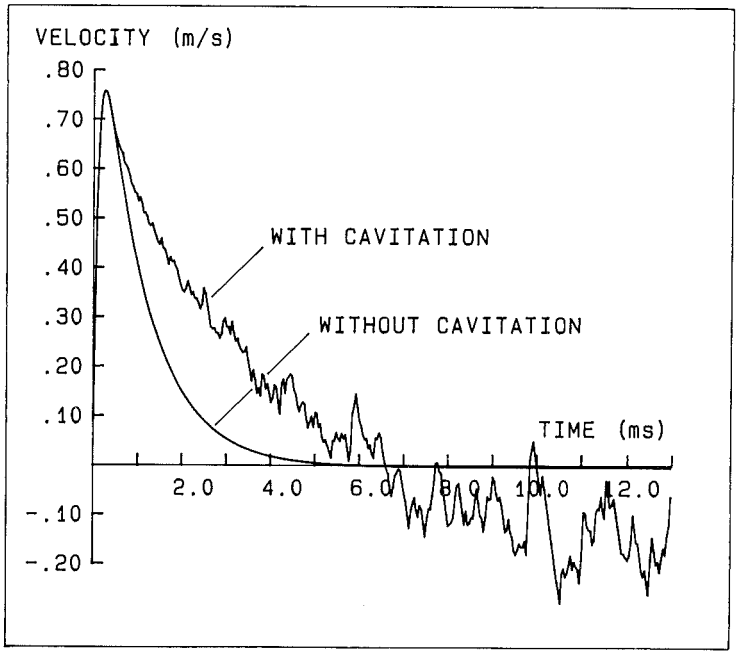

Figure 5.25. Upward velocity of the surface mass, D = 0

6. CONCLUDING REMARKS

6.1 Conclusions

This study is concerned with finite element modelling of fluid-structure interaction. The structure is not merely a boundary condition in a fluid domain, but the dynamic behaviour of the structure interacts with the fluid. Different primary variables are used in the fluid domain and different source functions for transient and harmonic analysis are described for every choice of primary variable. It is thus my belief that this work presents a general and concise description of situations in which different fluid 'load' conditions can be simulated. In the numerical examples, cases with both fluid and structural source functions are illustrated for both transient and harmonic cases.

Symmetric formulations are derived by using mixed fluid primary variables, one of which is basically similar to the one given by Ohayon [29], although the version presented here is applicable to general transient fluid source functions. The other formulations are new with respect to transient analysis, although recently and parallel to this work, similar formulations for eigenvalue problems have been proposed by Felippa [18].

Some nonlinear behaviour in the fluid domain is also taken into consideration. The model can handle wave propagation in which the speed of sound is a function of the primary variable. As a special application, the model is applied to cavitation in the fluid due to reflection against an elastic boundary.

The nonlinear model proposed in this study is preferable to the one presented by Newton [23]-[26] and Felippa [17] when a more sophisticated equation of state for a cavitating fluid is required and also if a nonlinear speed of sound is to be considered. Furthermore, it seems that special boundary conditions are more easily dealt with in the present formulation. The finite element model is verified against an analytical solution given by Bleich and Sandler [6] and the agreement between analytic and numerical results is very good.

All derivations are based on the weighted residual method and the Galerkin approach for choosing test functions, although reformulations using other principles for chosing test functions are possible.

6.2 Future developments

In numerical analysis of wave propagation, a crucial point is to minimize the overshoots at the wave front by increasing the diagonal dominance. There is a need to incorporate such ideas in fluid-structure interaction.

In the present work, an implicit routine is adopted for treating a cavitating fluid. It would be economic with regard to computer costs to investigate an explicit time stepping procedure. When submerged structures exposed to explosions are studied using the cavitating fluid concept, nonlinear structural behaviour such as buckling must be taken into consideration. Therefore such a phenomenon should be of interest in fluid-structure interaction.

Numerical implementation of symmetric formulations presented in this work is presently being carried out. A physical interpretation of eigenvectors obtained due to these symmetric systems is also of interest.

APPENDIX A: Notations

A	coupling matrix in connection with a symmetric formulation or matrix for discrete formulation of constitutive law in connection with nonlinear fluid
B	coupling matrix in connection with a symmetric formulation or matrix for discrete formulation of constitutive law in connection with nonlinear fluid
$\mathbf{b}$	body force acting in the fluid
c	speed of sound
C_c	fluid-structure coupling damping matrix
C_d	damping constant
C_f	fluid damping matrix
C_s	structure damping matrix
D	damping constant
$\mathbf{F}$	force acting on the structure
$\mathbf{F}_f$	structural load due to fluid interaction
$\mathbf{F}_s$	external structural load
g	acceleration due to gravity
I	identity matrix
K_c	fluid-structure coupling stiffness matrix
K_f	fluid stiffness matrix
K_s	structure stiffness matrix
L	differential operator

L_b	fluid load vector due to the body force
L_e	fluid load vector due to external time-dependent pressure
L_f	structure load vector due to fluid interaction
L_s	fluid load vector due to structure interaction
L_s^e	structure load vector due to external time-dependent load
L_q	fluid load vector due to added fluid mass
M_c	fluid-structure coupling mass matrix
M_f	fluid mass matrix
M_s	structure mass matrix
$\mathbf{n}$	unit vector
N_f	trial function in the fluid domain
N_s	trial function in the structure domain
p	fluid pressure, ambient value
p_s	fluid pressure, reference value
$\hat{p}$	fluid pressure, total value
P	fluid pressure vector
p_e	external time-dependent pressure
q	added fluid mass per unit volume and time

Q	added fluid mass per unit volume, $Q = \int_0^t q \, d\tau$
$\mathbf{r}$	vector (x,y,z)
S_1-S_4	fluid boundaries
t	time
$\mathbf{u}_f$	fluid displacement field
$\mathbf{u}_s$	structural displacement field
U_s	structure displacement vector
$\mathbf{v}$	fluid velocity field
V	material volume in the fluid
w	scalar test function
$\mathbf{w}$	vector test function
u_{sf}	structure displacement component interacting with the fluid
$\alpha(\rho)$	constitutive law linking density change to pressure change
$\beta(\rho)$	constitutive law linking density change to pressure change
β	Newmark time integration parameter
γ	Newmark time integration parameter
Δt	time step
ϕ	body force potential, $\mathbf{b} = \nabla\phi$
ψ	displacement potential field

Ψ fluid displacement potential vector

Π fluid density vector

ρ fluid density, ambient value

ρ_s fluid density, reference value

$\hat{\rho}$ fluid density, total value

$\sigma(\rho, \dot{\rho})$ constitutive law linking density change to pressure change

$\int_V$ volume integral

$\int_S$ surface integral

∇ the del operator, $\left[\frac{\partial}{\partial x}, \frac{\partial}{\partial y}, \frac{\partial}{\partial z}\right]$

$$\tilde{\nabla} = \begin{bmatrix} 0 & -\frac{\partial}{\partial z} & \frac{\partial}{\partial y} \\ \frac{\partial}{\partial z} & 0 & -\frac{\partial}{\partial x} \\ -\frac{\partial}{\partial y} & \frac{\partial}{\partial x} & 0 \end{bmatrix}$$

APPENDIX B

This appendix derives the formula (B5) for interchanging the order between space integration and time derivation used in section 2.2.

Suppose a fluid particle occupies the point $\mathbf{r} = (r_1, r_2, r_3)$ at time t and the point $\mathbf{r}_0 = (r_{01}, r_{02}, r_{03})$ at time 0.

Now consider the rate of change of some property $f(\mathbf{r}, t)$ assigned to a material volume V(t). Then

$$\frac{d}{dt}\left[\iiint_{V(t)} f(\mathbf{r},t)dV(\mathbf{r})\right] = \frac{d}{dt}\left[\iiint_{V(0)} f(\mathbf{r}(\mathbf{r}_0,t),t)\cdot J\ dV(\mathbf{r}_0)\right]=$$

$$= \iiint_{V(0)} \frac{d}{dt}\, f(\mathbf{r}(\mathbf{r}_0,t),t)\cdot J\ dV(r_0), \qquad (B.1)$$

where

$$J = \det\frac{\partial \mathbf{r}}{\partial \mathbf{r}_0} = \det\frac{\partial(r_1,r_2,r_3)}{\partial(r_{01},r_{02},r_{03})}.$$

But

$$\frac{d}{dt}(f(\mathbf{r}(\mathbf{r}_0,t),t)\ J) = J\ \frac{df(\mathbf{r}(\mathbf{r}_0,t),t)}{dt} +$$

$$+\ f(\mathbf{r}(\mathbf{r}_0,t),t)\ \frac{dJ}{dt} \qquad (B.2)$$

and

$$\frac{dJ}{dt} = \frac{d}{dt}\left[\frac{\partial \mathbf{r}}{\partial \mathbf{r}_0}\right] = \frac{d}{dt}\left[\frac{\partial(r_1,r_2,r_3)}{\partial \mathbf{r}_0}\right] =$$

$$= \frac{\partial(\dot{r}_1,r_2\ r_3)}{\partial \mathbf{r}_0} + \frac{\partial(r_1,\dot{r}_2,r_3)}{\partial \mathbf{r}_0} + \frac{\partial(r_1,r_2,\dot{r}_3)}{\partial \mathbf{r}_0}.$$

Because det(AB) = det(A)·det(B), where A and B are square matrices, we have

$$\frac{\partial(\dot{r}_1, r_2, r_3)}{\partial \mathbf{r}_0} = \det \begin{bmatrix} \frac{\partial \dot{r}_1}{\partial r_{01}} & \frac{\partial \dot{r}_1}{\partial r_{02}} & \frac{\partial \dot{r}_1}{\partial r_{03}} \\ \frac{\partial r_2}{\partial r_{01}} & \frac{\partial r_2}{\partial r_{02}} & \frac{\partial r_2}{\partial r_{03}} \\ \frac{\partial r_3}{\partial r_{01}} & \frac{\partial r_3}{\partial r_{02}} & \frac{\partial r_3}{\partial r_{03}} \end{bmatrix} =$$

$$= \det \begin{bmatrix} \frac{\partial \dot{r}_1}{\partial r_1} & 0 & 0 \\ 0 & 1 & 0 \\ 0 & 0 & 1 \end{bmatrix} \begin{bmatrix} \frac{\partial r_1}{\partial r_{01}} & \frac{\partial r_1}{\partial r_{02}} & \frac{\partial r_1}{\partial r_{03}} \\ \frac{\partial r_2}{\partial r_{01}} & \frac{\partial r_2}{\partial r_{02}} & \frac{\partial r_2}{\partial r_{03}} \\ \frac{\partial r_3}{\partial r_{01}} & \frac{\partial r_3}{\partial r_{02}} & \frac{\partial r_3}{\partial r_{03}} \end{bmatrix} = \frac{\partial \dot{r}_1}{\partial r_1} J$$

and

$$\frac{dJ}{dt} = \left[\frac{\partial \dot{r}_1}{\partial r_1} + \frac{\partial \dot{r}_2}{\partial r_2} + \frac{\partial \dot{r}_3}{\partial r_3}\right] J = (\nabla \cdot \dot{\mathbf{r}}) J. \qquad (B.3)$$

The last integration of (B.1) then yields

$$\int_{V(0)} \left[J \frac{df}{dt}(\mathbf{r}(\mathbf{r}_0, t), t) + f(\mathbf{r}(\mathbf{r}_0, t), t) \cdot J(\nabla \cdot \dot{\mathbf{r}})\right] dV(\mathbf{r}_0) =$$

$$= \int_{V(t)} \left[\frac{df}{dt}(\mathbf{r}, t) + f(\mathbf{r}, t)(\nabla \cdot \dot{\mathbf{r}})\right] dV(\mathbf{r}). \qquad (B.4)$$

Finally we have

$$\frac{d}{dt}\left[\iint_{V(t)} f(\mathbf{r},t)dV(\mathbf{r})\right] =$$

$$= \int_{V(t)} \left[\frac{df(\mathbf{r},t)}{dt} + f(\mathbf{r},t)(\nabla\cdot\dot{\mathbf{r}})\right]dV(\mathbf{r}_0). \qquad (B.5)$$

APPENDIX C

This appendix discusses the possibility of neglecting the convective terms when linearizing the fluid equations.

Eq. (2.13) states that $p = c^2\rho$. Replacing p by ρ in Eq. (2.10) yields

$$\frac{d\rho}{dt} + \rho_s \nabla\cdot\mathbf{v} = q, \tag{C.1}$$

$$\rho_s \frac{d\mathbf{v}}{dt} + c^2\nabla\rho = \rho_s\mathbf{b} - q(\mathbf{v}-\mathbf{v}_q). \tag{C.2}$$

Furthermore we have

$$\frac{d\rho}{dt} = \frac{\partial\rho}{\partial t} + \mathbf{v}\cdot\nabla\rho, \tag{C.3}$$

$$\frac{d\mathbf{v}}{dt} = \frac{\partial\mathbf{v}}{\partial t} + (\mathbf{v}\cdot\nabla)\mathbf{v}. \tag{C.4}$$

We want to be able to ignore the last term in Eq. (C.2), (C.3) and (C.4). Under what circumstances will this give a good approximation?

Substituting Eq. (C.3) and (C.4) into Eq. (C.1) and (C.2) respectively yields

$$\frac{\partial\rho}{\partial t} + \rho_s\nabla\cdot\mathbf{v} + \mathbf{v}\cdot\nabla\rho = q, \tag{C.5}$$

$$\rho_s \frac{\partial\mathbf{v}}{\partial t} + c^2\nabla\rho + \rho_s(\mathbf{v}\cdot\nabla)\mathbf{v} = \rho_s\mathbf{b} - q(\mathbf{v}-\mathbf{v}_q). \tag{C.6}$$

Solving Eq. (C.6) with respect to $\nabla\rho$ and substituting into Eq. (C.5) yields

$$\frac{\partial\rho}{\partial t} + \rho_s\nabla\cdot\mathbf{v} + \mathbf{v}\cdot\nabla\rho = q, \tag{C.5}$$

$$c^2 \frac{\partial\rho}{\partial t} + \rho_s(c^2\nabla\cdot\mathbf{v} - \mathbf{v}\cdot(\mathbf{v}\cdot\nabla)\mathbf{v}) - \rho_s\mathbf{v}\cdot\frac{\partial\mathbf{v}}{\partial t} =$$

$$= -\rho_s\mathbf{v}\cdot\mathbf{b} + (c^2 + \mathbf{v}\cdot(\mathbf{v}-\mathbf{v}_q))q. \tag{C.7}$$

Suppose that $|\mathbf{v}| \ll c$ and $|\mathbf{v}_q| \ll c$. Then we can neglect

$$(\mathbf{v}-\mathbf{v}_q)q \text{ in comparison with } c^2 q$$

and

$$\mathbf{v}\cdot(\mathbf{v}\cdot\nabla)\mathbf{v} \text{ in comparison with } c^2\nabla\cdot\mathbf{v}$$

The first deletion is obvious and the second deletion is due to:

$$\mathbf{v}\cdot(\mathbf{v}\cdot\nabla)\mathbf{v} = \sum_{i,j} v_j v_i \frac{\partial v_j}{\partial x_i}. \tag{C.8}$$

We can always choose the coordinate system so that at a specific point, $v_2 = v_3 = 0$, that is,

$$\mathbf{v}\cdot(\mathbf{v}\cdot\nabla)\mathbf{v} = v_1^2 \frac{\partial v_1}{\partial x_1}. \tag{C.9}$$

This quantity can be neglected compared to

$$c^2\nabla\cdot\mathbf{v} = c^2 \sum_i \frac{\partial v_i}{\partial x_i} \tag{C.10}$$

if $|\mathbf{v}| = v_1 \ll c$.

These size estimations imply that the influence of $(\mathbf{v}\cdot\nabla)\mathbf{v}$ and $q(\mathbf{v}-\mathbf{v}_q)$ in Eq. (C.6) on the system of equations given by Eqs. (C.5) and (C.6) are negligible compared to $\nabla\cdot\mathbf{v}$ and q in Eq. (C.5).

The result is a reduced system

$$\frac{\partial \rho}{\partial t} + \rho_s\nabla\cdot\mathbf{v} + \mathbf{v}\cdot\nabla\rho = q, \tag{C.5}$$

$$\rho_s \frac{\partial \mathbf{v}}{\partial t} + c^2\nabla\rho = \rho_s\mathbf{b}. \tag{C.11}$$

A physical interpretation of the cancellations resulting in Eq. (C.11) is that the influence of the variation in space of the fluid velocity field is mainly due to $\rho_s \nabla \cdot \mathbf{v}$ in Eq. (C.5). The influence of the added fluid mass is due mainly to density increase as long as the added fluid particles have a low velocity relative to the fluid velocity field.

In the same manner, we can eliminate of the influence of the density variation in space as expressed by $\mathbf{v} \cdot \nabla \rho$ in Eq. (C.5) compared to $c^2 \nabla \rho$ in Eq. (C.11). Multiply Eq. (C.5) by $\mathbf{v}$ and add Eq. (C.11) to the result. We have

$$\mathbf{v} \frac{\partial \rho}{\partial t} + \rho_s \mathbf{v}(\nabla \cdot \mathbf{v}) + \rho_s \frac{\partial \mathbf{v}}{\partial t} + (\mathbf{v}(\mathbf{v} \cdot \nabla \rho) + c^2 \nabla \rho) =$$

$$= q\mathbf{v} + \rho_s \mathbf{b}, \qquad \text{(C.12)}$$

$$\rho_s \frac{\partial \mathbf{v}}{\partial t} + c^2 \nabla \rho = \rho_s \mathbf{b}. \qquad \text{(C.11)}$$

Because

$$|\mathbf{v}(\mathbf{v} \cdot \nabla \rho)| = |\mathbf{v}||\mathbf{v} \cdot \nabla \rho| < |\mathbf{v}|^2 |\nabla \rho| << c^2 |\nabla \rho|$$

we can neglect $\mathbf{v}(\mathbf{v} \cdot \nabla \rho)$ in comparison with $c^2 \nabla \rho$. By substituting Eq. (C.11) in Eq. (C.12) we obtain

$$\mathbf{v}\left(\frac{\partial \rho}{\partial t} + \rho_s \nabla \cdot \mathbf{v} - q\right) = 0, \qquad \text{(C.13)}$$

$$\rho_s \frac{\partial \mathbf{v}}{\partial t} + c^2 \nabla \rho = \rho_s \mathbf{b}. \qquad \text{(C.11)}$$

Because $\mathbf{v} \neq \mathbf{0}$ we have the system given in Eqs. (2.11) and (2.12).

REFERENCES

[1] AMINI, S., WILTON, D.T.: An Investigation of Boundary Element Methods for the Exterior Acoustic Problem. Computer Methods in Applied Mechanics and Engineering, Vol. 54, pp. 49-65, 1985

[2] ARNOLD, D.N., BABUSKA, I., OSBORN, J.: Finite Element Methods: principles for their selection. Computer Methods in Applied Mechanics and Engineering, Vol.45, pp. 57-96, 1984.

[3] BERKHOFF, J.G.W.: Linear Wave Propagation Problems and the Finite Element Method, Finite Elements in Fluids, Vol. 1, Ed. Gallagher et al., Wiley, London, pp. 251-280.

[4] BETTESS, P.: Infinite Elements, International Journal of Numerical Methods in Engineering, Vol. 11, No. 1, pp. 53-64, 1977.

[5] BETTESS, P., ZIENKIEWICZ, O.C.: Infinite Elements in the Study of Fluid-Structure Interaction Problems, Second International Symposium on Computing Methods in Applied Science and Engineering, Versailles, France, 1975.

[6] BLEICH, H.H., SANDLER, I.S.: Interaction Between Structures and Bilinear Fluids, International Journal of Solids and Structures, Vol. 6, pp. 617-639, 1970.

[7] COLE, R.H.: Underwater Explosions, Princeton University Press, 1948.

[8] CRAGG, A.: The Transient Response of Coupled plate Acoustic Systems using Plate and Acoustic Finite Elements, Journal of Sound and Vibrations, Vol. 15, pp. 509-528, 1971.

[9] CRAGG, A.: The Use of Simple Three-Dimensional Acoustic Finite Elements for Determining the Natural Modes and Frequencies of Complex Shaped Enclosures, Journal of Sound and Vibration, Vol. 23, pp. 331-339, 1972.

[10] CRAGG, A.: An Acoustic Finite Element Approach for Studying Boundary Flexibility and Sound Transmission Between Irregular Enclosures, Journal of Sound and Vibration, Vol. 30, pp. 343-357, 1973.

[11] DAHLBLOM, O., PETERSON, A.: CAMFEM - Computer Aided Modelling Based on the Finite Element Method, Lund Institute of Technology, Division of Structural Mechanics, TVSM-3001, Lund, Sweden 1982.

[12] DANIEL, W.J.T.: Modal Methods in Finite Element Fluid-Structure Eigenvalue Problems, International Journal for Numerical Methods in Engineering, Vol. 15, pp. 1161-1175, 1980.

[13] DANIEL, W.J.T.: Performance of Reduction Methods for Fluid-Structure and Acoustic Eigenvalue Problems, International Journal for Numerical Methods in Engineering, Vol. 15, pp. 1585-1594, 1980.

[14] DUNCAN, D.B., GRIFFITHS, D.F.: The Study of a Petrov-Galerkin Method for First-Order Hyperbolic Equations. Computer Methods in Applied Mechanics and Engineering, Vol. 45, pp. 147-166, 1984.

[15] EVERSTINE, G.C.: A Symmetric Potential Formulation for Fluid-Structure Interaction. Journal of Sound and Vibration, Vol. 79, pp. 157-160, 1981.

[16] MANSOUR, A., SEIREG, A.: Simulating Explosions in Air-Solid-Liquid Spaces. Computer in Mechanical Engineering, pp. 26-32, January 1983.

[17] FELIPPA, C.A., DERUNTZ, J.A.: Finite Element Analysis of Shock-Induced Hull Cavitation. Computer Methods in Applied Mechanics and Engineering, Vol. 44, pp. 297-337, 1984.

[18] FELIPPA, C.A.: Symmetrization of Contained Compressible-Fluid Vibration Eigenproblem Communications in Applied Numerical Methods, Vol. 1, pp. 241-247, 1985.

[19] GLADWELL, G.M.L., ZIMMERMANN, G.: On Energy and Complementary Energy Formulations of Acoustic and Structural Vibrations Problems. Journal of Sound and Vibration, Vol. 3, pp. 233-241, 1966.

[20] GLADWELL, G.M.L.: A Variational Formulation of Damped Acousto-Structural Vibration Problems. Journal of Sound and Vibration, Vol. 4, pp. 172-186, 1966.

[21] HUGHES, T.J.R., TEZDUGAR, T.E.: Finite Element Methods for First-Order Hyperbolic Systems with Particular Emphasis on the Compressible Euler Equations. Computer Methods in Applied Mechanics and Engineering, Vol. 45, pp. 217-284, 1984.

[22] NEISHLOS, H., ISRAELI, M., KIVITY, Y.: The Stability of Explicit Difference Schemes for Solving the Problem of Interaction Between a Compressible Fluid and an Elastic Shell. Computer Methods in Applied Mechanics and Engineering, Vol. 41, pp. 129-143, 1983.

[23] NEWTON, R.E.: Effects of Cavitation on Underwater Shock Loading - Part 1. NPS-69-78-013, Naval Postgraduate School, Monterey, California, 1978.

[24] NEWTON, R.E.: Effects of Cavitation on Underwater Shock Loading - Plane Problem, Part 1. NPS-69-79-007PR, Naval Postgraduate School, Monterey, California, 1979.

[25] NEWTON, R.E.: Effects of Cavitation on Underwater Shock Loading - Plane Problem, Part 2. NPS-69-80-001, Naval Postgraduate School, Monterey, California, 1980.

[26] NEWTON, R.E.: Effects of Cavitation on Underwater Shock Loading - Plane Problem - Final Report. NPS-69-81-001A, Naval Postgraduate School, Monterey, California, 1981.

[27] Numerical Methods for Coupled Problems: Fluid Structure Interactions. Proceedings of the International Conference at University College, Swansea, 7th-11th September, 1981, Ed. Hinton, E., Bettes, P., Lewis, R.W.

[28] OHAYON, R., VALID, R.: True Symmetric Formulations of Free Vibrations of Fluid-Structure Interaction - Applications and Extensions. Numerical Methods for Coupled Problems, Proceedings of the International Conference in Swansea, 1981, Ed. Hinton, E., Bettes, P., Lewis, R.W.

[29] OHAYON, R., VALID, R.: True Symmetric Variational Formulations for Fluid-Structure Interaction in Bounded Domains - Finite Element Results. Numerical Methods in Coupled Systems, 1984. Ed. Lewis R.W., Bettes, P., Hinton, E., Wiley.

[30] OHAYON, R.: Transient and Modal Analysis of Bounded Medium Fluid-Structure Problems. Numerical Methods for Transient and Coupled Problems, Proceedings of an International Conference in Venice, 1984, Ed. Lewis, R.W., Hinton, E., Bettess, P., Shrefler, B.A.

[31] OHAYON, R.: Variational Analysis of a Slender Fluid-Structure System: The Elasto-Acoustic Beam. Numeta 85, Numerical Methods in Engineering: Theory and Applications, Proceedings of the International Conference in Swansea, 1985, Ed. Middleton, J., Pande, G.N.

[32] OLSON, L.G., BATHE, K-J.: Analysis of Fluid-Structure Interactions. A Direct Symmetric Coupled Formulation Based on the Fluid Velocity Potential. Computers and Structures, Vol. 21, No. 1/2, pp. 21-32, 1985.

[33] OLSON, L.G., BATHE, K-J.: An Infinite Element for Analysis of Transient Fluid-Structure Interactions. Engineering Computations, Vol. 2, pp. 319-329, 1985.

[34] PETERSON, A.: Finite Element Analysis of Structures at High Temperatures. Lund Institute of Technology, Division of Structural Mechanics, TVSM-1001, Lund, Sweden, pp. 57-66, 1984.

[35] PLESSET, M.S.: Cavitation in Real Liquids, Bubble Dynamics, Elsevier Publishing, Amsterdam, 1964.

[36] REID, S.R.,HENDRY, S.R.: Impact Response of Fluid-Backed Metal Beams. Computers and Structures, Vol. 20, No. 1-3, pp. 321-338, 1985.

[37] STANKO, M.J., SEIREG, A.: Finite Element Simulation for the Acoustical Response of Closed and Open Spaces. Computers in Mechanical Engineering, pp. 28-33, October 1982.

[38] SEGERLIND, L.J.: Applied Finite Element Analysis, John Wiley and Sons, New York, 1976.

[39] SHARAN, K.S.: Finite Element Analysis of Unbounded and Incompressible Fluid Domains. International Journal for Numerical Methods in Engineering, Vol. 21, pp. 1659-1669, 1985.

[40] SHARAN, K.S., GLADWELL, G.M.L.: A General Method for the Dynamic Response Analysis of Fluid-Structure Systems. Computers and Structures, Vol. 21, No. 5, pp. 937-943, 1985.

[41] SMITH: A Non-Reflecting Plane Boundary for Wave Propagation Problems. Journal for Computational Physics, Vol. 15, No. 3, pp. 466-503, 1974.

[42] SOMMERFELD: Partial Differential Equations in Physics. Academic Press, 1949.

[43] TONG, P.: Recent Advances in Matrix Methods of Structural Analysis and Design. The finite element method for fluid flow, University of Alabama Press, 1971.

[44] SZMIDT, K.: Discrete Radiation Boundary for a Semi-Infinite Layer of Fluid. Computer Methods in Applied Mechanics and Engineering, Vol. 40, pp. 245-260, 1983.

[45] WAWA, J.C., DiMAGGIO, F.L.: Dynamic Response of a Submerged Prolate Spheriodal Shell to a Longitudinal Shock Wave. Computers and Structures, Vol. 20, No. 6, pp. 975-989, 1985.

[46] VICHNEVETSKY, R.: Computer Methods for Partial Differential Equations, Vol. I, Prentice Hall, 1981.

[47] ZIENKIEWICZ, O.C., TAYLOR, R.L.: Coupled Problems - A Simple Time-Stepping Procedure. Communications in Applied Numerical Methods, Vol. 1, pp. 233-239, 1985.

[48] ZIENKIEWICZ, O.C.: Why Finite Elements?, Finite Elements in Fluids - Vol. 1. Viscous Flow and Hydrodynamics, 1975. Ed. Gallagher et al., John Wiley & Sons.

[49] ZIENKIEWICZ, O.C. et al.: Finite Elements in Fluid Mechanics - A Decade of Progress. Finite Elements in Fluids - Vol. 5, 1985. Ed. Gallagher, R.H. et al, Wiley.

[50] ZIENKIEWICZ, O.C., BETTESS, P.: Fluid Structure Interaction. Ocean Structural Dynamics Symposium '82, Proceedings Oregon State University, Corvallis, Oregon, 1982.

[51] ZIENKIEWICZ, O.C., PAUL, D.K., HINTON, E.: 'Cavitation in Fluid-Structure Response (with particular reference to dams under earthquake loading)', Earthquake Engineering and Structural Dynamics, Vol. 11, pp. 463-481, 1983.

[52] ZIENKIEWICZ, O.C.: The Finite Element Method. Third Edition, McGraw-Hill, 1977.

[53] Computational Methods in Mechanics, Vol. 1: Computational Methods for Transient Analysis. Ed. Belytschko, T., Hughes, T.J.R., North-Holland, 1983.

[54] LIU, W.K., HSI, .: A Method of Computation for Fluid Structure Interaction. Computers and Structures, Vol. 20, No. 1-3, pp. 311-320, 1985.

[55] 'Finite Elements in Fluids', Vol. 1-5, John Wiley 1972-1984, Ed. Gallagher et al.

[56] OWEN, D.R.J., HINTON, E.: Finite Elements in Plasticity: Theory and Practice. Pineridge Press Ltd., 1980.

[57] GEERS, T.L.: Doubly Asymptotic Approximations for Transient Motions of Submerged Structures. Journal of Acoust. Soc. Am. Vol. 64, Part 5, pp. 1500-1508, 1978.

[58] CHRISTIE, I., GRIFFITHS, D.F., MITCHELL, A.R., SANZ-SERNA, J.M.: Product Approximation for Non-Linear Problems in the Finite Element Method, IMA Journal of Numerical Analysis, Vol. 1, pp. 253-266, 1981.

[59] SPRADLEY, L.W., STALNAKER, J.F., RATLIFF, A.W.: Computation of three-dimensional Viscous Flows with the Navier-Stokes Equations, AIAA-80-1348, AIAA 13th Fluid and Plasma Dynamics Conference, Snowmass, Colorado, 1980.

[60] FLETCHER, C.A.J.: The Group Finite Element Formulation, Computer Methods in Applied Mechanics and Engineering, Vol. 37, pp. 225-243, 1983.

[61] FLETCHER, C.A.J., SRINIVAS, K.: On the Role of Mass Operators in the Group Finite Element Formulation, Computer Methods in Applied Mechanics and Engineering, Vol. 46, pp. 313-327, 1984.